UILU-ENG 83-3602

FCP Report No. 46

IMPROVEMENT OF WELD FATIGUE RESISTANCE

by

S.-T. Chang
Department of Metallurgy and Mining Engineering

and

F. V. Lawrence, Jr.
Professor of Civil Engineering and Metallurgy

A Report of the
FRACTURE CONTROL PROGRAM

College of Engineering, University of Illinois
Urbana, Illinois 61801-2983

January 1983

IMPROVEMENT OF WELD FATIGUE RESISTANCE

ABSTRACT

An analytical model was developed to predict the effect of post-weld treatment on weld fatigue resistance: shot-peening, high powered laser dressing and TIG dressing of the weld toe were studied.

Macro- and microstructural examinations were conducted to characterize microstructures, microhardness, toe geometries and fatigue crack initiation sites resulting from each of the post-weld treatment.

Residual stresses at shot-peened weld toe were estimated from empirical relationships and confirmed by X-ray measurements. A model was developed to estimate the stress concentration factor (K_t) for TIG and laser-dressed toe geometries with undercut. Most fatigue properties were estimated from hardness measured at the region of interest. Bending stresses were considered in the prediction of both the crack initiation and crack propagation life.

Fatigue tests of as-welded and post-treated ASTM A514/E110 and A36/E60S butt weldments were conducted to verify the analytically predicted total fatigue lives. The agreement between analytical predictions and experimental results were quite good. Utilizing the current fatigue crack initiation-progagation model, a general equation was established to calculate fatigue strength (S_a) from base metal tensile strength (S_u(BM)) for several post-treated weldments. To do this, several empirical relationships were found between S_u(BM) and the necessary material properties. Predicted S_a was compared with empirical data from open literature and good agreement was obtained.

ACKNOWLEDGEMENTS

This study was principally supported by the University of Illinois Fracture Control Program which is funded by a consortium of midwest industries.

The author wishes to thank gratefully Professor JoDean Morrow of the Department of Theoretical and Applied Mechanics for his advice and suggestions.

Grateful acknowledgements are made to Mr. Patrick Murzyn for his assistance in experimental portions of the study and providing some SEM micrographs, to Mr. G. H. Lafenhagen and Mr. R. B. Brown for their assistance in the operation of test equipment and to Mr. Jon Culton for his advice and assistance in laser-dressing the weldments.

The author is particularly indebted to Mr. Dan Cichlar and Metal Improvement Company (Chicago Division) for shot-peening the weldments and supplying much information on the shot-peening process and to Mr. W. P. Evans of Caterpillar Technical Center, Peoria, Ill., for his kind assistance in measuring residual stresses in shot-peened weldments.

TABLE OF CONTENTS

		Page
I.	INTRODUCTION	1
	1.1 The Fatigue Resistance of Weldments	1
	1.2 The Role of Geometrical Discontinuities	1
	1.3 Effect of Bending and Residual Stresses	2
	1.4 Imporving Weldment Fatigue Life Through Post-Weld Treatments	3
	1.4.1 Methods of Reducing the Stress Concentration	3
	1.4.2 Methods of Modifying the Residual Stresses	4
	1.4.3 Modification of Material Properties	7
	1.5 Scope	7
II.	A REVIEW OF THE INITIATION-PROPAGATION MODEL FOR WELDMENT FATIGUE LIFE PREDICTION	9
	2.1 Estimation of the Fatigue Crack Initiation Life (N_I)	10
	2.2 Estimation of the Fatigue Crack Propagation Life (N_p)	13
III.	EXPERIMENTAL PROGRAM AND RESULTS	17
	3.1 Materials	17
	3.2 Specimen Fabrication	17
	3.3 Post-Weld Treatments	17
	3.3.1 TIG-Dressing	17
	3.3.2 Laser-Dressing	18
	3.3.3 Shot-Peening	18
	3.4 Fatigue Testing and Results	19

		Page
	3.5 Microstructural Observations	20
	3.6 Fatigue Crack Initiation Sites	23
IV.	MODIFICATION OF THE INITIATION-PROPAGATION MODEL FOR POST-TREATED WELDMENTS	26
	4.1 Neuber's Rule for Both the Generally Elastic and Plastic Cases	26
	4.2 Neuber's Rule for Combined Axial and Bending Stresses	28
	4.3 Determination of a_I, a_m, a_f and Partitioning of the Crack Path	29
	4.4 Modification of the $K_f$max Concept for Plain Plate	30
	4.5 Application of the I-P Model to Shot-Peened Weldments	31
	4.5.1 Determination of Fatigue Properties	32
	4.5.2 Residual Stresses (σ_r)	32
	4.5.3 Initial Mean Stress	34
	4.5.4 Simulation of Shot-Peened Material Through Cross-Rolling	34
	4.5.5 Effect of Residual and Bending Stress on N_p	35
	4.6 Application of the I-P Model to TIG and Laser-Dressed Weldments	35
	4.6.1 Stress Concentration Factor (K_t)	35
	4.6.2 Material Properties and Residual Stresses	38
V.	COMPARISON OF PREDICTIONS WITH EXPERIMENTAL RESULTS	40
	5.1 Shot-Peened Weldments	40
	5.1.1 Effect of Bending Stress	40
	5.1.2 Shot Size and Intensity	41
	5.2 TIG and Laser-Dressed Weldments	41

		Page
	5.3 Summary	42
VI.	COMPARISION OF I-P MODEL PREDICTIONS WITH PUBLISHED DATA	44
	6.1 Sources of Data	44
	6.2 Predictive Equations and Assumptions	44
	6.3 Predicted Effect of Geometry, Size of Weldment, and Stress Ratio (R) on Fatigue Strength	46
	6.4 Comparisons of Predictions with Data for Weldment	47
VII.	THE RECOVERY OF WELDMENT FATIGUE LIFE	49
	7.1 Concepts	49
	7.2 Fatigue Life Recovery Resulting from Post-Weld Treatments	50
VIII.	CONCLUSIONS	53
TABLES		54
FIGURES		74
APPENDICES		125
A	OBSERVATIONS IN DEVELOPING LASER-DRESSING PROCESS	125
B	CROSS-ROLLING FOR SIMULATION OF SHOT-PEENING AND ITS SMOOTH SPECIMEN TESTS	128
C	MODEL TO PREDICT WELD FATIGUE STRENGTH FROM BASE METAL TENSILE STRENGTH	135
REFERENCES		146

LIST OF SYMBOLS AND ABBREVIATIONS

SYMBOLS

a, a_I, a_m, a_f, a_{th}	Crack length, initial, intermediate, final and threshold crack length
$\underline{a}$	Peterson's material constant
α, α_A, α_B	Geometry coefficient, geometry coefficient for axial and bending loads
b	Fatigue strength exponent
C, C_o	Crack growth rate material constants
C	Numerical value of stress concentration for big geometry
C_f, $C_f(R=0)$, $C_f(R)$	Crack opening factor, crack opening factor for zero to tension loading and crack opening factor for any stress ratio
d	Depth of surface notch
D_j, D_t	Damage for jth reversal, total damage
e, Δe, e_1	Remote strain, remote strain range, remote strain for the first reversal
ε, $\Delta\varepsilon$, ε_1, ε_r	Local strain, local strain range, local strain for the first reversal, residual strain
K, K'	Monotonic and cyclic strength coefficient
K_c	Fracture toughness
K_{open}, K_{max}, K_{min}	Crack opening, maximum and minimum stress intensity factor
ΔK, ΔK_{eff}	Range in stress intensity, effective range in stress intensity
K_t, K_t^g, K_t^n, K_t^s	Stress concentration factor, stress concentration factor for big geometry, surface notch and superposition
K_f, $K_{f,max}$	Fatigue notch factor, maximum fatigue notch factor
k	Mean stress relaxation exponent
M_k, M_s, M_t	Correction factor for stress concentration, free surface and specimen width

m	Crack growth rate constant
n, n'	Monotonic and cyclic strain hardening exponent
N_I, N_p, $N_T(N_f)$	Initiation, propagation and total fatigue life
$2N$	Reversals
p, q	Length of minor and major axis in an elliptical crack shape
ϕ	Angle between major axis and the point of interest on the crack front or edge preparation angle
ϕ_o	Correction factor for crack front shape
R	Stress ratio
r, r_g, r_n	Radius of notch roots
r_M	Radius for $K_{f,max}$ condition in complex geometry
S, ΔS, S_1	Remote stress, remote stress range, remote stress for the first reversal
S_1^B, ΔS_2^B	Static bending stress, cyclic bending stress range
σ, $\Delta\sigma$, σ_1, σ_r	Local stress, local stress range, local stress for the first reversal, residual stress
S_a, σ_a	Remote and local stress amplitude
S_a	Fatigue strength
S_o, σ_o	Remote and local mean stress
$\sigma_{o,i}$, $\sigma_{o,2N}$	Initial mean stress and current mean stress
σ_f'	Fatigue strength coefficient
S_u, $S_u(BM)$, $S_u(HAZ)$	Ultimate tensile strength, ultimate tensile strength for base metal and heat affected zone
S_u^b, S_u^p	Ultimate tensile strength before peening and after peening
S_y	Yield strength
t	Weld plate thickness
θ	Flank angle of weld
W	Specimen width

ABBREVIATIONS

A, B	Axial, Bending (as superscript or subscript)
AISI	American Iron & Steel Institute
ASTM	American Society for Testing and Materials
AW	As-weld
BHN	Brinell hardness number
BM	Base metal
DPH	Diamond pyramid hardness number
FEM	Finite element method
GMA, GTA	Gas metal arc welding process, gas tungsten arc welding process
HAZ	Heat affected zone
HS	High strength streel
I-P	Initiation-Propagation
LD	Laser dressing
MRL	Maximum recoverable life
MS	Mild steel
OM	Optical microscope
PP	Plain plate
p, w, t	plain plate, as-welded and post-treated (as superscript or subscript)
QT	Quenched and tempered steel
R_c	Rockwell C hardness number
r_{crit}	Critical radius for $K_{f,max}$ condition
RL	Recovered life
SAE	Society of Automotive Engineers
SEM	Scanning electron microscope

SP, SP(cyc)	Shot-peening, shot-peened and cycled
SS	Smooth specimen
TD	TIG dressing
TIG	Tungsten inert gas welding process
UTS	Ultimate tensile strength
VHN	Vickers hardness number
WM	Weld metal

I. INTRODUCTION

1.1 The Fatigue Resistance of Weldments

The fatigue resistance of a welded structure is almost always governed by that of its welds; consequently, years of research have been devoted to the understanding and the improvement of weld fatigue behavior. Post-weld treatments for fatigue life improvement such as shot-peening and tungsten inert gas (T.I.G.) dressing, have been developed. Some treatments provide better results than others, and there are one or two methods by which the complete recovery of the "lost" fatigue life can be effected. The basic mechanisms by which the various treatments improve weld fatigue resistance need to be better understood in order to develop new and more effective methods.

1.2 The Role of Geometrical Discontinuities

Fatigue cracks always initiate and propagate at the most highly strained regions in a welded structure, and the local stresses and strains of these locations control the fatigue process there. These highly strained regions are either external discontinuities (reinforcement, undercut, or overfill) or internal discontinuities (porosity, shrinkage crack, slag inclusions, lack of penetration, or lack of fusion). Because of the high concentration of stress and strain in these locations, localized plastic strains can occur even when the nominal strains are elastic. The critical discontinuities are seldom located in the base metal of a weld (Fig. 1); most fatigue cracks initiating at internal defects do so in tempered weld metal; external discontinuities such as the weld toe initiate cracks in the grain-coarsened heat affected-zone (high wetting angles) or in untempered, highly diluted weld metal (low wetting

angles). In general, the location which has greatest stress concentration and least fatigue resistance is most likely to initiate the dominant fatigue crack. The fatigue properties of the materials in these critical regions (weld metal and heat affected zone) are generally unavailable and difficult to obtain experimentally; using the empirical relationships between the strain-controlled fatigue properties and hardness established by Landgraf (1) and others, the fatigue properties in these critical regions can be estimated.

1.3 Effect of Bending and Residual Stresses

Because it is impossible to avoid misalignment and/or angular distortion in weld joint during fabrication and fatigue testing, large bending stresses are usually induced in axially loaded weldments. Burk and Lawrence (2) showed that the bending stresses induced during axial loading were a function of distortion angle, applied axial load, the ratio of the length of specimen to its thickness, and the Young's modulus of the material.

Residual stresses can be either detrimental or beneficial to the fatigue life of a weld. Tensile residual stresses are produced in weld metal or the weld toe area when the contraction of the cooling weld metal is restrained by adjacent material. Generally, the magnitude of the residual stress cannot exceed the yield strength of the surrounding material (3). Even though early work (4,5) suggested that residual stresses had a negligible effect on weld fatigue strength, Dugdale (6) concluded that tensile residual stresses would reduce the fatigue strength of welded structures with a pronounced notch (weld toe or weld defects) by arguing that weldments were similar to the machine-notched base metal specimens which he tested. Trufyakov (7) and Serensen, et al. (8), demonstrated that tensile residual stresses significantly reduced the fatigue strength of weldments. Gurney (9) observed the beneficial effects of

compressive residual stresses induced by spot heating and local compressions in plates with fillet welded attachments.

Stress ratio (R) has an important influence on the long-life fatigue strength of welded joints when residual stresses are involved (9-14). However, thermal stress relief has a negligible effect on weld fatigue resistance for pulsating tension (R=0) (13-15) but is more effective as the stress ratio becomes negative (12,16,17).

1.4 Improving Weldment Fatigue Life through Post Weld Treatments

The three most important factors influencing weld fatigue behavior are: the severity of the stress concentration (geometry), the sign and magnitude of the residual stresses, and the material properties of the critical region. Consequently, all post-weld treatments causing improvement are involved in the control of one or more of these three major factors.

1.4.1 Methods of Reducing the Stress Concentration

The effect of grinding on weld fatigue resistance was investigated by Dutschinskii (18), Harrison (19), Gurney (20) and Suhr (21) who found that grinding the weld profiles or lightly grinding the weld toes imparted substantial improvements in fatigue strength. Grinding altered the failure location from the toe to internal weld defects, particularly for high strength steel weldments. The S-N curves obtained by Gurney for ground and as-welded specimens were nearly parallel over the whole fatigue life regime investigated. This observation suggests the potential of grinding as a life improvement technique for both the short and long life regimes. The weak point of the grinding method for fatigue life improvement is that it is an expensive process and that there is the danger of undercutting when attempting to grind out slag inclusions completely.

TIG (GTA) dressing is a technique which may be utilized to reduce the local stress concentration by remelting the weld toe material to a shallow depth to produce a more generous weld toe radius. Harrison (22), Millington (23), Haagensen (24), Watkinson, et al. (25), Kado et al. (26) and Minner and Seeger (27) have conducted fatigue tests on TIG dressed weldments and have shown a significant increase in the long life fatigue strength over as-welded weldments. Watkinson et al. reported that at long lives, the fatigue failures in the TIG dressed fillet welds often occurred not at the dressed weld toes but at other locations having more severe stress concentrations: the weld root, weld face, etc.

Kado et al. (28) and Baxter et al. (29) utilized the plasma arc dressing which produced an ultra-high temperature by supplying electrical energy to a gas. This process remelts the weld toe at greater dressing speeds due to a higher applied energy than is possible with TIG dressing. This treatment produces a great increase in fatigue resistance of weldments due to a reduction in stress concentration and an increase in hardness at the weld toe.

It is clear that modification of the weld profile to reduce local stress concentrations simply by eliminating the sharp notches at the weld toe can result in a significant improvement in fatigue resistance. However, the big problems with the conventional dressing methods are the inconsistency of the resulting geometries and undercut at the boundary between dressed and undressed surfaces due to a lack of precise process control.

1.4.2 Methods of Modifying the Residual Stresses

Stress-relief can reduce the tensile residual stresses of as-welded welds to the corresponding yield strength of the base metal at the temperature at which stress relief was conducted. Braglia (14) and Testin (30) showed that

stress relief increased the long life fatigue strength of mild steel fillet welds by approximately 90% under completely reversed (R=-1) loading condition, and that the beneficial effects of the stress relief treatment diminished rapidly in the 5×10^5 to 10^6 cycle regime and became negligible below 2×10^5 cycles.

Peening is a cold-working process which consists of bombarding the surface of the component, usually either with a high-velocity stream of metal particles (shot-peening) or with a pneumatic or a multiple-wire hammer (hammer-peening) in order to induce a compressive residual stress in the surface layer. Among the peening techniques, shot-peening is probably the most effective. Shot-peening is the controlled impingement of a stream of high velocity shot on a metal surface. As each individual shot bombards the work piece, it forms a depression through plastic deformation of the surface, thereby radially deforming the surface and causing tensile stresses. As the shot bounces off, the stress state changes, and the resultant surface stresses at equilibrium are compressive. Faulkner et al. (31) found no difference in the result of fatigue tests between weldments treated by three different types of peening method, although the depths of the work-hardened layers were significantly different between the differently peened weldments. On the other hand, Gurney (32) compared the results of weld fatigue tests performed by several investigators (20,33-36) and showed that the solid-tool hammer peening gave the best results among the three different peening techniques.

Although peening has been used fairly extensively for the improvement of fatigue resistance of mechanical parts such as coil and leaf springs, shafts and axles, its application to welded components has been fairly limited. However, experimental work has shown that peening causes significant improvements in weld fatigue strength. Watkinson et al. (25) observed 65% and

170% fatigue strength increases in pulsating tension tests by peening transverse non-load-carrying fillet welds of low (40 ksi) and high (107 ksi) yield strength steels, respectively. Booth (37) showed that hammer peening of fillet welds in mild steel can prolong the fatigue life to that of the plain plate. Nacher (38) tested both butt welds and fillet welds treated by multiple wire type of peening tool and observed an 87% (as maximum) increase in fatigue strength at 2×10^6 cycles under pulsating tension loadings. Several researchers investigated the effect of shot-peening on weld fatigue resistance. Doty (39), Nacher (40) and Baron et al. (41) observed fatigue strength improvements between 33% and 37% by conventional shot-peening of transverse butt welds. Robakowski (42) reported an increase in fatigue strength of only 18% at 2×10^6 cycles by peening. However, Konishi (43) obtained a 100% increase in weld fatigue strength for high tensile structural steel treated by normal shot peening. Nordmark (44) and Hedström (45) observed plain plate failures of shot-peened aluminum alloy welds. Recently, Braglia (14) demonstrated that the long life fatigue strength of transverse fillet welds in reversed bending could be increased 90% by either shot or needle peening.

Tensile overloading which commonly occurs in many structures like pressure vessels and boilers during their hydrotesting can plastically deform the most highly stressed areas such as the weld toe or weld root. A compressive residual stress state can be induced in these critical areas upon release of the load. Gurney (46) and Harrison (47) have shown that the long life fatigue strength of welds increases in proportion to the level of overstress. Albrecht et al. (48) showed that overloads can alter the initial tensile mean stresses by introducing compressive residual stresses at the weld toe and thus delay fatigue crack initiation. Albrecht et al. found that

periodic overloads reestablished the compressive residual stresses at the weld toe and were therefore more beneficial in delaying initiation than a single overload.

Local heating of a region can set up high compressive stresses around the hot spot, which cause it to deform plastically. Upon cooling, the hot spot is then subjected to tensile residual stresses and the surrounding area to compressive residual stresses.

1.4.3 Modification of Material Properties

Material properties in critical regions such as the HAZ can vary considerably depending on the heat input, joint details, plate thickness and weld process. However, the resulting differences in microstructures and hardness generally have only a minor effect on weld fatigue resistance because severity of the notch and the residual stress effects generally overshadow the metallurgical variables. Therefore, no method which improves weld fatigue resistance by improving material properties has been utilized. However, improvement of material properties usually accompanies most post-weld treatments.

1.5 Scope

All the post-weld treatments discussed above have been developed and investigated only in a phenomenological or qualitative manner. Though Burk and Lawrence (49) have introduced a model which predicts the influence of stress concentration, material properties, and residual stresses and stress ratio (R) on the fatigue resistance of weldments, no unified theoretical analysis for the development of welds with an improved fatigue resistance currently exists.

The purpose of this investigation was first to develop analytical means to predict the weld fatigue behavior of several conventional (shot-peening and TIG dressing) and a newly proposed (laser-dressing) post-treated weldments and to prove the analytical predictions through comparison with actual data. Second, rational and effective ways of developing of welds with an improved fatigue resistance were studied. A maximum recoverable life (MRL) concept was introduced and the conditions for complete recovery of lost fatigue life were discussed for several post-treated weldments. This investigation was limited to ASTM A514 and ASTM A36 structural steels.

II. A REVIEW OF THE INITIATION-PROPAGATION MODEL FOR WELDMENT FATIGUE LIFE PREDICTION

Currently, there are two different types of model to predict weld fatigue life: Maddox (50) and El Haddad (51) have developed propagation models in which the total fatigue life (N_T) is predicted solely through estimates of fatigue crack propagation life (N_p). Lawrence et al. (52,53) have developed a hybrid, initiation-propagation model in which the total fatigue life (N_T) is predicted by combining estimates of the fatigue crack initiation life (N_I) and the fatigue crack propagation life (N_p):

$$N_T = N_I + N_p \tag{1}$$

Each of these models have advantages and disadvantages. The propagation models of Maddox and El Haddad are currently favored by many investigators of weld fatigue and presume the existence of a crack or crack-like-defect which is large enough to propagate. These models have the virtue of involving only a single crack propagation analysis. However, the difficulties of the propagation models include estimating the initial crack size and/or behavior of very small cracks and estimating the influence of residual and mean stresses.

The initiation-propagation (I-P) model has the disadvantage of requiring two separate analyses but attempts to circumvent the small crack problem through the use of smooth specimen fatigue data to estimate the life (N_I) devoted to fatigue crack initiation and early propagation. A strong point of this I-P model is that it can estimate the influence of residual stresses. The I-P model is quite general and can be applied to sound welds or to welds

containing internal defects (54). The I-P model is particularly effective in the long life regime, since the initiation life becomes dominant at long lives at which most weld structures are designed to operate.

The I-P model has been used successfully in predicting the fatigue resistance of weldments under constant-amplitude loadings. It also provides a systematic means for predicting the fatigue behavior of weldments when one or more of the variables influencing their fatigue resistance is altered as is the case with most post-weld treatments.

2.1 Estimation of the Fatigue Crack Initiation Life (N_I)

Using the modified Basquin relationship (55), the fatigue crack initiation life (N_I) can be estimated:

$$\sigma_a = (\sigma_f' - \sigma_o)\ (2N_I)^b \tag{2}$$

where $\sigma_a = (\frac{\Delta\sigma}{2})$ is the stabilized notch-root stress amplitude, σ_f' is the fatigue strength coefficient, σ_o is the mean stress including weld residual and remote mean stresses (after the initial set-up cycle), $2N_I$ is the reversals to fatigue crack initiation, and b is the fatigue strength exponent.

If the mean stress relaxes during cycling, the current mean stress ($\sigma_{o,2N}$) has been found to obey a power function for a constant strain amplitude (49) (see Fig. B-5):

$$\sigma_{o,2N} = \sigma_{o,i}(2N-1)^k \tag{3}$$

where: $\sigma_{o,i}$ is the initial mean stress, 2N is the elapsed reversals and k is the relaxation exponent. Larger strain amplitudes and higher initial mean stresses cause a more rapid relaxation of mean stress.

A mechanics analysis to estimate the local notch-root (weld toe) stresses and strains (from the remote stresses and strains) is required. Topper, Wetzel and Morrow (56) found that it is useful in solving notch fatigue problems if the fatigue notch factor (K_f) is substituted for the elastic stress concentration factor (K_t) in Neuber's rule (57) to relate the remote (S,e) and local (σ,ε) stressses and strains:

$$K_f = \left(\frac{\sigma\ \varepsilon}{S\ e}\right)^{\frac{1}{2}} \tag{4}$$

When the remote stress and strain ranges result in only elastic behavior, as can be assumed in most cases after the initial set-up cycle, Eq. 4 can be expressed:

$$\frac{(K_f\ \ \Delta S)^2}{E} = \Delta\sigma\Delta\varepsilon \tag{5}$$

Using the equation for the cyclic stress-strain behavior, $\Delta\sigma$ can be determined by (numerically) solving the following equation:

$$\frac{(K_f\ \ \Delta S)^2}{E} = \Delta\sigma \left\{\frac{\Delta\sigma}{E} + 2\ \left(\frac{\Delta\sigma}{2K'}\right)^{1/n'}\right\} \tag{6}$$

where: K' is the cyclic strength coefficient and n' is cyclic strain hardening exponent. For long-life fatigue ($N_I > 10^6$ cycles), generally elastic conditions prevail at the notch root ($\Delta\sigma = E \cdot \Delta\varepsilon$); and, thus, $\Delta\sigma$ becomes:

$$\Delta\sigma = K_f\ \ \Delta S \tag{7}$$

Combining Eqs. 2 and 7:

$$\frac{\Delta S}{2} K_f = (\sigma_f' - \sigma_o) [2N_I]^b \quad (8)$$

The fatigue notch factor (K_f) can be estimated using Peterson's empirical relationship (58):

$$K_f = 1 + \frac{K_t - 1}{1 + \frac{a}{r}} \quad (9)$$

where: r is the notch root radius, and a is a material parameter which can be estimated for steels using the ultimate tensile strength of the material in the region of interest (59):

$$a = (300/S_u)^{1.8} \times 10^{-3} = (300/BHN/2)^{1.8} \times 10^{-3} \text{ inches} \quad (10)$$

A difficulty arises in determining the appropriate value of K_f because the notch root radius of a discontinuity such as a weld toe is unknown and variable. Observations through microscopic examination of weld toes, for example, lead to the conclusion that a weld toe has all possible values of notch-root radius along its length. This conclusion has led to the idea of using the worst possible, the maximum, value of K_f for a given weld shape, $K_{f,max}$ (52).

The elastic stress concentration factor (K_t) can be estimated using finite element methods as a function of assumed notch root radii (r) for a given weld geometry (60). Assuming a general form of K_t for welds (see Fig. 2):

$$K_t = 1 + \alpha(t/r)^{\frac{1}{2}} \quad (11)$$

where α is a constant determined by weld geometry and type of loading and t is the plate thickness. Substituting Eq. 11 into Eq. 9 and differentiating with respect to "r" leads to the maximum value of K_f, $K_{f,max}$ (see Fig. 3), when $r = \underline{a}$:

$$K_{f,max} = 1 + (\alpha/2)\ (t/\underline{a})^{\frac{1}{2}} = 1 + 0.093\ \alpha\ S_u^{0.9} t^{0.5} \text{ (for steels)} \quad (12)$$

Combining Eq. 2 and Eq. 3, the <u>damage</u> due to the jth reversal (D_j) is:

$$D_j = \frac{1}{2N_j} = \left\{\frac{\sigma_f' - \sigma_{o,i}}{\sigma_a}(2N_j - 1)^k\right\}^{-1/b} \quad (13)$$

Using the Palmgren-Miner's damage summation rule (61,62), the initiation life can be estimated by solving the following equation for $2N_I$ using proper numerical methods:

$$D_t = \sum_{j=1}^{2N_I} D_j = \int_1^{2N_I} D_j\, d(2N_j) = 1 \quad (14)$$

where: D_t is the total accumulated damage.

2.2 Estimation of the Fatigue Crack Propagation Life (N_p)

Generally, the fatigue crack propagation life (N_p) can be estimated by integrating the Paris power law (63) from the initial crack length (a_I) to the final crack length (a_f):

$$N_p = \frac{1}{C} \int_{a_I}^{a_f} (\Delta K)^{-m} da \quad (15)$$

where: C and m are material constants and ΔK is the stress intensity factor range:

$$\Delta K = Y \Delta s \, (\pi a)^{\frac{1}{2}} \tag{16}$$

For a weld whose geometry is generally complex, the geometry factor (Y) for a given weld shape should be determined and the effect of mean and bending stresses should be considered in the estimation of N_p.

The geometry factor (Y) for a particular weld shape can be determined by the superposition of the following factors (64):

$$Y = \frac{M_k M_s M_t}{\phi_o} \tag{17}$$

where: M_k is a correction factor for the induced stress distributions due to the geometrical discontinuity of the weld during loading, M_s is a correction factor for free surface ($M_s = 1.12$), M_t is a correction factor for finite width (W):

$M_t = (\sec \pi a/2W)^{1/2}$ for a center crack and

$M_t = \sin^2(\pi a/2W) + \sec^2(\pi a/2W)$ for a single edge crack.

ϕ_o is a correction factor for crack front shape and expressed as follows for an elliptical crack shape:

$$\phi_o = \int_0^{\pi/2} \left[1-\left(1-\frac{p^2}{q^2}\right) \sin^2\phi\right]^{\frac{1}{2}} d\phi \tag{18}$$

where: p is the length of minor axis of ellipse, q is the length of major axis and ϕ is the angle between major axis and the point of interest on the crack front; $\phi_o = \pi/2$ for a semi-circular crack (p=q) and ϕ_o=1 for a very long

TABLE 5

Cyclic and Fatigue Properties of Base, Cross-Rolled, Weld,
and Heat-Affected Materials for ASTM A36/E60S-3 Welds

(71,81)

Material	A36-BM	A36-HAZ	E60S-3-WM	Cross-Rolled*
Cyclic Yield Strength, 0.2% Offset, ksi (MPa)	48.0 (232)	58.0 (400)	55.8 (385)	73.5 (507)
Cyclic Strain Hardening Exponent, n'	0.227	0.178	0.155	0.285
Cyclic Strength Coefficient, K', ksi (MPa)	198 (1365)	175 (1207)	146 (1007)	432 (2979)
Fatigue Strength Coefficient, σ_f', ksi (MPa)	150 (1034)	120 (827)	131 (904)	224 (1544)
Fatigue Ductility Coefficient, ε_f'	0.352	0.282	0.607	0.079
Fatigue Strength Exponent, b	-0.113	-0.064	-0.075	-0.119
Fatigue Ductility Exponent, c	-0.514	-0.534	-0.548	-0.387
Transition Fatigue Life, $2N_{tr}$, Reversals	33,182	9,743	28,022	5,930

* A36 plates of 5/8" thickness were cross-rolled in 60% reduction and strain aged for 1 hour at 100°C. These test pieces were cut from the plate which Higashida used (71).

TABLE 6

Welding and TIG-Dressing Parameters

Parameter	A514/E110	A36/E60S-3	TIG-Dressing*
Plate Thickness, in. (mm)	0.5 (12.7)	0.625 (15.9)	---
Electrode Diameter, in. (mm)	0.0626 (1.6)	0.0626 (1.6)	---
Voltage, (v)	30	35	20
Current, amps	290	500	200
Travel Speed, ipm (mm/sec)	17 (7.2)	15 (6.4)	12 (5.1)
Preheat Temp, °F (°C)	205 (96)	72 (22)	72 (22)
Heat Input, kJ/in. (kJ/mm)	30.7 (1.2)	70 (2.8)	20.0 (0.8)
Shielding Gas Composition	Ar-2% O_2	Ar-5% O_2	Ar

* Same parameters were used to TIG-dress both A514/E110 and A36/E60S-3 weldments.

TABLE 7

Laser-Dressing Parameters

Beam impignement angle	80°
Shielding gas impingement angle	0°
Beam power, kw	4.5 (A514), 5.5 (A36)
Focussing mirror	f7
Distance to focus from surface, in. (mm)	1.25-1.5 (31.8-38.1)
Travel speed, in/min. (mm/sec)	13 (5.5)
Surface coating	Krylon flat black
Shielding gas	Ar
Shielding gas pressure, psi (MPa)	60 (0.414)
Shielding gas flow rate, ft^3/min (cm^3/sec)	4 (464)
Heat input, KJ/in.	20.8 (A514), 25.4 (A36)

TABLE 8

Shot-Peening Parameters*

Air jet nozzle size, in (mm)	0.25 (6.4)
Shot nozzle size, in (mm)	0.5 (12.7)
Angle of impingement	45°
Air pressure, psi (MPa)	80 (0.55)
Length of oscillation, in (mm)	4 (101.6)
Cycle time, min	5
Travel speed, in/min (mm/min)	1.6 (40.6)
Shot size,** in (mm)	0.033 (0.84)
Almen intensity	.019A

*Recommended and performed by Metal Improvement Company
**SAE 330 = 0.033 in., SAE 230 = 0.023 in., SAE 170 = 0.017 in., SAE 110 = 0.017 in.

TABLE 9

Almen Intensity Produced by Various Shot Size for the Selected Parameter (Table 8)

Shot Size (SAE)	110	170	230	330
Almen Intensity	.009A	.012A	.016A	.019A

TABLE 10

Fatigue Test Results for As-welded and Shot-peened A514/E110 Specimens (R = 0)

Condition	Designation	Δ Stress (ksi) Axial	Δ Stress (ksi) Bending	Life (Cycles)	Failure Site	Comments
As-Welded	T1WA	65	± 4.3	59,970	weld toe	no straightening
	T1WB	65	± 3.2	72,410	weld toe	no straightening
	T1WC	65	± 1.9	77,340	weld toe	no straightening
	T1W2	65	± 1.0	94,340	weld toe	
	T1W4	80	± 1.1	26,690	weld toe	
	T1W5	80	± 0.8	34,690	weld toe	
	T1W6	65	± 0.3	84,850	weld toe	
Shot-Peened	T1P1 (330)	80	± 1.3	130,630	weld toe	
	T1P2 (330)	80	± 1.2	104,260	weld toe	
	T1P3 (330)	80	± 1.5	112,900	weld toe	
	T1P4 (330)	80	± 1.5	116,720	weld toe	
	T1P5 (330)	80	± 1.2	130,990	weld toe	
	T1P330	65	± 0.6	7,125,400+	--	no failure
	T1P230	80	± 1.1	459,450	weld toe	
	T1P170	80	± 0.3	74,130	weld toe	
	T1P110	80	± 0.6	103,350	weld toe	

TABLE 11

Fatigue Test Results for TIG-dressed and Laser-dressed A514/E110 Specimens (R = 0)

Condition	Designation	Δ Stress (ksi)		Life (Cycles)	Failure Site	Comments
		Axial	Bending			
TIG-Dressed	T1TA	65	± 2.9	665,430	TIG toe	no straightening
	T1TB	65	± 0.6	356,740	TIG toe	no straightening
	T1TC	65	± 1.9	280,900	TIG toe	no straightening
	T1T1	80	± 1.0	65,290	TIG toe	
	T1T2	65	± 1.3	254,990	TIG toe	
	T1T3	80	± 0.6	71,810	TIG toe	
	T1T5	80	± 1.6	31,740	TIG toe	
	T1T6	65	± 0.0	317,800	notch	notch created by TD
Laser-Dressed	T1L1	(65)	± 1.2	1,000,000-	--	no failure
	T1L2	65	± 1.3	1,136,770	plain plate	
	T1L3	65	± 0.4	308,270	plain plate	
	T1L4	65	± 2.1	813,160	plain plate	
	T1L5	80	± 0.2	52,770	laser toe	undercut
	T1L6	80	± 2.0	85,310	laser toe	undercut
	T1L7	80	± 0.9	61,210	laser toe	undercut
	T1L8	80	± 0.4	92,200	plain plate	
	T1L9	80	± 1.8	43,920	laser toe	bad undercut

TABLE 12

Fatigue Test Results for As-Welded, Shot-Peened
TIG-Dressed, and Laser-Dressed A36/E60S-3 Specimen (R = 0)

Condition	Designation	Δ Stress (ksi.) Axial	Bending S_1^B	Bending ΔS_2^B	Life (Cycles)	Failure Site	Comments
As-Welded	AW1	32	- 1.9	- 2.1	2.32×10^6	--	no failure
	AW2	35	- 2.6	- 2.2	8×10^6	--	no failure
	AW3	40	+ 1.8	--	154,700	weld toe	bending corrected
	AW4	40	- 9.3	--	576,500	weld toe	
	AW1'	45	- 8.6	+ 4.4	166,100	weld toe	retested AW1
Shot-Peened	AP1	40	-12.1	+ 4.8	1,103,410	smooth surface	
	AP2	40	-10.9	+ 4.1	4,798,770	weld toe	
	AP3	45	-15.2	+ 6.8	243,720	weld toe	
	AP4	50	- 5.6	--	85,490	weld toe	
TIG-Dressed	AT1	40	+ 9.1	--	1,142,110	TIG toe	
	AT2	40	+ 9.3	--	946,900	smooth surface	
	AT3	40	+ 9.7	--	333,000	TIG toe	bad undercut
	AT4	45	+10.9	--	259,140	TIG toe	
	AT5	45	+ 6.1	--	224,700	TIG toe	
Laser-Dressed	AL1	40	+ 1.3	--	765,190	undercut	bending corrected
	AL2	40	+ 4.6	--	561,130	undercut	
	AL3	40	+ 4.7	--	872,520	undercut	
	AL4	45	+ 9.9	--	120,040	undercut	
	AL5	45	+ 8.8	--	191,210	undercut	
	AL6	45	- 5.1	--	203,960	undercut	

Table 13

Residual Stresses Measured and Predicted for on the Surface of a Shot-Peened A36/E605-3 Bead-on-Plate Weldment

Specimen	Location	Estimated Value (ksi) Using Eq. 47	Measured Value ksi	Average
	Toe (left)	- (53 ∿ 64)	- 71.6 ± 5.2 - 77.5 ± 5.1 - 61.1 ± 4.4	- 70.1 ± 8.3
A36 p7	Weld Metal (center)	- (46 - 55)	- 53.9 ± 6.6 - 46.5 ± 5.5	- 50.2 ± 6.1
	Toe (right)	- (53 ∿ 64)	- 56.4 ± 6.0 - 67.2 ± 6.1	- 61.8 ± 7.6
	Toe (left)	- (53 ∿ 64)	- 65.5 ± 4.3 - 61.7 ± 8.0	- 63.6 ± 6.2
A36 p2	Weld Metal (center)	- (46 - 55)	- 61.9 ± 4.5 - 37.4 ± 7.3 - 42.3 ± 5.9 - 56.4 ± 4.4	- 49.5 ± 11.5
	Toe (right)	- (53 ∿ 64)	- 49.8 ± 5.9 - 55.0 ± 6.2	- 52.4 ± 6.1

TABLE 14

Coefficients for Axial and Bending Loads (66)

Loading type	ϕ	θ	a_1	a_2	a_3	a_4	a_5
Axial	90°	0°	1.0	0	0	0	0
		10°	1.364	-7.09	42.84	-104.20	87.52
		20°	1.563	-10.97	66.25	-161.05	135.20
		30°	1.717	-14.03	84.72	-205.97	172.92
		45°,60°	1.831	-16.57	100.54	-244.88	205.74
Bending	90°,120°	0°	1.0	-2.0	0	0	0
		10°	1.056	-6.07	28.68	-74.84	66.81
		20°	1.278	-10.93	61.57	-162.15	145.48
		30°	1.434	-14.25	83.80	-220.78	198.11
		45°,60°	1.540	-17.09	103.47	-273.51	245.95

Table 15

The Effects of Parameters in Eq. 54 on r_M and $K^s_{f.max}$

	Simple As-Weld			Dressed Weld with Undercut		
	Condition	r	$K_{f.max}$	Condition	r_M	$K^s_{f.max}$
Material Properties	$\underline{a}$ ↑	↑	↓	$\underline{a}$ ↑	↑	↓
Size	t ↑	-	↑	d ↑	↓	↑
Stress field	α ↑	-	↑	C ↑	↑	↑

Note: ↑ represents an increase and ↓ represents a decrease.

TABLE 16

Methods Proposed to Determine the Three Major Factors
in Calculating Crack Initiation Life for Each Post-Treated Weldment

Post-Weld Treatments	K_t	K_f	σ_r	Material Properties
As-Weld	As-welded K_t: $K_t = 1+\alpha(t/r)^{\frac{1}{2}}$	K_f, max	$+\sigma_{ys}$(BM)	Hardness or Simulated HAZ properties
Over-Stress	As-welded K_t	K_f, max	$-\sigma > -\sigma_{ys}$	"
Stress-Relief	As-welded K_t	K_f, max	zero	"
Shot-Peening				
H.S. St. (A514)	As-welded K_t	K_f, max	$\sigma_{r,H} = -(0.1\ BHN + 80)$	Hardness
Mild St. (A36)	As-welded K_t	K_f, max	$\sigma_{r,m} = -(0.5 \sim 0.6)\ Su$	Simulation by X-rolling or Hardness
TIG-Dressing				
Original Toe (TIG Bead)	As-welded K_t	$K_f(r)$	$+\sigma_{ys}$(BM)	Hardness
New Toe	Proposed Method	K_f, max	$+\sigma_{ys}$(BM)	Hardness or Simulated HAZ properties
Laser-Dressing				
Original Toe (Laser Bead)	As-welded K_t	$K_f(r)$	$+\sigma_{ys}$(BM)	Hardness
New Toe	Proposed Method	K_f, max	$+\sigma_{ys}$(BM)	Hardness or Simulated HAZ properties
Plain Plate	$K_t = 1+2(d/r)^{\frac{1}{2}}$	K_f, max	near zero	Tested properties

TABLE 17

Weld Geometry, Parameters and Residual Stresses Required to Estimate Crack Initiation Life

Butt Weld ($\phi = 90^o$)	θ	α_A	α_B	BHN*	a in. (mm) x 10^{-3}	d in. (mm) x 10^{-3}	K_f^A, max	K_f^B, max	Assumed σ_r ksi (MPa)
A514/E110									
t = 0.5"									
PP	-	2	-	303	4.15 (106)	1.4 (35)	1.58	-	-
AW	45^o	0.27	0.165	398	2.00 (51)	-	3.13	1.52	120 (827)
TD	0	2	-	477	1.37 (35)	5.8 (147)	3.06	-	120 (827)
LD	0	2	-	410	1.87 (47)	1.3 (33)	1.84	-	120 (827)
SP	45^o	0.27	0.165	437	1.72 (44)	0.5 (14)	3.30	2.41	-125.5(-865)
A36/E60S-3									
t = 0.625"									
PP	-	2	-	166	11.30 (287)	2.1 (53)	1.49	-	-
AW	60^o	0.27	0.165	220	6.09 (155)	-	2.33	1.84	40 (276)
TD	0	2	-	473	1.39 (35)	8.2 (208)	3.43	-	40 (276)
LD**	30^o	0.23	-	460	1.45 (37)	9.2 (234)	4.12	-	40 (276)
SP	60^o	0.27	0.165	326	3.48 (88)	0.7 (18)	2.80	2.10	-50(-345)

*Hardness of crack initiation sites (100 μm from the surface).

**For Laser-dressed A36/E60S-3, C = 1.2 and $\gamma_M = 1.56 \times 10^{-3}$ in. (40×10^{-3} mm). For all others, C = 1, $\gamma_M = \underline{a}$.

TABLE 18

Material Constants and Parameters Required to Estimate Crack Propagation Life

Propag. Region Material	C in/cycle (mm/cycle) x 10^{-10}	m	K_{IC} ksi (MPa)	a_I in. (mm)	a_m in. (mm)	ΔS(ksi)	a_f (inches) :40	45	50	65	80
A514F/E110											
Plain plate	1.5 (38.1)	3.25	150 (1034)	0.009 (0.229)	-		-	-	-	1.4	0.93
AW & SP HAZ	66 (1676)	2.25	-	0.0024 (0.061)	0.081 (2.06)		-	-	-	-	-
AW & SP BM	1.5 (38.1)	3.25	150 (1034)	-	0.081 (2.06)		-	-	0.34	0.32	0.30
LD HAZ	66 (1676)	2.25	-	0.01 (0.254)	0.031 (0.79)		-	-	-	-	-
LD BM	1.5 (38.1)	3.25	150 (1034)	-	0.031 (0.79)		-	-	-	1.4	0.92
TD HAZ	66 (1676)	2.25	-	0.01 (0.254)	0.045 (1.14)		-	-	-	-	-
TD BM	1.5 (38.1)	3.25	150 (1034)	-	0.045 (1.14)		-	-	-	1.4	0.92
A36/E60S-3											
Plain plate	3.6 (91.4)	3.0	45 (310)	0.01 (0.254)	-		0.33	0.26	0.21	-	-
AW & SP HAZ	66 (1676)	2.25	-	0.01 (0.254)	0.06 (1.52)		-	-	-	-	-
AW & SP BM	3.6 (91.4)	3.0	45 (310)	-	0.06 (1.52)		0.325	0.25	0.20	-	-
LD HAZ	66 (1676)	2.25	-	0.002 (0.051)	0.03 (0.76)		-	-	-	-	-
LD BM	3.6 (91.4)	3.0	45 (310)	-	0.03 (0.76)		0.31	0.25	-	-	-
TD HAZ	66 (1676)	2.25	-	0.003 (0.076)	0.047 (1.19)		-	-	-	-	-
TD BM	3.6 (91.4)	3.0	45 (310)	-	0.047 (1.19)		0.43	0.40	-	-	-

TABLE 19

Coefficients of Eq.55 for Each Post-Weld Treatment and Base Metal Heat Treatment

Post-Weld Treatment	Base Metal Heat-Treatment	A	B	C	D
Plain Plate	-	1	50	50	0.1865
As-Weld	Hot-Rolled	0.94	50	$\frac{100}{3}$	0.1343
	Normalized	0.72	70	$\frac{100}{3}$	0.1343
	Quench. & Temp.	0.30	100	$\frac{100}{3}$	0.1343
Stress-Relief	-	1.50	50	$\frac{100}{3}$	0.1343
Over-Stress	Hot-Rolled	2.06	50	$\frac{100}{3}$	0.1343
	Normalized	2.28	30	$\frac{100}{3}$	0.1343
	Quench. & Temp.	2.70	0	$\frac{100}{3}$	0.1343
Shot-Peening	S_u(HAZ) < 125 ksi	2.55	50	$\frac{50}{1.8}$	0.1582
	S_u(HAZ) > 125 ksi	2.12	130	$\frac{50}{1.8}$	0.1582

TABLE 20

Estimated Conditions for Complete Recovery of Lost Fatigue Life

Treatment	σ_r			Maximum K_f^t/K_f^p*			Maximum $K_{f,max}^t$		
	MS	HL	QT	MS	HL	QT	MS	HL	QT
Stress Relief	0	0	0	1.3	1.3	1.4	1.8	1.9	2.1
Over Stress	-35	-50	-100	1.6	1.7	2.0	2.2	2.4	3.1
TIG or Laser** Dressing	35	50	100	2.0	1.8	1.2	2.8	2.6	1.9
Shot-Peening	-50	-70	-115	1.9	2.0	2.3	2.6	2.9	3.6

*K_f^p, max (MS) = 1.37
K_f^p, max (HL) = 1.42
K_f^p, max (QT) = 1.58

**$\sigma_f'^t$(MS) = 270 ksi.
$\sigma_f'^t$(HL) = 275 ksi. (Assumed)
$\sigma_f'^t$(QT) = 300 ksi.

Table 21

The Average Recovery (%) of the Lost Fatigue Life Resulting from the Post-Weld Treatments for A514/E110 and A36/E60S Bead on Plates.

Materials	ΔS(ksi)	Shot-Peening	TIG-Dressing	Laser-Dressing
A514/E110	80	70%	20%	25%
	65	100%	30%	100%
A36/E60S	45	75%	75%	45%
	40	100%	100%	65%

FIGURES

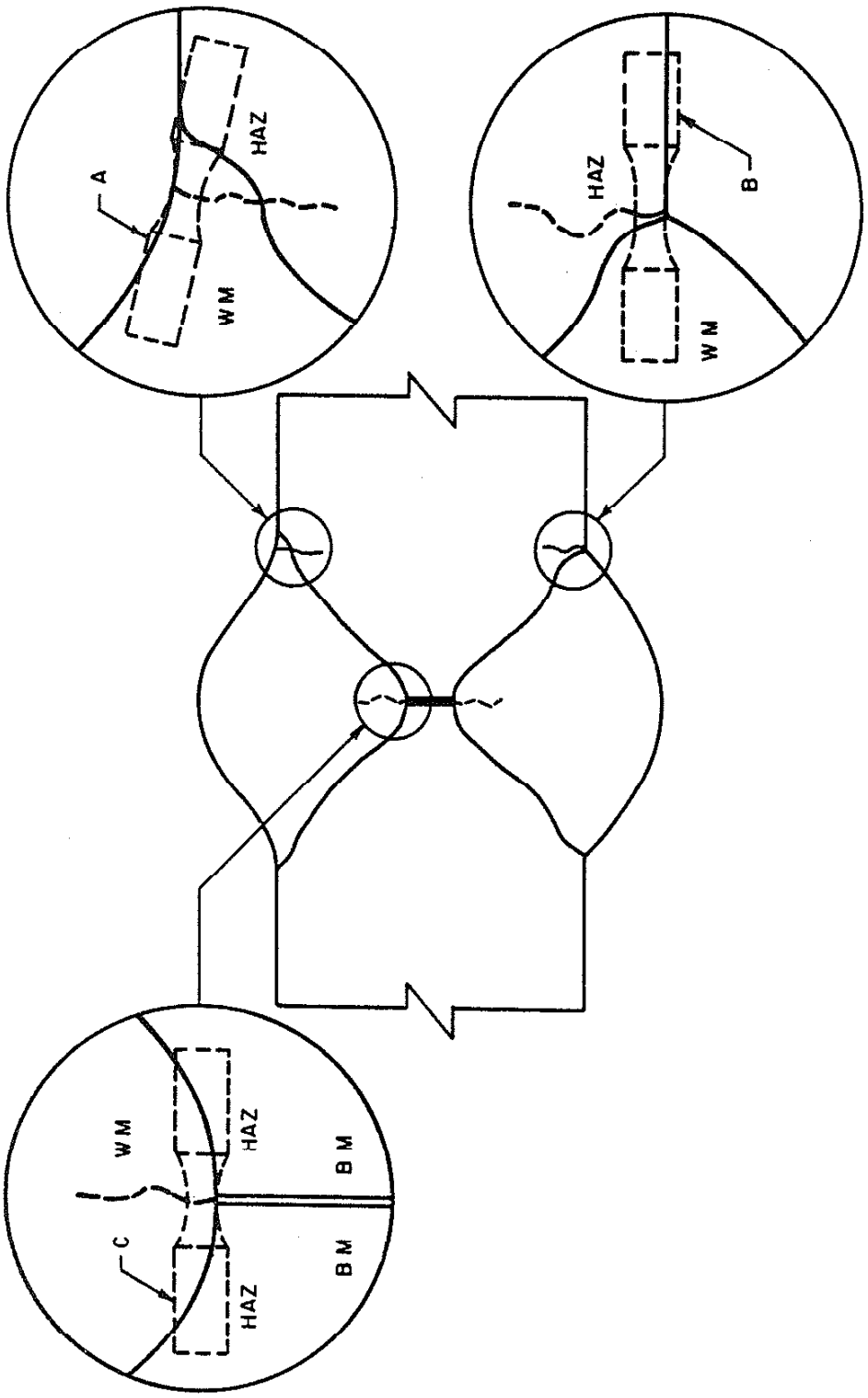

Fig. 1 Typical Locations of Fatigue Crack Initiation in a Butt Weld. Fatigue Cracks Can Initiate: in Diluted, Untempered Weld Metal (A); in the Heat Affected Zone Close to the Line of Fusion (B); and in Tempered Weld Metal (C).

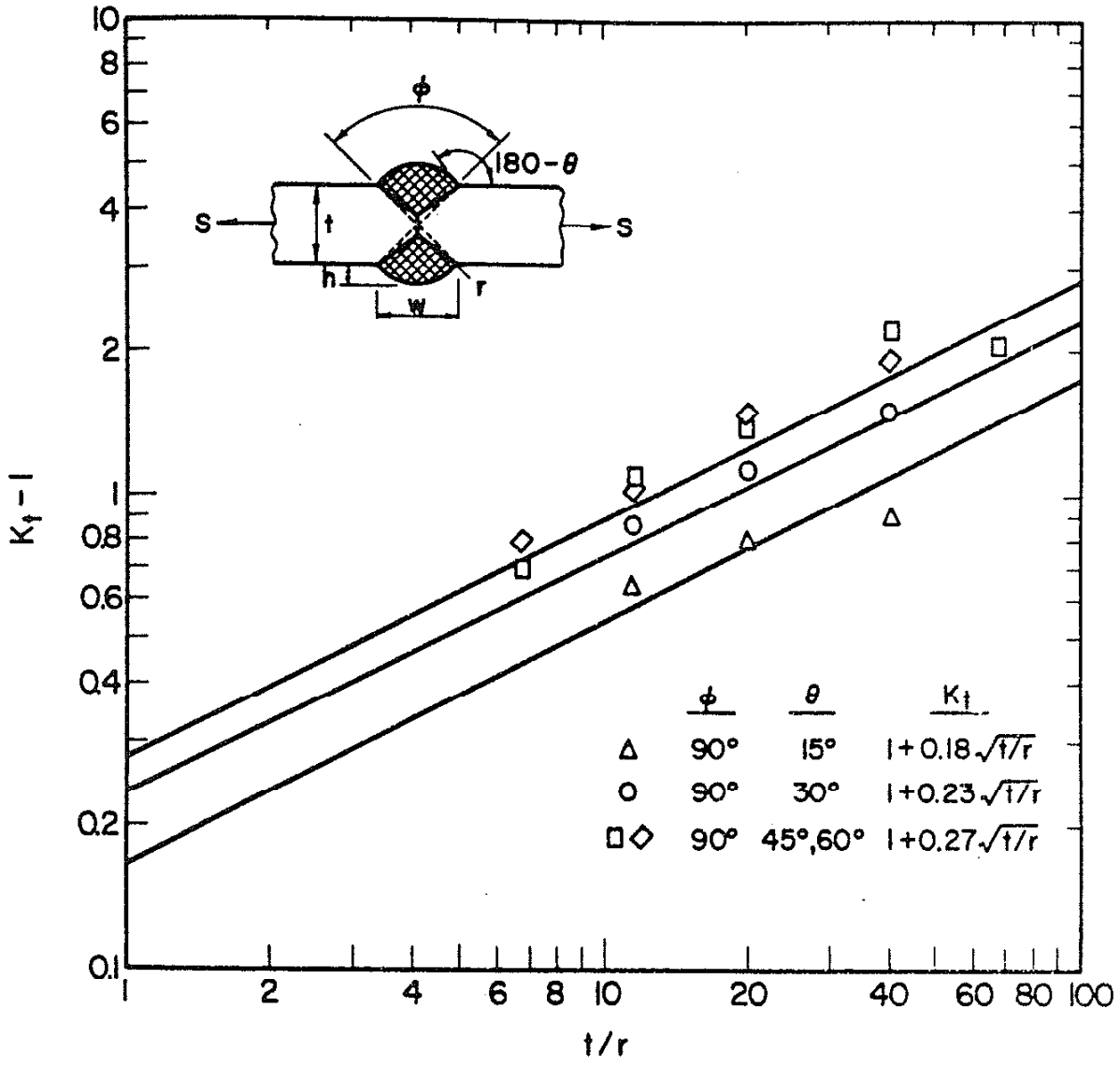

Fig. 2 Theoretical Stress Concentration Factor (K_t) as a Function of Weld Toe Root Radius and Butt Weld Geometry (ϕ = 90°, θ = 15°, 30°, 45°, 60°).

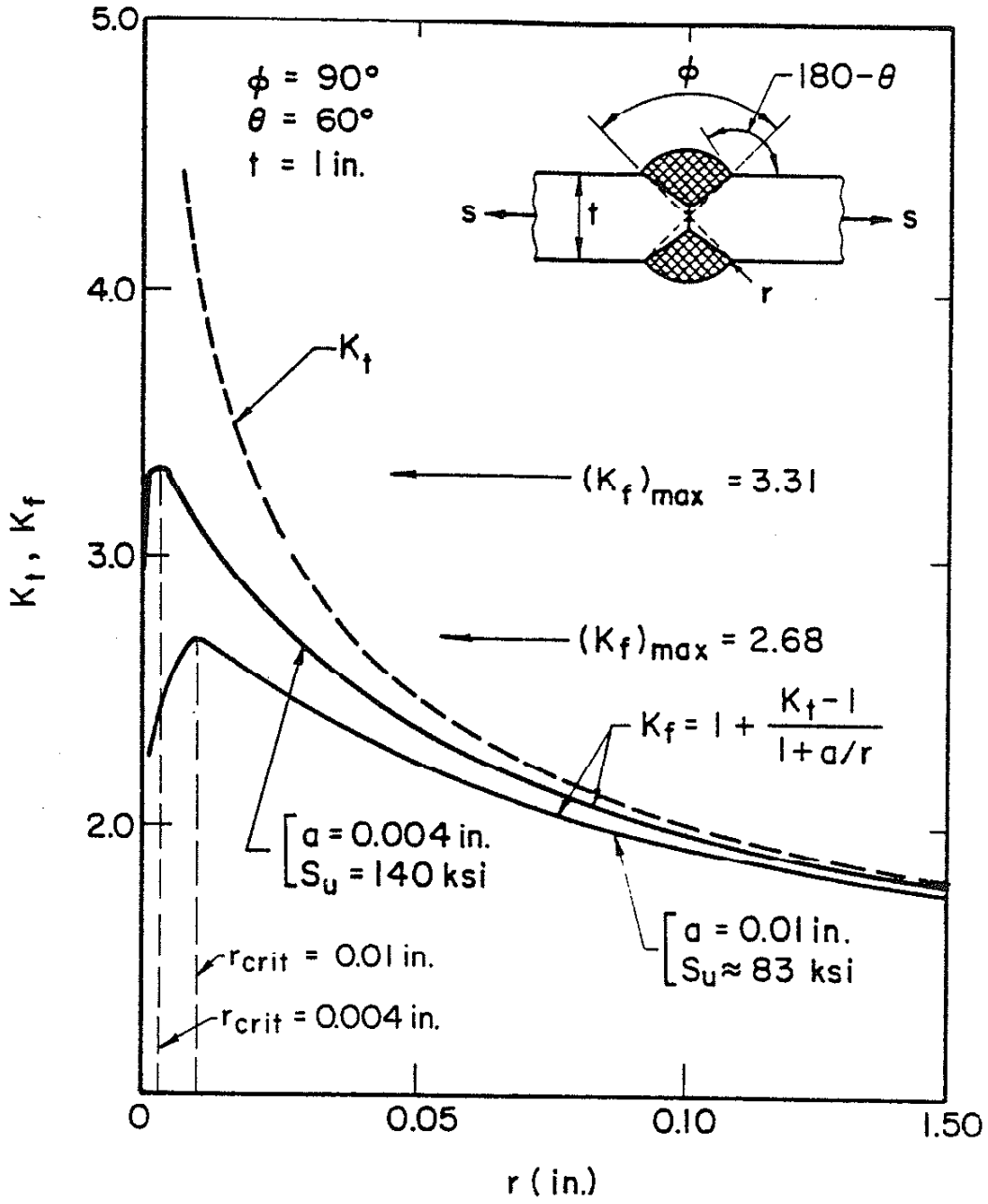

Fig. 3 Maximum Fatigue Notch Factor (K_f, max) and Its Variations With Strength Level (Su) and Consequent Changes in the Material Parameter a. K_f,max Occurs at r = a.

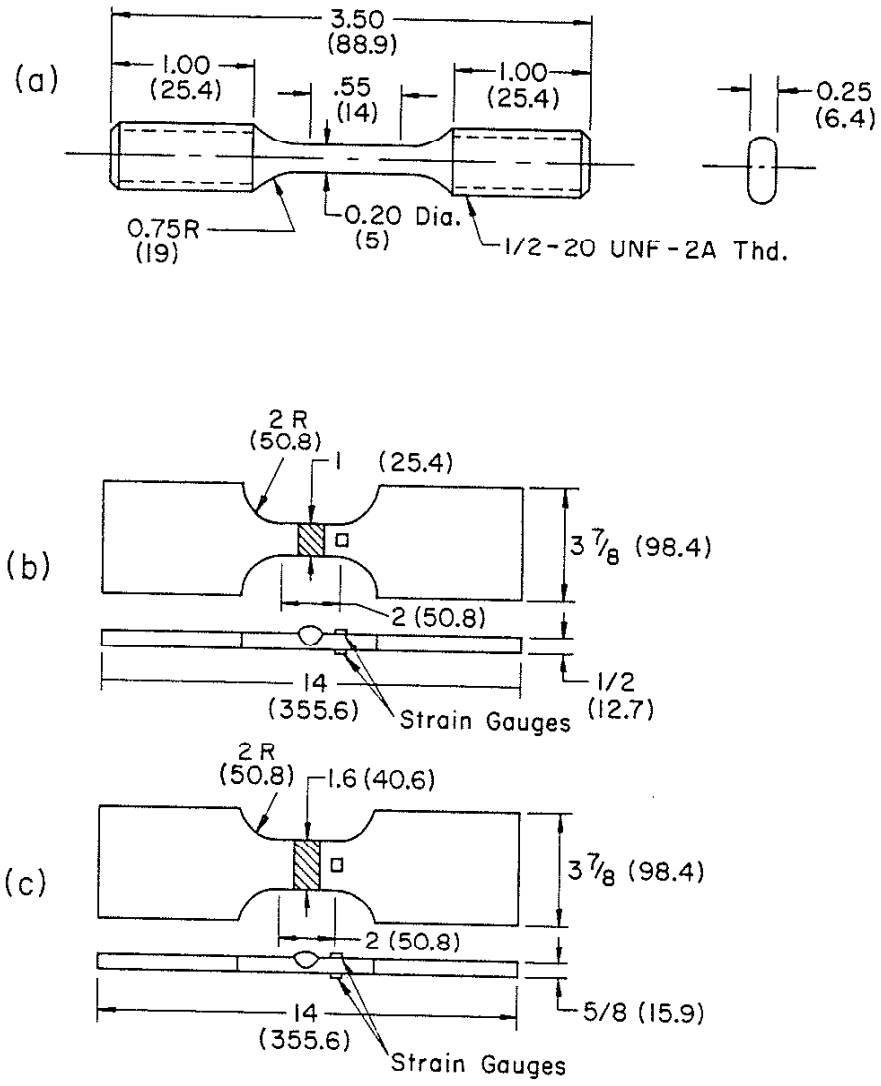

Fig. 4 (A) Cross-Rolled Smooth Specimen of A36 Simulating Shot-Peening.
(B) Specimen of As-Welded and Post-Treated A514/E110 Bead on Plate.
(C) Specimen of As-Welded and Post-Treated A36/E60S Bead on Plate.
(All Dimensions Are Inches (mm)).

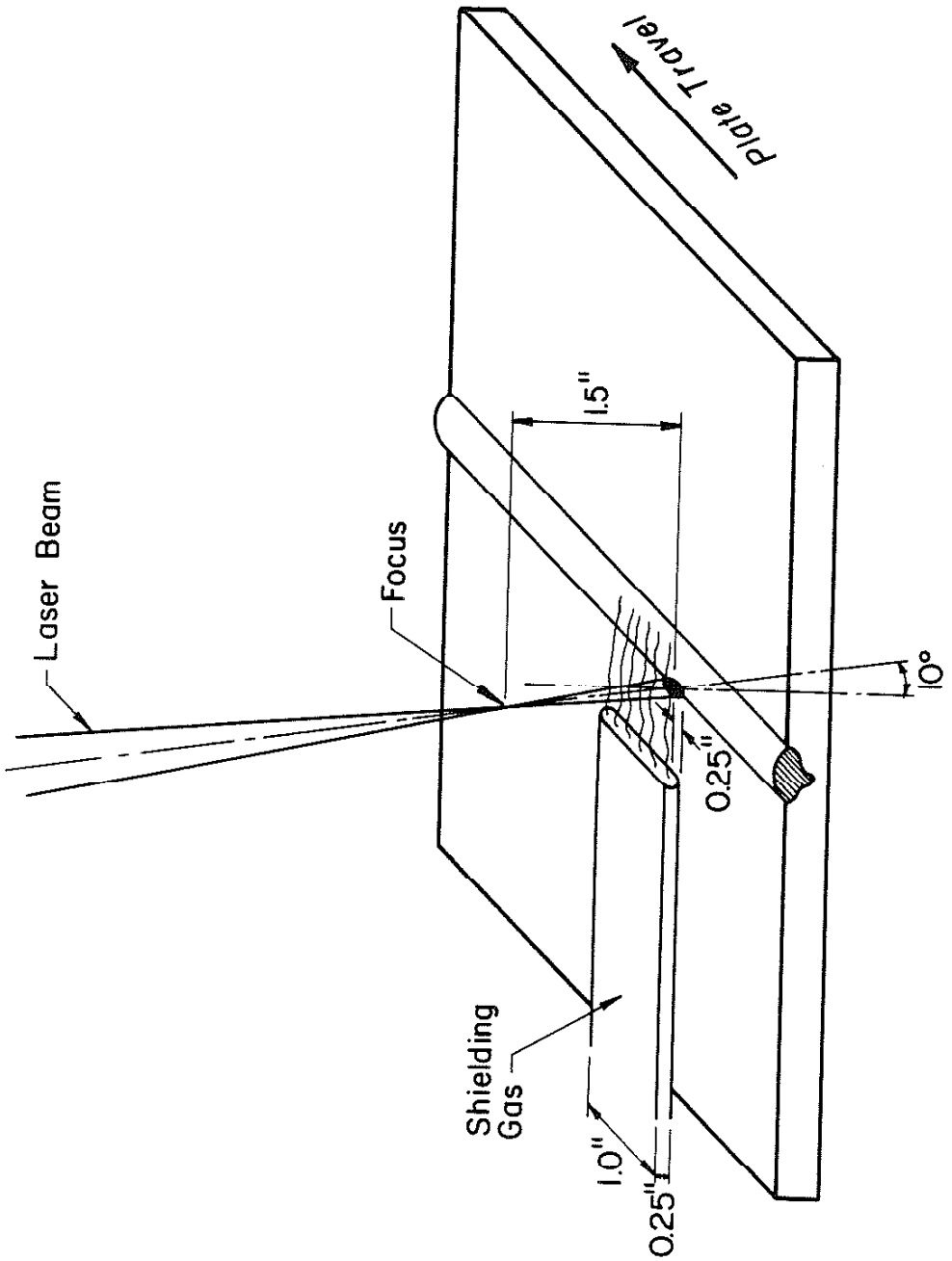

Fig. 5 Laser-Dressing Geometry Used in This Study

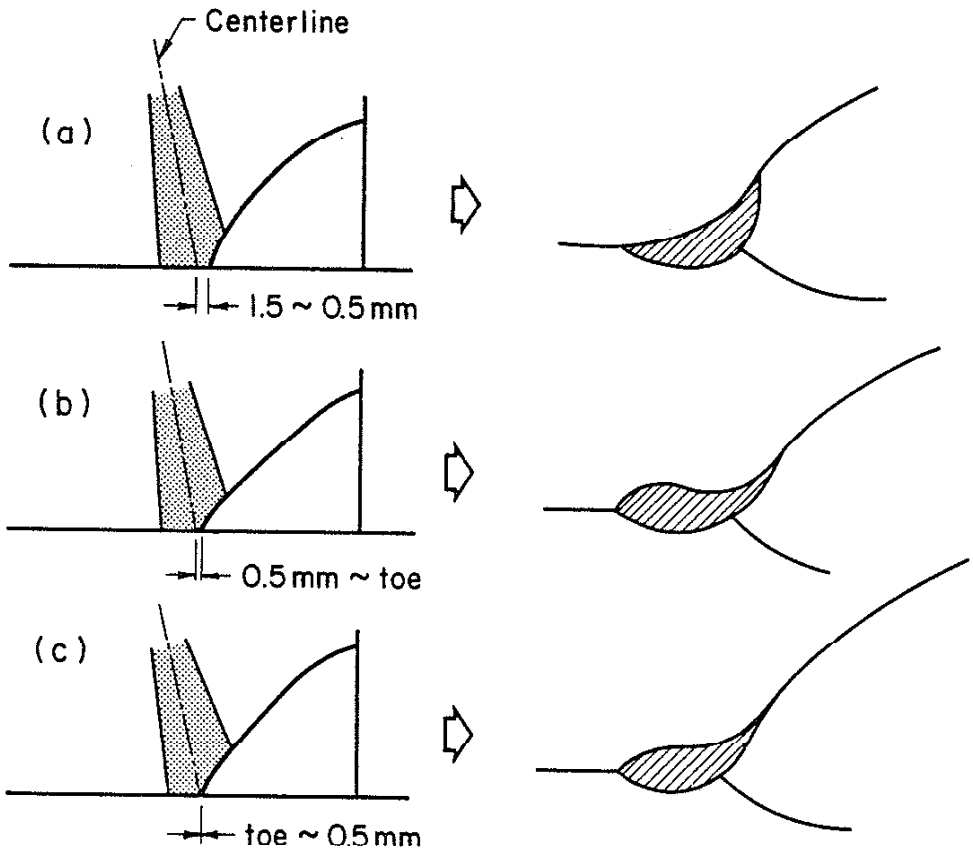

Fig. 6 Position of Laser Beam and Resultant Profiles after Kado et al. (28)

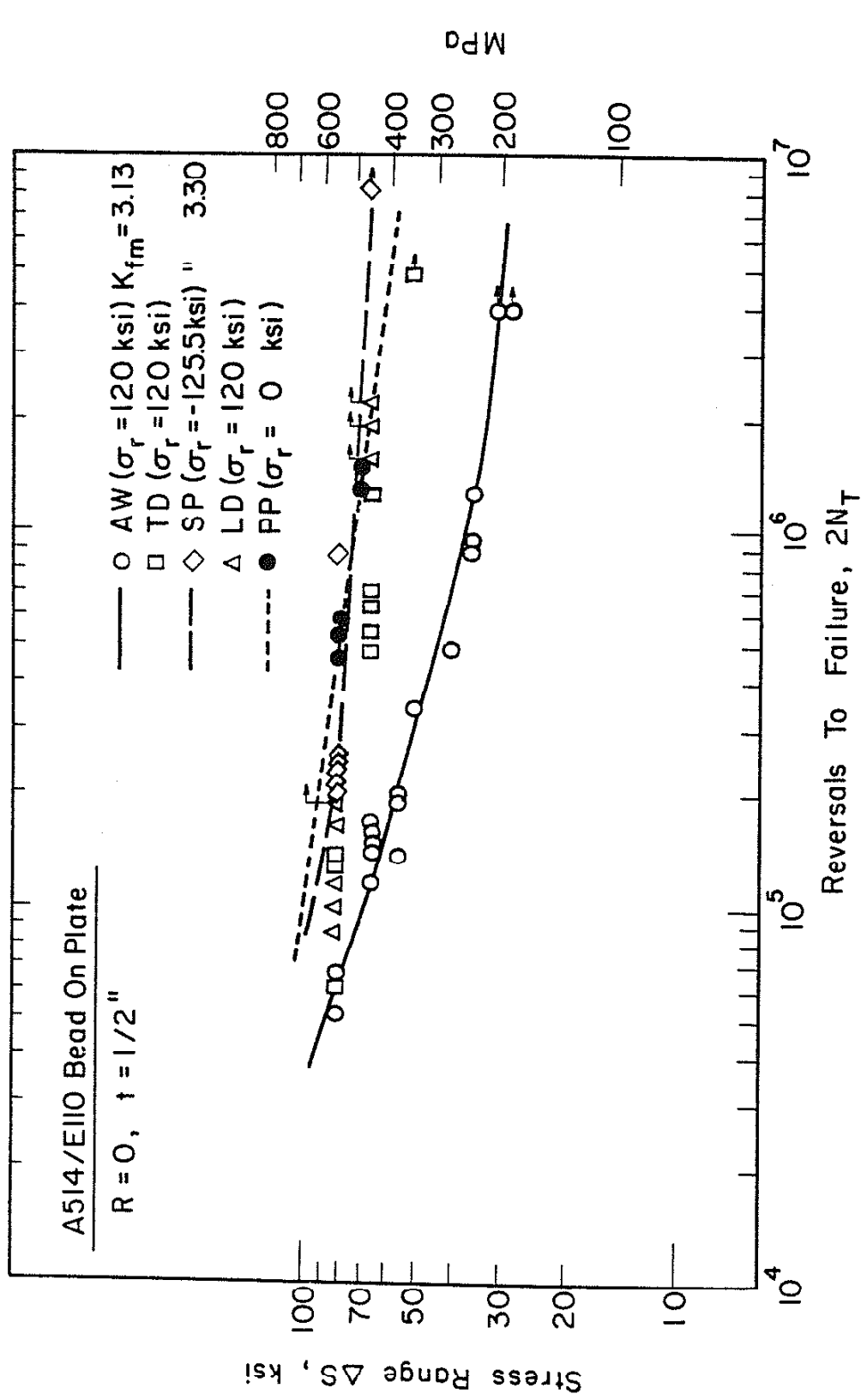

Fig. 7 Fatigue Test Results for As-Welded and Post-Treated A514/E110 Bead on Plate Specimens and Total Fatigue Life Predictions (Lines) for Plain Plate, As-Welded and Shot-Peened Specimens.

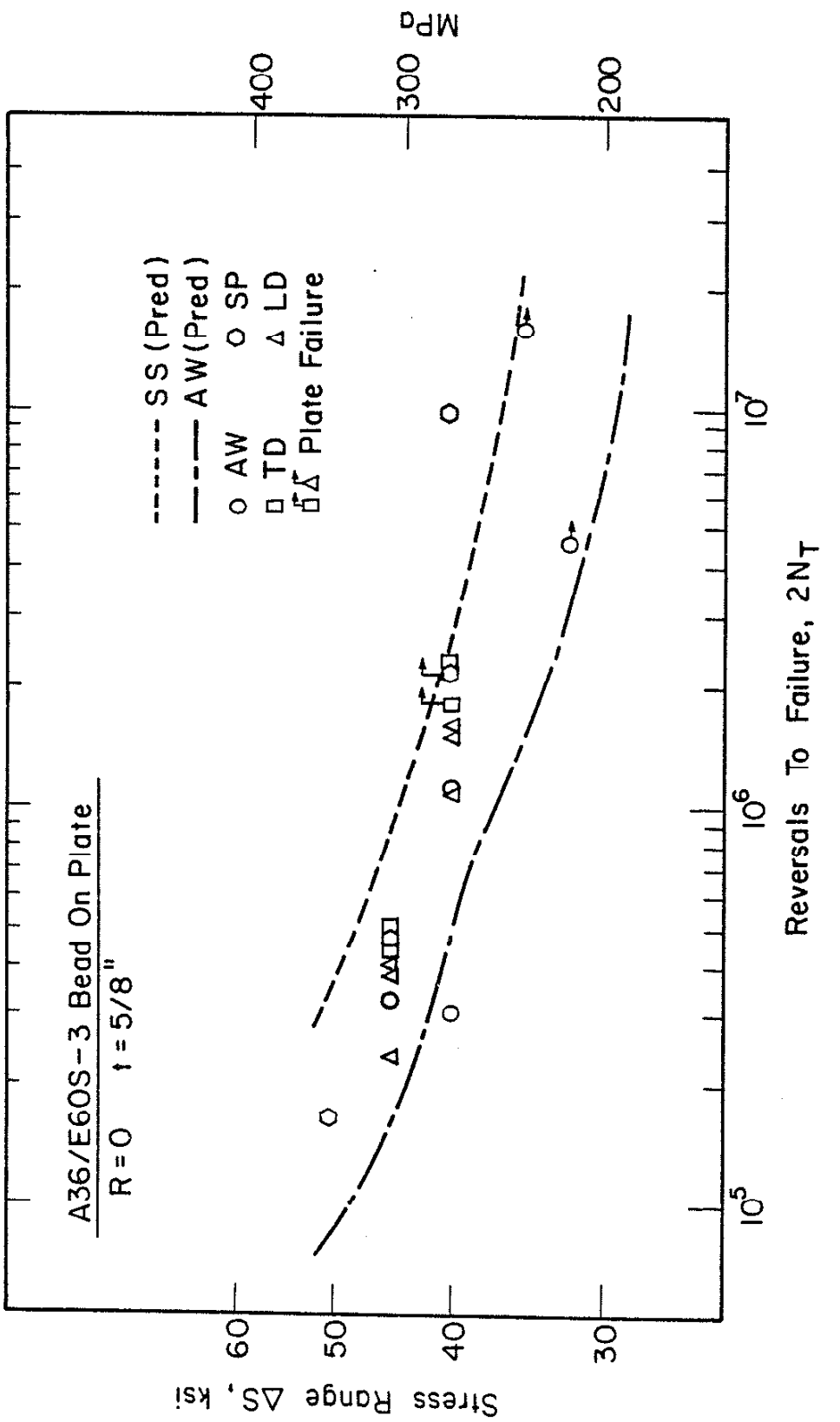

Fig. 8 Fatigue Test Results for As-Welded and Post-Treated A36/E6CS Bead on Plate Specimens and Total Fatigue Life Predictions for Smooth and As-Welded Specimens. (AW = As-Welded; SP = Shot-Peened; TD = TIG-Dressed; LD = Laser-Dressed; SS = Smooth Specimen)

(a)

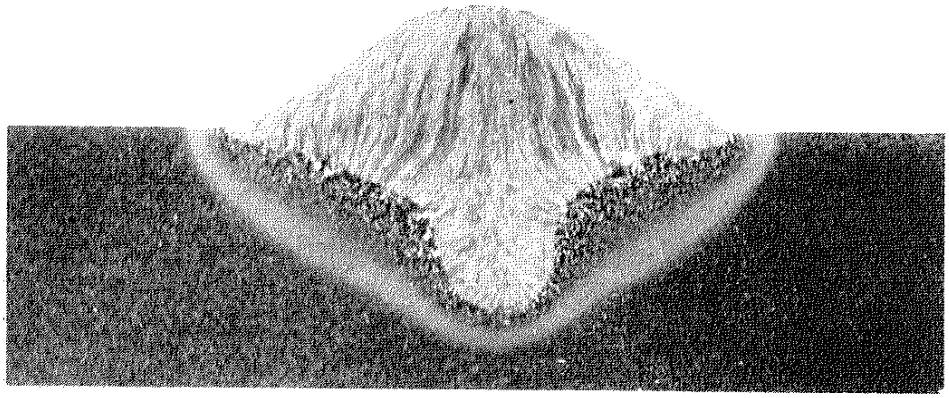

(b)

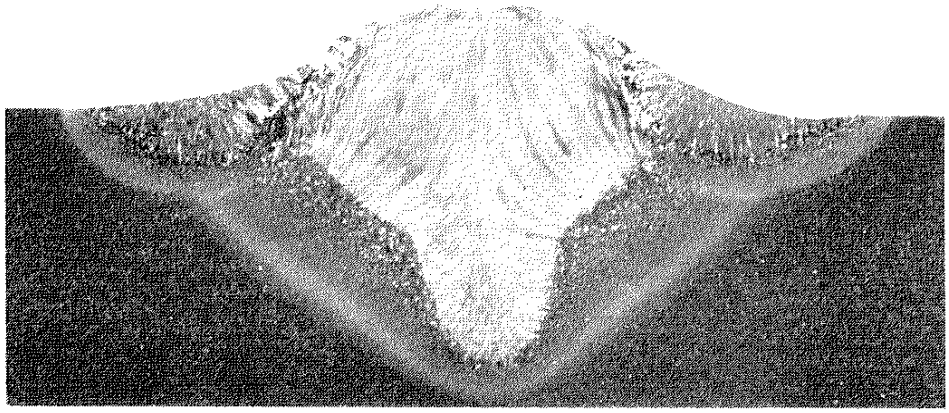

(c)

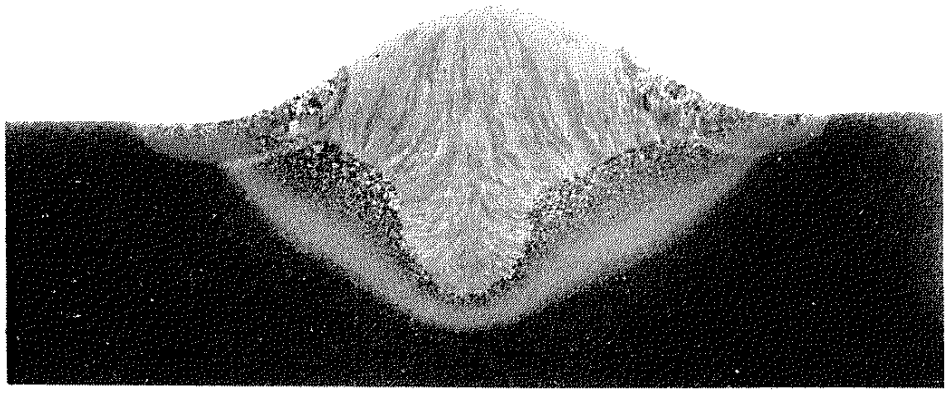

Fig. 9 Macrographs (5.8x) of Cross-Sections for (a) As-Welded and Shot-Peened; (b) TIG-Dressed; and (c) Laser-Dressed A514/E110 Weldments.

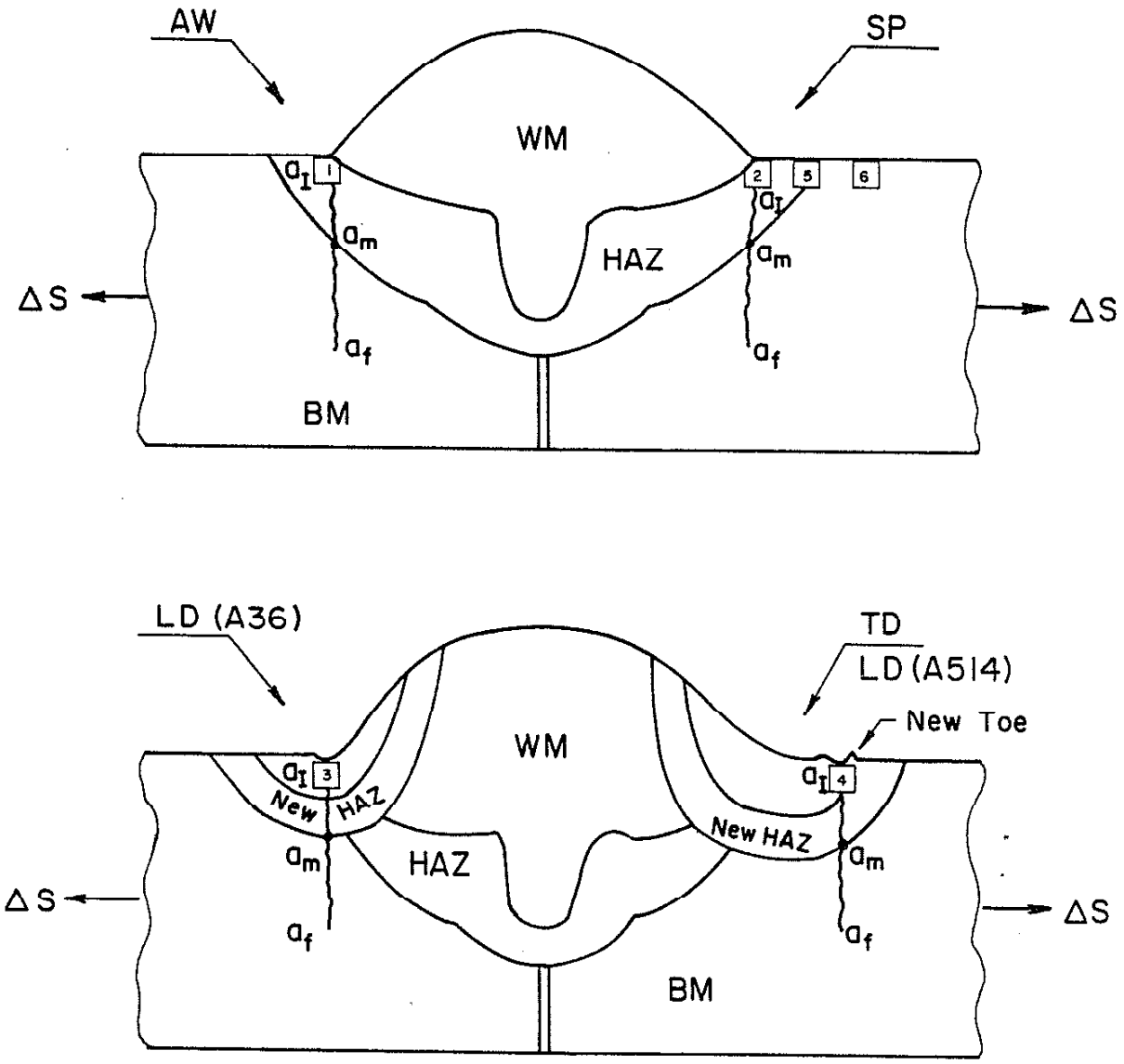

Fig. 10 Schematic Diagram of Cross-Sections of As-Welded and Post-Treated Weldments for Both A36 and A514 Steels. (AW = As-Welded; SP = Shot-Peened; LD = Laser-Dressed; TD = TIG-Dressed) Fatigue Crack Paths are Indicated.

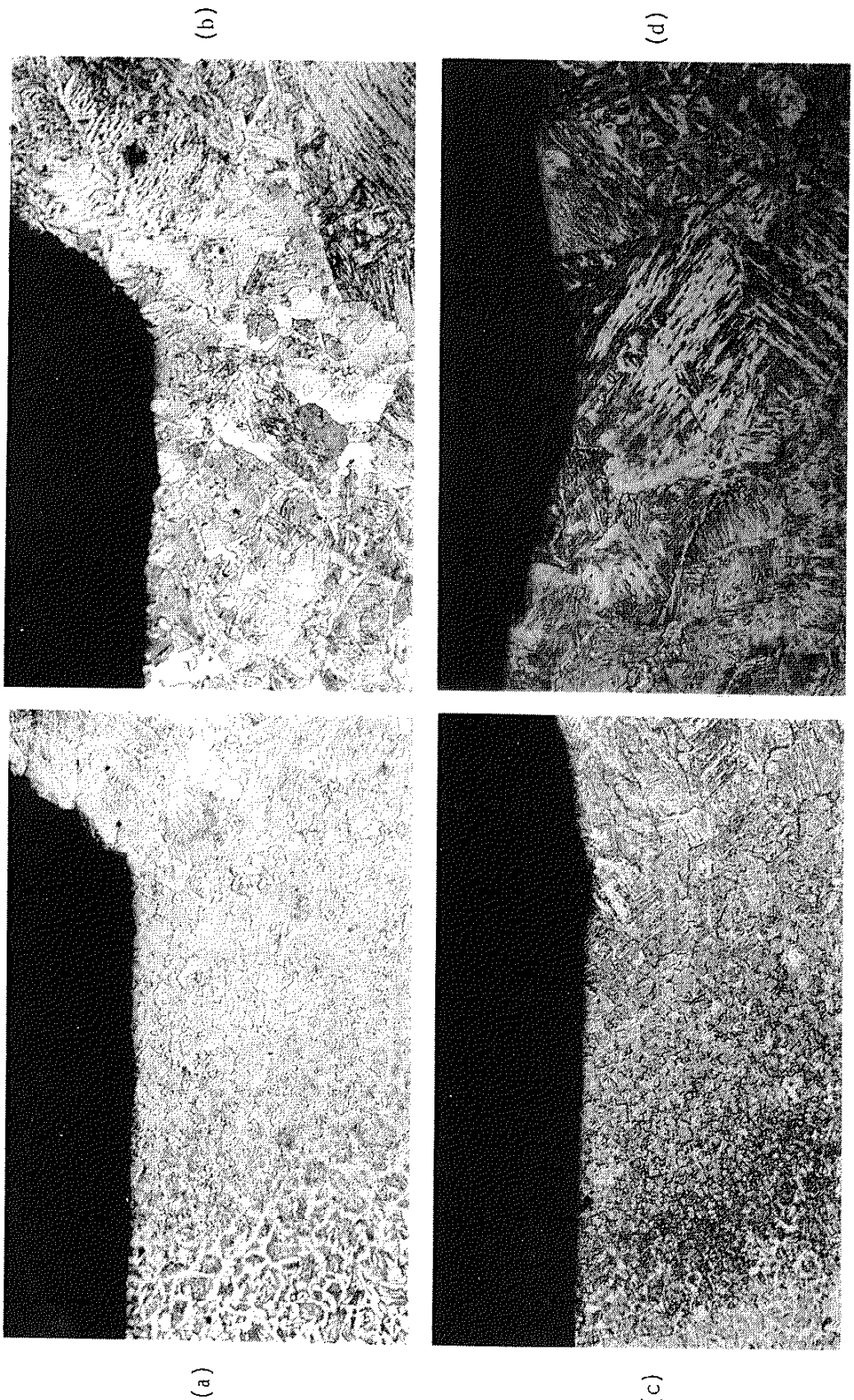

Fig. 11 Microstructures of A36/E60S Bead on Plate; (a) As-Welded HAZ (70x) Showing Toe Located at Grain-Coarsened HAZ Adjacent to the Fusion Line; (b) Enlarged View (300x) at Toe of (a); (c) TIG-Dressed New HAZ (70x) Showing New Toe with Undercut at Grain-Coarsened HAZ Adjacent to the New Fusion Line; (d) Enlarged View (300x) of the New Toe with Undercut of (c): Widmanstätten Structure Gererated at Tip of Undercut.

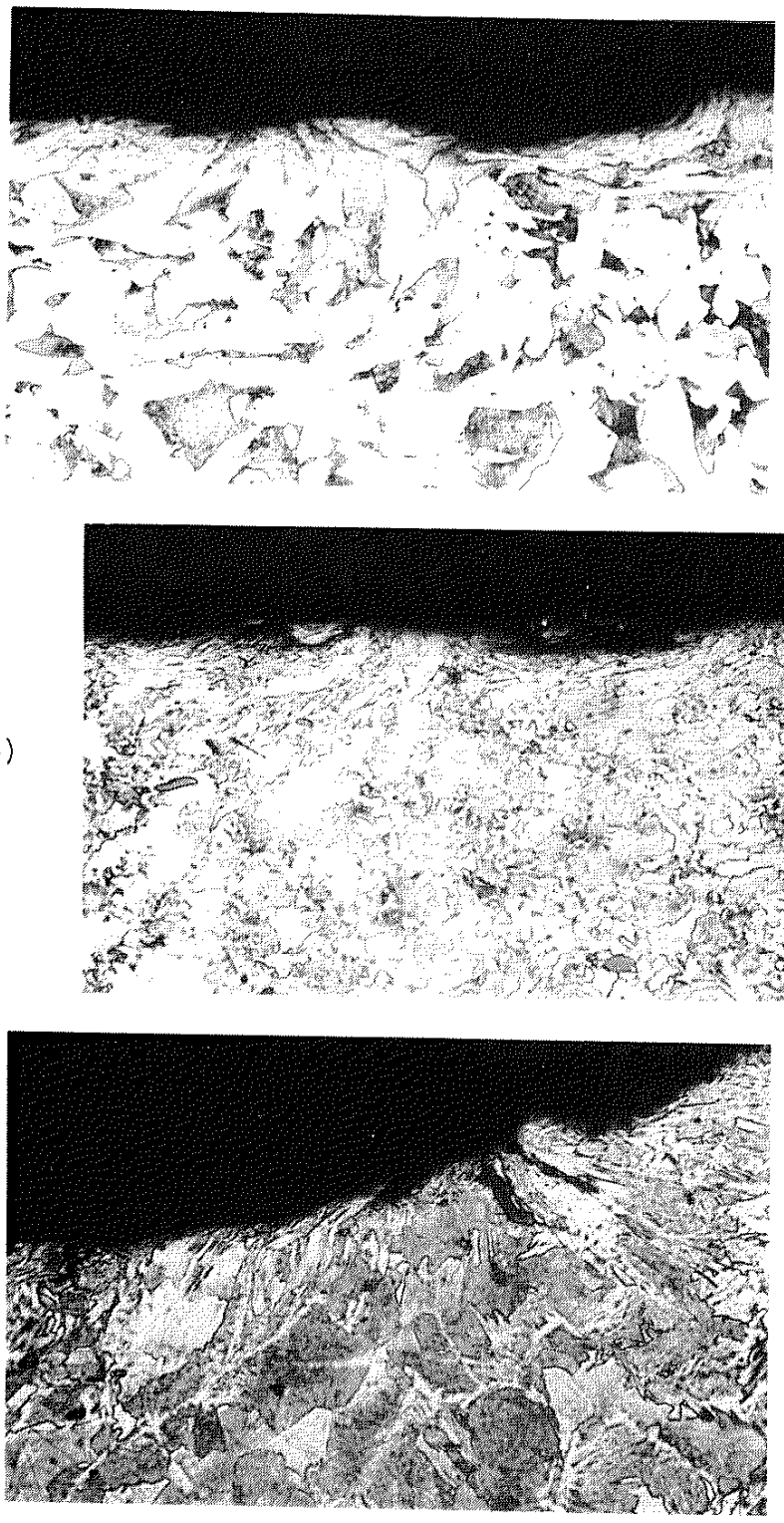

(a)

(b)

(c)

Fig. 12 Micrographs (450x) of A36/E60S Showing the Effect of Shot-Peening on the Surface Layers of (a) Base Metal, (b) Subcritical HAZ, (c) Grain-Coarsened HAZ (Toe).

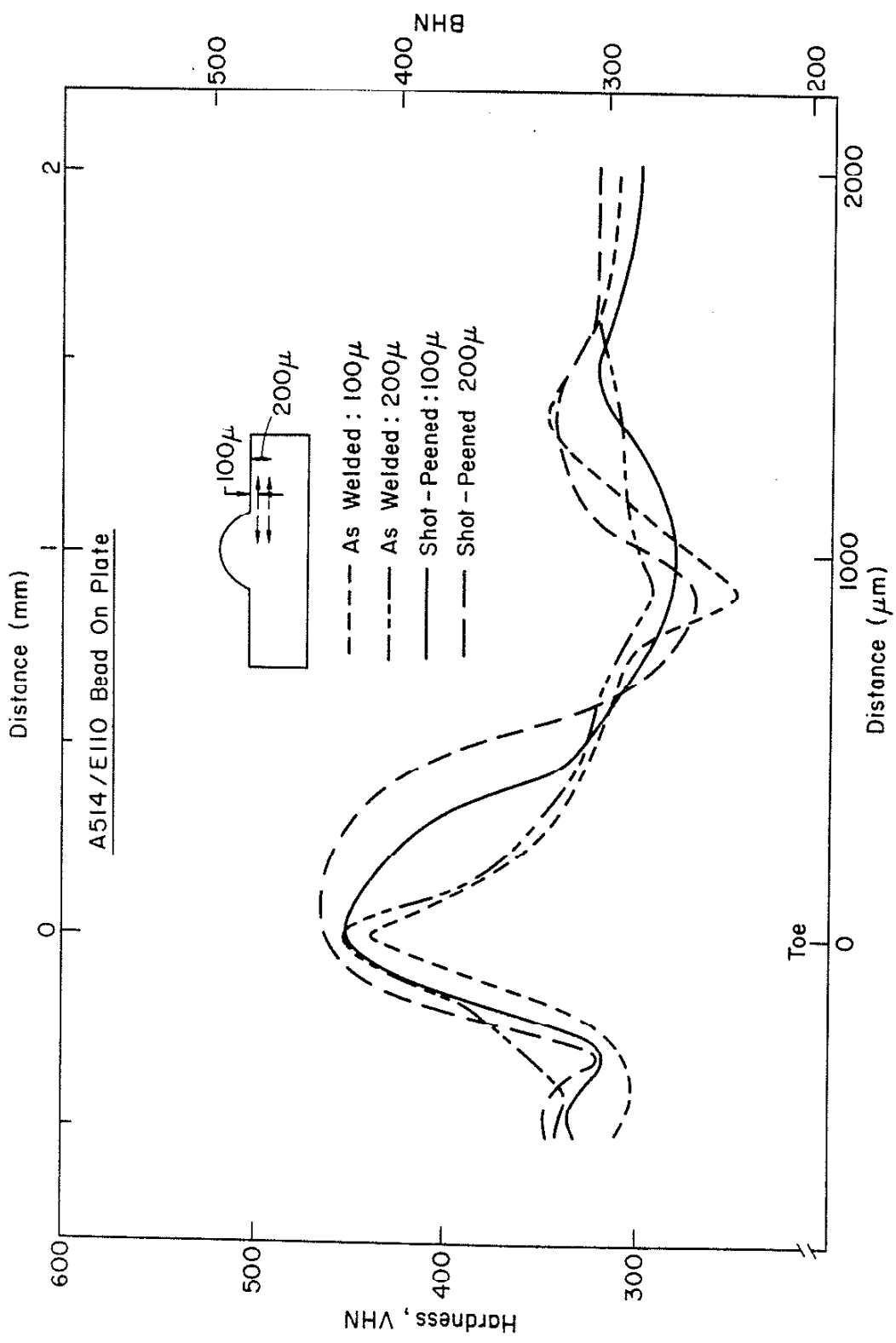

Fig. 13 Microhardness Traverse at a Depth of 100μ and 200μ below the Surface for As-Welded anc Shot-Peened A514/E110 (Positive Direction into BM).

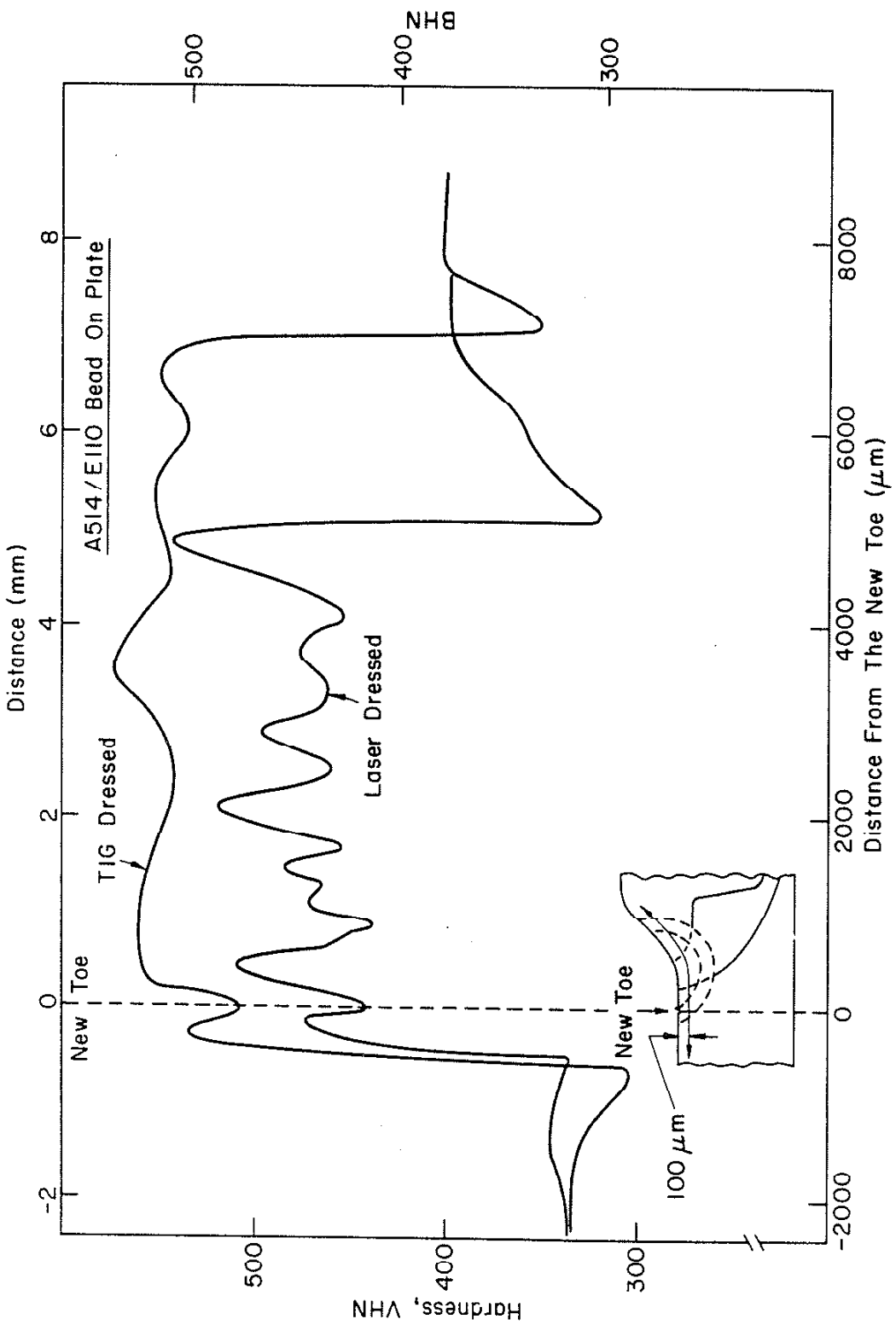

Fig. 14 Microhardness Traverse at 100μ below the Surface for TIG-Dressed and Laser-Dressed A514/E110 (Positive Direction into WM).

continuous crack ($p/q\tilde{-}0$) extending across the whole width of weldment.

The most influential factor in Eq. 17 for a weldment is M_k which is usually a function of crack length (a) for a given weld geometry. Lawrence proposed a method to determine M_k using elastic superposition and Emery's solution (65) for an open edge crack subject to any arbitrary stress system and obtained an expression for M_k for axial or bending stress (2):

$$M_k = 1.1\ a_1+0.6635\ a_2(\frac{a}{t})+0.5255\ a_3(\frac{a}{t})^2+0.4566\ a_4(\frac{a}{t})^3+0.4153\ a_5(\frac{a}{t})^4 \quad (19)$$

The coefficients a_1 through a_5 vary with loading type and weld geometry.

The effect of the notch root residual stresses on the fatigue crack propagation life is usually neglected: see Sec. 4.5.5. The effect of bending on the stress intensity factor should, however, be considered. The stress intensity factor for combined axial (ΔK_A) and bending (ΔK_B) loads can be obtained by superposing both the ΔK_A and ΔK_B:

$$\Delta K = \Delta K_A + \Delta K_B \quad (20)$$

By combining Eqs. 16, 17, 19, and 20:

$$\Delta K = \frac{M_s M_t(\Delta S_A\ M_K^A + \Delta S_B\ M_K^B)}{\phi_o}(\pi a)^{1/2} \quad (21)$$

where M_K^A and M_K^B are M_k for axial and bending loads, respectively.

The mean stress effect on crack propagation rate can be accounted for using the crack opening concept. The crack opening stress concept results in a new stress intensity factor, the effective stress intensity factor (K_{eff}) (67-70) and a new coefficient Co:

$$\frac{da}{dN} = C_o(\Delta K_{eff})^m \tag{22}$$

where $\Delta K_{eff} = K_{max} - K_{open}$ $(K_{open} > K_{min})$ or

$$\Delta K_{eff} = K_{max} - K_{min} \quad (K_{min} > K_{open}) \tag{23}$$

Since crack opening factor (C_f) is defined as $C_f = \Delta K_{eff}/\Delta K$, the following relationship can be derived for C_o:

$$C_o = C/C_f^m(R=0) \qquad \text{for } R = 0 \tag{24}$$

and

$$C_o = C[C_f(R)/C_f(R=0)]^m \qquad \text{for } R \neq 0 \tag{25}$$

The crack opening factors (C_f) for several materials are given as function of stress ratio as result of FEM in Ref. 49.

III. EXPERIMENTAL PROGRAM AND RESULTS

3.1 Materials

ASTM-A514 grade F and ASTM-A36 structural steels were selected for this investigation. The welding electrodes, Murex Hylox 110 (ASTM E110) and Linde 82 (ASTM E60S-3) were used for A514 welds and A36 welds, respectively. The chemical composition of both the base and filler metals are given in Table 1. The monotonic, cyclic and fatigue properties of the base metals and the simulated heat-affected-zones (HAZs) are given in Tables 2-5.

3.2 Specimen Fabrication

The A514 steel plates were ground and the A36 steel plates were machined to remove mill scale, and thus to avoid fatigue failure at the surface irregularities of the as-received plain plate. Bead-on-plate weldments were fabricated by depositing a weld bead on one side of a steel plate using a semi-automatic GMA welding apparatus the process parameters of which are given in Table 6. The machined A36 plates were restrained by confining them with clamps to limit distortion during welding. Any post-weld treatment was performed without restraint prior to saw-cutting. Test pieces were saw-cut in strips from the welded and post-welded treated plates and machined to the dimensions shown in Fig. 4.

3.3 Post-Weld Treatments

3.3.1 TIG-Dressing

Several of the A514 and A36 as-welded plate weldments were TIG (or GTA)

dressed by remelting the weld toe to produce a more generous weld toe radius using a semi-automatic, TIG (GTA) welding torch and argon shielding gas. The TIG dressing parameters are listed in Table 6.

3.3.2 Laser-Dressing

Several of the as-welded plate weldments were laser dressed at their weld toes using an AVCO-Everett high-power CO_2 Laser with argon shielding gas. This laser produces a beam of 10.2 μm continuous radiation at powers up to 10 kw. The process parameters (Table 7) and experimental gemoetries (Fig. 5 and 6) to obtain desirable toe configuration were established after a series of preliminary tests for the particular geometries and materials used in this investigation: see Appendix A. The surfaces of the weld toes were coated with Krylon, ultra-flat black paint to maximize the absorption of energy. A fixed laser beam defocused with a f_7 focusing mirror to an annular circle of 0.25 inches diameter was used to obtain a proper irradiated area and to avoid any possible damage caused by refocusing of the beam through back reflection. The beam impingement angle was 10° from the plate normal. The plates were moved horizontally beneath the beam at a constant speed. Argon shielding gas was directed along the weld toe at 4 $ft.^3$/min. through an oblong (1" x 1/4") nozzle positioned to give maximum coverage to the molten and cooling regions during the treatment: see Fig. 5.

3.3.3 Shot-Peening

Shot-peening was performed by the Metal Improvement Co. (MIC). The weld toe region was bombarded with round steel shot under controlled conditions to produce a surface layer with compressive stresses. All the process parameters used for the materials under investigation are listed in Table 8, and the Almen intensity variations with shot size and other parameters are listed in Table 9. The uniformity and full coverage of shot-peening was insured by

Peenscan, an MIC process which utilizes a fluorescent die and ultra-violet light.

3.4 Fatigue Testing and Results

Two Micro-Measurements strain gauges (0.25", 120 ohm) were attached to both sides of each specimen using M-bond 200 adhesive (cyanoacrylate) to monitor bending stresses. A proper distance (one-third of the plate thickness) from the weld toe (or new toe) to the strain gauges (53,74) was maintained so that the monitored strains would be independent of the weld toe stress concentration and would approximate the nominal surface strain. Specimens were fatigue-tested in a 100 kip. MTS machine with self-aligning grips using a sine wave form, load control, a zero-to-max stress cycle (R = 0) and a frequency of 5 Hz.

Two methods were employed to solve the bending stress problems which developed during nominal axial loading due to the fact that the specimens were not perfectly straight. The first method was to correct the bending before fatigue testing. The bending strain was measured under small axial loads prior to cycling, and any bending strain was eliminated by forcing the grips and specimen into alignment through minor grip adjustments. In this manner, the bending stress was reduced to less than 2% of the axial stresses for the case of A514 F weldments and 4% for A36 weldments. The second method was to fatigue-test in the conventional manner but to consider the bending stress effects quantitatively in the prediction of N_T as described in Sec. 2.2 and 4.2. This latter method was applied only to the A36 weldments. Most of as-welded A36/E60S specimens which were confined by clamps to avoid distortion during fabrications were bent during welding and had a negative bending moment induced at toe during axial loading. The TIG and laser dressing treatments

remelted and resolidified the toe region and eliminated the negative bending effect and introduced a positive bending moment at the toe. However, shot-peening did not eliminate the distortions introduced during welding; the peened specimens exhibited the greatest effects of bending moment, especially at long lives.

The fatigue test results for as-welded, shot-peened, and TIG and laser-dressed specimens are shown in Tables 10-12 and Figs. 7 and 8 for both A514 and A36 steels. Among the techniques investigated, shot-peening increased the fatigue life the most, followed closely by laser-dressing, and lastly by TIG-dressing.

3.5 Microstructural Observations

Each post-weld treatment produced characteristic changes in macro-geometry, microstructure, mechanical properties and fatigue crack initiation site. Regions of interest were examined with both optical (OM) and scanning electron microscopes (SEM). Microhardness traverses were performed at the regions with a Leitz microhardness tester.

The macrographs shown in Fig. 9 are the general appearances of the post-treated A514/E110 weldments. The general appearance of the microstructures and the associated fatigue crack paths are schematically diagrammed in Fig. 10 for each post-treated weld toe region. In each case, the heat affected zone (HAZ) is bounded by base metal (BM) on one side and by weld metal (WM) on the other and is composed of three regions: the subcritical HAZ, the grain-refined HAZ, and the grain-coarsened HAZ: see Fig. 11a.

TIG and laser dressing melted together the original WM, HAZ, and BM producing a remelted zone (dressed beads) and a new, associated HAZ (new HAZ): see Figs. 9b and 9c. The remelted regions in the laser-dressed specimens are

shallower and microstructurally much less distinct due to the lower heat input in the process and thus the more rapid cooling. Although the total amount of heat delivered by the laser beam was slightly higher than the heat input in the TIG process (see Tables 6 and 7), a lower heat input resulted from the fact that a considerable amount of beam energy was reflected even when the surface was black-coated.

Peening produced no distinct changes in the weld macro-geometries for both materials, as shown in Fig. 9a. However, the surfaces of the shot-peened A36/60S weldments showed a tremendous distortion, as is characteristic of shot-peened metal surfaces (75) and as can be seen in Figs. 12a, 12b, and 12c which are the micrographs taken from locations 6 (base metal), 5 (subcritical HAZ), and 2 (grain-coarsened HAZ) identified in Fig. 10. The depth of the surface regions distorted by shot-peening was greatest (0.02 mm) in base metal, followed closely (0.013 mm) by the subcritical HAZ, and was least (almost undiscernible (0.006 mm)) in the grain-coarsened HAZ. This finding indicates that harder materials result in a shallower depth of distortion and would explain why it was very difficult to identify any observable change on the shot-peened surfaces of A514/E110 weldments through OM. These weldments generally exhibited much higher hardnesses in the as-weld condition than did A36/E60S weldments.

The microhardness traverses for various post-treated weld toe regions studied are plotted in Figs. 13-18. In the as-welded HAZ, the grain-coarsened and grain-refined HAZs were inherently harder than any of the surrounding materials, but the subcritical HAZ had a hardness nearly the same as that of the BM: see Figs. 13 and 16. The elevation of hardness due to shot-peening was proportional to the original hardness of steels before peening: see Fig.

C-3, also Figs. 13 and 16. In fact, the hardness of the peened materials studied was invariably 1.2 times the original hardness.

As shown in Fig. 15 and 18, peening increased the hardness to a depth of 0.04 inches for the A514/E110 and 0.02 inches for the A36/E60S. Just below this depth the hardness decreased sharply to a minimum value which was lower than that of the unpeened condition. This hardness distribution inward from the toe showed the same general profile as the reported distributions of residual stresses (78), suggesting that the residual stresses might be a function of hardness. After 112,900 cycles of fatigue cycling (specimen TIP3), the hardness of the peened surface decreased to a value of nearly those of the unpeened material: see Fig. 15.

Generally, the new HAZs and dressed beads of both TIG and laser processed weld toes exhibited significantly higher hardness than found in the as-welded toe regions of both materials: see Figs. 14 and 17. However, hardnesses at potential fatigue crack sites (new toe) of the TIG and laser dressed A514/E110 were nearly the same (laser) or slightly higher (TIG) than the hardness at the toe of the as-welded A514/E110: see Fig. 15. Slightly lower hardness values were observed around the new toe regions in the laser-dressed specimens of both materials (Figs. 14 and 17) which exhibited generally smaller new HAZs compared to the TIG dressed specimens. The smaller remelted zone of laser-dressed compared to that of TIG dressed specimens exhibited greater hardness fluctuations (Figs. 14 and 17) because the smaller heat-input of laser dressing gave higher cooling rates and thus less diffusion time and a less homogeneous microstructure, which in turn caused more fluctuations in hardness. Furthermore, laser dressing resulted in generally higher hardnesses in the remelted zone of the A514 materials but lower hardnesses for the A36 materials in comparison with TIG dressing, presumably because of the above

mentioned more rapid cooling and the difference in hardenability between these two classes of materials.

Hardness traverses along possible crack paths for the as-welded and post-treated weldments (Figs. 15 and 18) generally showed two different regions of hardness--the HAZ (and remelted zone) and the BM zone--which may have different fatigue crack propagation properties and thus have different fatigue crack growth rates.

3.6. Fatigue Crack Initiation Sites

Each post-weld treatment modified the notch geometry and/or location and surface conditions of the notch to a different extent. SEM micrographs of as-welded and post-weld treated toe profiles are shown in Figs. 19 and 20 for both steels.

The as-welded toe profiles in Figs. 19a and 20a clearly show the variation of toe radius along its length. The variability of the toe radius apparent in these figures supports the $K_{f,max}$ concept. The as-weld toe is located at the intercept between the fusion line and the plate surface (Fig. 9a), and fatigue cracks initiate right at the toe (Fig. 20a) and grow downward through the grain-coarsened HAZ adjacent to the fusion line: see Fig. 21a.

Shot-peening may slightly modify the local gemoetry but generally not enough to eliminate the sharp notch root radii (Fig. 21b) and invalidate the use of $K_{f,max}$. Though shot-peening cannot change the macro-geometry ("α" remains constant in Eq. 12) and the failure site (Fig. 20b), it does result in a higher $K_{f,max}$ value than that of the as-welded condition by increasing the tensile strength (S_u) in Eq. 12. Despite this increase, shot-peening tremendously increases the fatigue life. This great life increase may be partly caused by the improvement of material properties but mostly by the induced compressive

residual surface stresses. Therefore, the major factor of importance in shot-peened treatment is the magnitude of compressive residual stresses at the surface of the toe. This compressive residual stress lowers the initial surface mean stress ($\sigma_{o,i}$) to a level below which little or no damage occurs during cycling. As the cycling continues though, the initial mean stress, $\sigma_{o,i}$, begins to relax. Since the fatigue crack occurs at the weld toe, the $K_{f,max}$ concept might provide a reasonable description of the shot-peened weldments if consideration is given to the altered material properties and the residual compressive stresses and their relaxation.

Dressing treatments significantly altered the curvature of the original toe and produced a new toe at the intersection between the dressing bead and the plate surface with the associated new HAZ: see Figs. 9b and 9c. This new toe generally was undercut to some degree (see Figs. 19c, 19d, 20c, and 20d), which in fact plays an important role in the fatigue fracture of the dressed welds.

Properly executed laser-dressing with high degree of control over the location and motion of the molten pool, could produce a very straight new fusion line with very smooth, nearly imperceptible undercut along the length of new toe, as in the example for A514/E110 shown in Fig. 19d. Most of these well-dressed specimens failed at small discontinuities in the plate surface, outside the dressed region. However, if the original weldments had irregular toe geometries along their lengths, then even laser-dressed samples exhibited a considerable amount of undercut at the new toe, and fatigue cracks initiated there. Furthermore, as in the case of most of the laser-dressed A36/E60S weldments, if the original toe was very steep, even laser-dressed weldments did not have a smoothly dressed toe with a large radius. Rather, a steep radius was presented with a severe undercut around the middle of the dressed bead. Most fatigue cracks started here rather than at the new toe (at which a small

undercut existed) because of the compound stress concentration (see Fig. 20d) of this region.

The less controllable TIG arc resulted in a somewhat erratic fusion line with significant periodic undercut along the length of the new toe: see Fig. 19c. Most TIG failures initiated at this undercut: see Fig. 20c. Figure 11c shows the microstructure of a new HAZ of a TIG-dressed weldment. The new toe was located at grain-coarsened HAZ adjacent to the new fusion line, which is similar to the toe in the as-welded weldment: see Fig. 11a. The as-quenched martensites shows a Widmanstätten structure at the tip of the undercut (Fig. 11d) and resulted in a great increase in microhardness. Fig. 22a is a OM fractograph of a TIG-dressed specimen. Fig. 22b shows clearly that the fatigue crack initiated at an undercut and propagated inward.

In TIG and laser dressed weldments, most fatigue cracks initiated at the undercut produced during the dressing treatments; thus in order to apply the I-P model, a new analysis of the stress field surrounding the dressed weld toe was required which takes into consideration the degree of undercut and the altered toe geometry.

IV. MODIFICATION OF THE INITIATION-PROPAGATION MODEL FOR POST-TREATED WELDMENTS

The post-weld treatments used in this study significantly altered one or more of the major factors which influence the total fatigue life: geometry, residual stresses, and material properties. In applying the I-P model to post-treated weldments, some new concepts had to be introduced to account for the changes induced in the welds.

4.1 Neuber's Rule for Both the Generally Elastic and Plastic Cases.

Lawrence and Burk (49) modified Neuber's Rule to incorporate the effects of residual stress. Their results can only be applied to the case of elastic remote conditions. Consequently, it was necessary to further modify Neuber's Rule to deal with the more general cases, i.e. both elastic and plastic remote conditions.

The residual stress (σ_r) and residual strain (ε_r) at the weld toe may be simulated as shown in Fig. 23 for the first reversal (O-A in Fig. 24). A remote stress of σ_r/K_f and remote strain of ε_r/K_f are then applied to produce a local stress and local strain equal to the residual stress (σ_r) and residual strain (ε_r). The applied remote stress (S) and remote strain (e) are then superposed to give $S + \sigma_r/K_f$ and $e + \varepsilon_r/K_f$ which are substituted for the remote stress (S) and strain (e) in Eq. 4. If the remote stress and strain behave as shown in Figs. 24a and 24b (for example, R = 0), the local stress-strain response can be bounded as shown in Fig. 24c. The first reversal (O-A) is bounded by:

$$(K_f S_1 + \sigma_r)\ (K_f e_1 + \varepsilon_r) = \sigma_1\ \varepsilon_1 \qquad (26)$$

where $S_1 = (\Delta S/1-R)$ represents the maximum stress (S_{max}) at the first reversal for an arbitrary R:

$$\text{Since } R = \frac{S_{min}}{S_{max}} \text{ and } \Delta S = S_{max} - S_{min}, \quad S_{max} = \Delta S/1-R \tag{27}$$

The subsequent reversals (A-B-C-D) will be bounded by the following equation expressed in terms of the stress and strain ranges:

$$(K_f \cdot \Delta S)\ (K_f \cdot \Delta e) = \Delta\sigma \cdot \Delta\varepsilon \tag{28}$$

In these subsequent reversals, the remote stress-strain response can be assumed to be elastic (A-B-C-D in Fig. 24b), i.e. $\Delta e = \Delta S/E$. Therefore, subsequent reversals are bounded by:

$$(K_f \cdot \Delta S)^2/E = \Delta\sigma \cdot \Delta\varepsilon \tag{29}$$

The initial mean stress ($\sigma_{o,i}$) can be calculated using Eqs. 6, 26, and 29:

$$\sigma_{o,i} = \sigma_1 - \Delta\sigma/2 \tag{30}$$

For residual stresses less than the yield point: $\sigma_r = E \cdot \varepsilon_r$.
If the first reversal (O-A) of the remote stress strain behavior is elastic, $e_1 = S_1/E$ and Eq. 26 becomes:

$$(K_f \cdot S_1 + \sigma_r)^2/E = \sigma_1 \cdot \varepsilon_1 \tag{31}$$

Equation 31 is the same equation as derived by Lawrence and Burk (49).

4.2 Neuber's Rule for Combined Axial and Bending Stresses

Using finite element analyses Lawrence and Ho (53) showed that the stress concentration factor of a weld toe for pure bending (K_t^B) has a form similar to that for axial loading (K_t^A):

$$K_t^B = 1 + \alpha_B (t/r)^{1/2} \tag{32}$$

where: α_B is geometry coefficient for pure bending which is generally smaller than α_A which is geometry coefficient for pure axial loading. It is assumed that the fatigue notch factor for bending loads (K_f^B) may be estimated using Peterson's formula. Therefore, $K_{f,max}^B$ occurs when r = a where the maximum fatigue notch factor for axial loading ($K_{f,max}^A$) occurs.

Bending stresses can be treated (like residual stresses) as mechanical prestresses, and thus can be superposed on the axial stresses. The first reversal Neuber parameter for an arbitrary R is:

$$\sigma_1 \quad \varepsilon_1 = (K_{f,m}^A \quad S_{max}^A + \sigma_r + K_{f,m}^B \quad S_{max}^B)\ (K_{f,m}^A \quad e_{max}^A + \varepsilon_r + K_{f,m}^B \quad e_{max}^B) \tag{33}$$

And similarly, the second reversal Neuber parameter (Eq. 28) will be:

$$\Delta\sigma \quad \Delta\varepsilon = (K_{f,m}^A \quad \Delta S^A + K_{f,m}^B \quad \Delta S^B)(K_{f,m}^A \quad \Delta e^A + K_{f,m}^B \quad \Delta e^B) \tag{34}$$

If the remote axial and bending stresses are within the elastic range, Eqs. 33 and 34 become:

$$\sigma_1 \quad \varepsilon_1 + (K^A_{f,m} \quad S^A_{max} + \sigma_r + K^B_{f,m} \quad S^B_{max})^2/E \tag{35}$$

and

$$\Delta\sigma \quad \Delta\varepsilon = (K^A_{f,m} \quad \Delta S^A + K^B_{f,m} \quad \Delta S^B)^2/E \tag{36}$$

The local stress and strain range and the initial mean stress can be determined using Eqs. 6 and 30.

4.3 Determination of a_I, a_m, a_f and Partitioning of the Crack Path

During fatigue crack growth in a weld, the crack usually passes through different material regions (HAZ and BM). Therefore, these different regions should be considered separately, and the corresponding material constants for crack propagation for each region should be used to obtain more accurate estimates of N_p. Thus, in addition to a_I and a_f, a_m (see Fig. 10) should be deterimined from the fracture surfaces. Then Eq. 15 can be partitioned into:

$$N_p = \int_{a_I}^{a_m} f(HAZ)\, da + \int_{a_m}^{a_f} f(BM)\, da \tag{37}$$

where: f(HAZ) is $\frac{1}{C}(\Delta K)^{-m}$ for HAZ material and
f(BM) is $\frac{1}{C}(\Delta K)^{-m}$ for base metal.

A number of theories have been proposed to estimate the crack initiation size (a_I) which has a strong influence on N_p, but none of them has been widely accepted. In this investigation, a_I was estimated using the strategy proposed recently by Chen (76):

$$q = \frac{K_{f,max}^{-1}}{K_t - 1} = \exp\,(-35\,\alpha(t/a)^{1/2} a_I/t) = 1/2 \tag{38}$$

Thus, $$a_I = 0.18788\ t^{1/2}/(\alpha\ S_u) \tag{39}$$

The final crack size (a_f) was approximated using the fracture toughness concept:

$$a_f = 1/\pi\ \left(\frac{K_c}{Y\ \Delta S}\right)^2 \tag{40}$$

N_p is not very sensitive to a_f.

4.4 Modification of the $K_{f,max}$ Concept for Plain Plate

The I-P model was applied to the fatigue behavior of plain plate using the concept of the "equivalent elliptical surface notch" of a semi-infinite plate and the $K_{f,max}$ concept. As-rolled plain plates usually contain unavoidable manufacturing notches which are considerably more severe than the normal surface roughness on their surface, and fatigue cracks can be expected to initiate there. The K_t for an "equivalent elliptical surface notch" (77) is:

$$K_t = 1 + 2(d/r)^{\frac{1}{2}} \tag{41}$$

where, "r" is the notch root radius and "d" is average depth of the most severe surface notches. Thus, $K_{f,max}$ can occur at r = $\underline{a}$, i.e.,

$$K_{f,max} = 1 + (d/\underline{a})^{\frac{1}{2}} \tag{42}$$

The depth "d" can be measured using a profilometer or by taking magnified photos of polished sections. The surface roughness profiles for plain plate

(as-received), shot-peened surfaces, and smooth (machined) surface of A36 base metal were measured using a profilometer and one of the most severe profiles for each case is shown in Fig. 25. A depth from graphical centerline[1] to a valley would be a reasonable value for "d". Unfortunately, all the severe manufacturing notches could not be included in the scan. Thus, it was not possible to determine the exact graphical centerline. The middle point of the height from the peak to the valley of the most severe roughness profile detected was taken as the graphical centerline, and the depth from that line to the valley was defined as an effective depth, d_{eff}, i.e. d_{eff} = 1/2 D as shown in Fig. 25.

A comparison between the predictions for plain plate and actual data is shown in Fig. 26, and it can be seen that the agreement was very good. This application gives further evidence of the validity of I-P model and provides a bench mark for the improvement of weldment fatigue life through post-weld treatments since the fatigue life of a weldment cannot exceed that of the plain plate which it joins.

4.5 Application of the I-P Model to Shot-Peened Weldments

The most difficult problem in the prediction of N_I for shot-peened weldments was to determine the tensile and fatigue properties of the material in the shot-peened surface region. It is impossible to obtain smooth specimens of sufficient size for direct testing of the material because of its shallow depth (~ 0.02 inches).

---

[1]The graphical centerline is the line about which roughness is measured and is a line parallel to the general direction of the profile such that the sums of the areas of the profile which lie on either side of it are equal.

4.5.1 Determination of Fatigue Properties

Micro-hardness traverses showed that the hardness varied significantly even within a microscopically small region and that the hardness at locations of interest was altered by shot-peening: see Figs. 13, 15, 16, and 18. Since crack initiation takes place very near the surface, the material at the depth (a_I) will respond to the local stresses and determine the crack initiation life of the structure. Therefore, the material properties determined from hardness[1] measured at the depth of crack initiation (a_I) were used in the prediction of N_I. Empirical functions of hardness due to Landgraf (1) were generally used to estimate the fatigue properties of the regions of interest (Fig. 27).

$$S_u = 1/2 \text{ BHN} \quad \text{(ksi)} \tag{43}$$

$$\sigma_f' = \sigma_f \text{ (corrected for necking)}$$

$$= S_u + 50 = 0.5 \text{ BHN} + 50 \quad \text{(ksi)} \tag{44}$$

$$b = -\frac{1}{6} \log (2 \sigma_f'/S_u) = -\frac{1}{6} \log \left[2 + \frac{200}{\text{BHN}}\right] \tag{45}$$

Young's modulus (E) was assumed to be unaffected by the post-weld treatments.

4.5.2 Residual Stresses (σ_p)

A relationship for the maximum compressive residual stresses of high strength steels as a function of tensile strength or hardness before peening was obtained from experimental data in the literature (78) (Fig. 28):

---

[1]This hardness measured within the possible depth of a crack initiation was also used to estimate the "a" value in the Peterson's formula (Eq. 10).

$$\sigma_r = -(0.21\ S_u + 80) = -(0.1\ BHN + 80) \qquad \text{(ksi)} \qquad (46)$$

The depth of the compressive stress layer as a function of Almen intensity is shown in Fig. 29. Experimental data on the magnitude of residual stresses for shot-peened mild steels were not available. However, as a rule of thumb, σ_r for peened mild steels is usually assumed to be the negative value of 50-60% of the tensile strength before peening (79):

$$\sigma_r = -(0.5 \sim 0.6)\quad S_u \qquad (47)$$

This assumption was confirmed by measurement[1] of the residual stresses of shot-peened A36/E60S bead-on-plate weldments. The longitudinal (axial) residual stresses were measured at both the toes and at the top of the welds using an X-ray residual stress apparatus. The irradiated spot was 0.1 inches longitudinal and 0.5 inches transverse with an X-ray penetration depth of less than 0.001 inches. The results are given in Table 13. The measured residual stresses at the toe agreed very well with the estimated values based on S_u of the HAZ and WM before peening using Eq. 47. The weld metal showed slightly smaller absolute values of residual stresses than the toe (HAZ). Further investigation showed that in the longitudinal direction, no difference was observed between the residual stresses measured at the edge and mid-points along the length of the toe.

[1]Measurement was done at the Caterpillar Technical Center, Peoria, Illinois by Mr. W.P. Evans, staff engineer.

4.5.3 Initial Mean Stress

In order to determine the initial mean stress ($\sigma_{o,i}$), the monotonic and cyclic properties of the notch root material must be known. As previously discussed, it is nearly impossible to determine the properties of that shallow region altered by shot-peening. A model was developed to calculate the initial mean stress ($\sigma_{o,i}$) of a shot-peened weld toe without knowledge of the plastic behavior (i.e., K, n, K', n') for the material in the region of interest. Generally, the residual stress should not exceed the yield strength of the surrounding material; therefore, the maximum compressive residual stress of shot-peened HAZ (σ_{ys}(HAZ)) is within the elastic range (point P, in Fig. 30). If the local stress range $\Delta\sigma$ (which is equal to $K_f \cdot \Delta S$) does not exceed a certain range (Δ in Fig. 30), the upper limit (Q) will be below the stabilized cyclic yield strength of HAZ material (σ'_{ys}(HAZ)), and thus it will be within the elastic range, too. Therefore, the local stress range ($\Delta\sigma$), strain range ($\Delta\varepsilon$), and the initial mean stress ($\sigma_{o,i}$) can be easily determined without knowing the σ-ε behavior (K, K', n, n') for shot-peened materials if the base metals' Young's modulus (E) is known. The relaxation exponents (k) of shot-peened HAZ material were assumed to be the same as those of unpeened HAZ material for A514/E110 weldments.

4.5.4 Simulation of Shot-Peened Material through Cross-Rolling

If the local stress-strain behavior of peened weld was in the plastic range, the σ-ε curve was necessary for the set-up cycle analysis. To do this, the material properties of cross-rolled A36 steel were used in the analysis. The material properties of heavily cross-rolled specimens were assumed to be similar to those of the shot-peened layer, because both processes impart heavy plastic deformations. A36 steel plates were heavily cross-rolled to

simulate shot-peening. Cross-rolling was used to reduce the anisotropy caused by unidirectional rolling. Smooth specimen tests were run under strain control for fatigue properties and mean stress relaxation information. All the details and test results are given in Appendix B. Mean stress relaxation exponents (k) as function of strain amplitude for the materials under investigation are shown in Fig. 31.

4.5.5 Effect of Residual and Bending Stress on N_p

The effect of compressive residual stress induced by shot-peening on N_p was neglected for the following reasons: In the long life region, N_I is much greater than N_p; thus, the difference in N_p caused by compressive residual stress should not make any significant difference in the total life (N_T). In the short life region, the high stress imposed may relax the residual stress rapidly, and probably washout completely the residual stress before the crack starts to propagate.

Bending stresses were considered in the estimation of N_p using Eq. 21. The coefficients of Eq. 19 for the geometries under investigation are listed in Table 14.

4.6 Application of the I-P Model to TIG and Laser-Dressed Weldments

Early experiments showed that both dressing processes altered the geometry of the weld toe and produced a new toe at which there was a slight undercut. Most of the TIG dressed and some poor laser-dressed weldments had a severe undercut at which most of their fatigue cracks initiated.

4.6.1 Stress Concentration Factor (K_t)

To determine K_t of a new toe, a model was developed which considered the geometry of the new toe with undercut to be a big notch (weld toe) with a small surface notch (undercut): see Fig. 32. The stress concentration

factor (K_t^g) for a weld toe was calculated by Mattos and Lawrence (60) using FEM:

$$K_t^g = 1 + \alpha(t/r_g)^{\frac{1}{2}} \tag{48}$$

where: t is plate thickness and r_g is radius of big geometry. The stress concentration factor for a general surface notch is:

$$K_t^n = 1 + 2(d/r_n)^{\frac{1}{2}} \tag{41}$$

where d is notch depth (undercut depth) and r_n is notch root radius. If a weld toe has a surface notch, the stress concentration factor (K_t^s) at the surface notch root can be estimated by superposing the two value of K_t: see Fig. 32b:

$$K_t^s = K_t^g \times K_t^n \tag{49}$$

Substituting Eqs. 41 and 48 into Eq. 49:

$$K_t^s = \{1 + \alpha(t/r_g)^{\frac{1}{2}}\}\{1 + 2\ (d/r_n)^{\frac{1}{2}}\} \tag{50}$$

Here, t and α are known and r_g can be measured.

Therefore, K_t^s can be expressed:

$$K_t^s = C\ \{1 + 2(d/r_n)^{\frac{1}{2}}\} = C + 2C\ (d/r_n)^{\frac{1}{2}} \tag{51}$$

where C (≥ 1) is a constant representing the calculations of the first term

with known values in Eq. 50. Thus, the fatigue notch factor (K_f^s) can be expressed:

$$K_f^s = 1 + \frac{K_t^s - 1}{1 + \underline{a}/r_n} = 1 + \frac{C - 1 + 2C(d/r_n)^{\frac{1}{2}}}{1 + \underline{a}/r_n} \tag{52}$$

For $K_{f,max}^s$ condition:

$$\frac{dK_f^s}{d\, r_n} = 0 \tag{53}$$

As a result, $K_{f,max}^s$ occurs when $r_n = r_M$:

$$r_M = \left[\frac{\underline{a}(C-1) + \{(C-1)^2\underline{a}^2 + 4\underline{a}C^2d\}^{\frac{1}{2}}}{2Cd^{\frac{1}{2}}}\right]^2 \tag{54}$$

Since notch depth "d" can be measured, r_M can be evaluated numerically. Therefore, $K_{f,max}^s$ can be estimated by substituting the value of r_M into Eq. 52.

The depth of the undercut at possible crack initiation sites was measured using a profilometer for each kind of dressed weldment. The profiles and depths are shown in Fig. 33. The root radius of undercut showed sufficient variation to support the use of the $K_{f,max}$ condition in each case. For the case of a surface notch on a flat surface, C is unity. Then, from Eq. 54, $K_{f,max}$ occurs when $r_M = \underline{a}$, which is the same result as Lawrence et al. (52) found in a simple, as-welded weld geometry.

The effect of the dressed weld geometries on the undercut at the new toe for the specimens under investigation was studied using the above model. The measured distance (x) from the new toe to the point of tangency between the base plate and the flank of the remelted material was greater than 0.125" for

all the dressed specimens. The measured radii (r) of the dressed beads were greater than 0.125 inches ($r > 0.125$ in.) in all cases. The solid line in Fig. 34 represents the case of $r = 0.125$ inches and shows that no stress concentration due to the weld toe is possible if the ratio x/t is greater than 0.15 The ratio x/t for all specimens studied was greater than 0.2; thus, no effect of the modified weld toe on the undercut at the new toe was possible ($C = 1$ in Eq. 51 and $r_M = \underline{a}$). However, the fatigue crack initiation sites of laser-dressed A36 specimens were not at the undercut of the new toe but at the undercut at the point of tangency: see Fig. 20d. For these sites the value of C was 1.2 and thus $r_M = 1.56 \times 10^{-3}$ in. The effects of the parameters in Eq. 54 on r_M and $K^S_{f,max}$ are listed in Table 15 and compared with those for the as-weld case. The most effective way to increase fatigue life by changing the parameters in Eq. 54 was found to be the reduction of the "C" value by decreasing the stress concentration of the bigger notch and to reduce the undercut depth "d".

4.6.2 Material Properties and Residual Stresses

The hardness surveys (Figs. 15 and 18) showed that both the TIG and the laser dressing treatments generally gave a much higher hardness at the crack initiation sites than that of the original as-welded toe. Hence, the HAZ fatigue properties determined for the as-weld toe are inappropriate and would give conservative estimates of the fatigue life. In these cases, hardness measurements[1] (see Sec. 4.5.1) were used to estimate the fatigue properties of the dressed toes.

[1]The fatigue properties calculated for the as-welded A36/E60S weldments using Landgraf's correlations with hardness predicted extraordinarily long fatigue lives and much too high values of σ'_f. The fatigue properties of the HAZ for as-welded A36 weldments estimated from Higashida's correlations for A36 materials (Fig. 35), recently reconfirmed by work of Yung (81), do not follow the trends reported by Landgraf for other steels.

Monotonic and cyclic properties of the HAZ for dressed weldments were assumed to be the same as those of the as-welded HAZ. Higashida (71) and Yung (81) determined the monotonic and cyclic properties (Table 2-5) and the mean stress relaxation exponents (k) (Fig. 31) for HAZ materials prepared using electrical resistance simulation.

V. COMPARISON OF PREDICTIONS WITH EXPERIMENTAL RESULTS

Table 16 summarizes the methods for predicting N_I for post-treated weldments using the I-P model. Tables 17 and 18 list all the values and parameters used in the estimations of N_I and N_p, respectively.

5.1 Shot-Peened Weldments

The predictions shown in Fig. 7 for as-welded and shot-peened A514/E110 bead on plates agree well with the experimental results. Shot-peening gave a slight increase in the value of $K_{f,max}$ (see Table 17) by elevating the S_u of the material, but the induced compressive residual stresses and the improved material properties caused a tremendous net increase in N_I.

5.1.1 Effect of Bending Stress

For single-V butt welds, if compressive bending stresses are induced at weld toe side by properly controlled angular distortion during fabrication, these compressive bending stresses will improve weld fatigue resistance. However, for double V butt welds and cruciform joints, bending stresses always produce a detrimental effect on weld fatigue resistance because of the existence of positive bending stresses at one or the other of the weld toes (or roots).

For shot-peened A36/E60S bead on plate weldments, predictions with and without bending stresses are shown in Fig. 36. The predictions agree well with experimental results when bending is considered. At 40 ksi. (which is the yield strength of the base metal), the fatigue life increased to about 5×10^6 cycles. This increase was caused mainly by the induced compressive residual stresses and partly by the induced compressive bending stresses on weld-toe side due to the anglular distortion of these one-side, bead-on plate specimens.

5.1.2 Shot Size and Intensity

To obtain improvement of the weld toe geometry by shot-peening, the shot-size would have to be small enough to hit the sharp corner of the toe to eliminate the $K_{f,max}$ condition ($r = \underline{a}$). However, the shot-size also need to be large enough to produce a compressive residual stress layer of sufficient depth, that is, at least of a depth a_I (see Table 9 and Fig. 29). For a maximum improvement in N_I, the maximum value of the compressive residual stress should also be located within the depth a_I[1]. Faulkner and Bellow (31) performed tests on butt joints treated by three different peening methods: shot-peening, multiple-wire-hammer peening, and solid-tool-hammer peening. No difference in fatigue strength was found between the three, all three giving improvements of between 55% and 65% at 2×10^6 cycles. But the depth of the work-hardened layer was 0.016 in. as a result of shot-peening, 0.035 in. for multiple-wire-hammer peening, and 1.059 in. for a solid-tool-hammer peening which implies that compressive layers deeper than a_I ($\leq$ 0.01 in.) do not cause any further improvement.

5.2 TIG and Laser-Dressed Weldments

Predictions and experimental results for TIG and laser dressed specimens for both materials are shown in Figs. 37-40. As shown in Table 17, TIG dressing treatments reduced the flank angle (θ) at the new toe to zero degrees, but the $K_{f,max}$ for TIG dressing treatment was still nearly the same as for as-welded A514/E110 and slightly bigger than for the A36/E60S weldments due to a deep undercut at the TIG toe. The great improvement in material

[1] Shot-peened TIP230 showed much longer life than others (Table 9) which indicated that the optimum shot size might be 0.023-in. (SAE 230) for the A514/E110 weldment and shot peening parameters used (Table 8).

properties at the critical location offsets this notch effect giving a considerable increase in N_I. Furthermore, the gross geometrical improvement imparted a significant increase in N_p and thus a great increase in the total fatigue life.

Laser-dressed A514/E110 specimens had only a very shallow undercut at their new toes which reduced the $K_{f,max}$ value tremendously and increased the fatigue life to that of plain plate at the lower stress levels (65 ksi). At higher stress levels where N_p is dominant, the higher strength materials resulting from laser-dressing have a shorter N_p than plain plate. For laser-dressed A36/E60S specimens, the sharper geometrical notch (C = 1.2) and deeper undercut at the laser dressed bead resulted in a shorter total fatigue life than that of the TIG dressed specimens through reductions in N_I at long lives and N_p at short lives: see Fig. 8.

5.3 Summary

Among the post-weld treatments studied, shot-peening was the most effective. However, the compressive residual stresses induced which are the main cause of improvement do have the disadvantage of being eliminated by heat or relaxed by high plastic strains. Peening is more beneficial for high strength materials because of the higher compressive residual stresses possible and at long lives because of lesser mean stress relaxation.

Both the TIG and laser-dressing methods produced a tremendous improvement in the material properties of the remelted regions. However, undercut which often is associated with these treatments is very detrimental to the weld fatigue resistance. Therefore, the most important consideration in dressing a weldment is to establish parameters which produce minimal undercutting. Changes in geometry and material properties are permanent; thus an improvement

in geometry may be the most secure method of fatigue life improvement. From such a viewpoint, laser-dressing, which has a lot of limitations at the present, is a promising treatment for future study.

VI. COMPARISON OF I-P MODEL PREDICTIONS WITH PUBLISHED DATA

6.1. Sources of Data

The fatigue strength predictions for several geometries and post-weld treatments of double-V steel butt weldments were made and compared with available data from the Fatigue Data Bank compiled by W.H. Munse and coworkers (82) and from studies reported in the open literature (83,84) for which the information required for the use of the I-P model existed.

The fatigue strength at $2x10^6$ cycles was calculated and compared because fatigue strength data for $2x10^6$ cycles is available in the literature and because for such long lives, the propagation life, the effect of mean stress relaxation on initiation life, and cyclic hardening or softening effects are small enough to be neglected in the estimation of total fatigue life. Therefore, fatigue crack initiation life (N_I) was assumed to be equal to the total fatigue life (N_T).

The principal difficulty applying the I-P model was determining appropriate values of HAZ material properties and residual stresses (σ_r). Empirical relationships were found between S_u(BM) and the material properties for as-welded and shot-peened weldments. Details of the prediction of fatigue strength (S_a) are given in Appendix C.

6.2 Predictive Equations and Assumptions

Equations C10, C19 and C21 have a form similar to Eq. 55. The appropriate values of σ_r (see Eqs. 46-47 and C11-C13) are substituted for each case:

$$S_a = \frac{(A \cdot S_u + B)(2N_I)^{-\frac{1}{6}\log 2_3\left(1 + C \cdot \frac{1}{S_u}\right)}}{\left\{1 + D \cdot \alpha_A \; S_u^{0.9} \; t^{0.5}\right\}\left\{1 + \frac{1+R}{1-R}(2N_I)^{-\frac{1}{6}} \log 2\left(1 + C \cdot \frac{1}{S_u}\right)\right\}} \qquad (55)$$

where A, B, C and D are the coefficients for the several post-weld treatments and plain plate: see Table 19. Note: "t" in Eq. 55 will be replaced by "d" for plain plate case and S_u is the S_u of the BM.

The fatigue strength (at 10^6 cycles, R = -1, and $\phi = 90°$) of steel weldments predicted by Eq. 55 as functions of S_u(BM) and θ is plotted in Fig. 41 for hot-rolled steels. For as-welded weldments ($\sigma_r = +S_y$), the fatigue strength continues to increase with increasing S_u(BM) up to 90 ksi; the increase in fatigue strength coefficient (σ_f') due to the increase in S_u(BM) is partially offset by the increase in residual stresses (σ_r) and $K_{f,max}$ value: see Eq. C10. However, above 90 ksi. the fatigue strength becomes almost independent of S_u(BM): the increase in σ_f' due to the S_u(BM) increase is almost completely offset by the increase in the $K_{f,max}$ and σ_r. Therefore, increasing S_u(BM) may have little effect on the fatigue strength of as-welded weldments for hot-rolled steels. This phenomenon was reported by Munse (85). For stress-relieved weldments ($\sigma_r = 0$), the fatigue strength continues to increase with increasing S_u(BM) because the increase in σ_f' due to the increase in S_u(BM) is only partially offset by the increased $K_{f,max}$. The higher strength steels should show the greatest benefit from over-stressing or inducing compressive residual stresses ($\sigma_r = -S_y$) at the weld toe.

The fatigue strength of low strength steels may not be improved much by post-weld treatments because the possible improvement of fatigue strength through such treatments becomes small as the base metal strength, S_u(BM), is reduced. However, the fatigue strength of plain plate becomes less than that

of over-stressed weldments for the very low strength steels as shown in Fig. 41; thus, complete recovery of the lost fatigue strength due to welding is possible through over-stressing for the given conditions.

6.3 Predicted Effect of Geometry, Size of Weldment, and Stress Ratio (R) on Fatigue Strength

Fatigue strength greatly depends on the geometry of the weldment, that is, on the value of $K_{f,max}$. Increasing the flank angle (θ) causes an increase in the value of $K_{f,max}$ and a decrease in fatigue strength (S_a): see Fig. 2 and Eq. C4. The dependence of S_a on flank angle (θ) becomes greater as θ becomes smaller as shown in Figs. 41 and 44 - 46.

Figs. 42 and 43 show the effect of thickness (t) on the fatigue strength of as-welded and shot-peened weldments. Increasing thickness (t) causes a decrease in weld fatigue strength due to an increase in $K_{f,max}$: see Eq. C4. Thus, in general, N_I depends strongly upon weld size (t); N_p also depends upon "t" (Eq. 19) but to a lesser degree. The dependence of weld fatigue strength on thickness (t) becomes greater as "t" becomes smaller. As shown in Figs. 42 and 43 for example, weld fatigue strength can be improved up to that of plain plate by shot-peening for a wide range in base metal strengths if the thickness is small. However, if the thickness (t) is 1.5 inches or larger and if S_u(BM) is 100 ksi or above, complete recovery of the lost fatigue strength can never be obtained through shot-peening for the weldments studied.

Increasing the stress ratio (R) causes an increase in the value of $\frac{1+R}{1-R}$ in Eq. 55 thus decreasing the weld fatigue strength (S_a), as is shown in Figs. 42-45.

6.4 Comparisons of Predictions with Data for Weldments

Figures 44 through 46 show predictions of fatigue strength as function of S_u(BM) at $N_f = 2x10^6$ with the average data principally from Munse's Data Bank (82) for two different thicknesses (t = 3/4" and 1/2") of as-welded butt welds and plain plate. Since the flank angle (θ) was not always reported, a value of 30 to 45 degrees was assumed in most cases. Most of steels which had tensile strengths above 80 ksi. were not hot-rolled steels but quenched and tempered steels. A small number of normalized steels were studied in the strength range between 80-100 ksi. Since each different kind of heat treatment gives a different trend of S_y as a function S_u(BM) (see Eqs. C11-C13), the predictions for hot-rolled steels were plotted up to S_u(BM) of 80 ksi and the predictions for normalized and Q-T steels were plotted for S_u(BM) above 80 ksi. Since plain plate was assumed to have zero residual stresses, its particular heat treatment was assumed not to matter. Fairly good agreement is seen between predictions and actual data for both the as-welded welds and plain plate.

For quenched and tempered steel weldments (above 80 ksi.), increasing the strength (S_u(BM)) actually decreases the fatigue strength due to the combined effects of increasing σ_r and $K_{f,max}$ as shown in both predictions and actual data in Figs. 44 and 45.

In Fig. 47, the predicted fatigue strength and experimental data obtained in this study are plotted. An excellent agreement was obtained between predictions and test data. Complete recovery of lost life was obtained by shot-peening for both the mild (A36) and high strength (A514) steels.

In Fig. 48, predictions of fatigue strength for stress-relieved weldments were plotted with the small amount of data available in the literature. Since stress-relief can reduce the tensile residual stresses of as-welded welds only

to the yield strength of the base metal corresponding to the temperature at which stress relief was conducted, the actual residual stress may not be completely relieved. Furthermore, material properties at the weld toe may be degraded due to a decrease in hardness during the stress-relief. The data for stress-relieved weldments were well below their predicted fatigue strengths and represented almost no improvement over the fatigue strength of as-welded weldments.

Figure 49 gives a comparison of predicted fatigue strengths using Eq. 55 with data for plain plates and as-welded and post-treated weldments with various geometries for several steels. Good agreement was observed between the predictions and data except for the stress-relieved and hammer peened weldments. Most hammer peened weldments were tested in the short life range which would relax the induced compressive residual stresses shortening the fatigue life. The given fatigue strength at $N_f = 2 \times 10^6$ was calculated from the short life data. If specimens with compressive residual stresses were tested at R = -1 with higher stress amplitude, the bigger negative stress amplitude added to the compressive residual stresses might exceed the negative yield strength of the material at the critical region, giving less compressive mean stress. These facts might cause much lower actual fatigue strength than predicted. Therefore, the possibility of overestimation in the prediction of shot-peened weld fatigue strength for the case of R = -1 should be pointed out.

Equation 55 can predict the effect of each factor (i.e., $S_u(BM)$, σ_r, α, t, R, etc.) on the weld fatigue. The fatigue strength (S_a) of weldment for combined axial and bending stresses can also be predicted by modifying Eq. 55. Detailed discussions are given in Appendix C.5.

VII. THE RECOVERY OF WELDMENT FATIGUE LIFE

7.1 Concepts

The fatigue resistance of a weldment can never exceed the fatigue life of the plain plate which it joins; therefore, no fatigue improvement scheme can lead to lives in excess of that of the plain plate. This fact leads to the concept of maximum recoverable life (MRL) that is, the difference between plain plate and weldment fatigue life and to the concept of recovered life (RL), the net increase in fatigue life due to a post-weld treatment. The MRL and RL can be predicted using the I-P model discussed:

$$2N_I^P = \left[\frac{\Delta S\ K_f^P}{2(\sigma_f'^P - \sigma_o^P)}\right]^{\frac{1}{b_p}} \tag{56}$$

$$2N_I^W = \left[\frac{\Delta S\ K_f^W}{2(\sigma_f'^W - \sigma_o^W)}\right]^{\frac{1}{b_w}} \tag{57}$$

and

$$2N_I^t = \left[\frac{\Delta S\ K_f^t}{2(\sigma_f'^t - \sigma_o^t)}\right]^{\frac{1}{b_t}} \tag{58}$$

where: $2N_I^P$, $2N_I^W$, $2N_I^t$ = Initiation life of plain plate, as-welded and post-treated weldment, respectively,

K_f^P, K_f^W, K_f^t = Fatigue notch factor for plain plate, as-welded and post-treated weldment, respectively,

$\sigma_f'^P$, $\sigma_f'^W$, $\sigma_f'^t$ = Fatigue strength coefficient for plain plate, as-welded and post-treated weldment HAZ, respectively,

σ_o^p, σ_o^w, σ_o^t = Mean stress for plain plate, as-welded and post-treated weld toe, respectively,

b_p, b_w, b_t = Fatigue strength exponent for plain plate, as-welded and post- treated weldment HAZ, respectively, and

ΔS = Remote stress range.

The maximum recoverable life (MRL) and the recovered life (RL) resulting from a post-weld treatment at long lives are:

$$MRL = 2N_T^p - 2N_T^w \simeq 2N_I^p - 2N_I^w \tag{59}$$

and

$$RL = 2N_T^t - 2N_T^w \simeq 2N_I^t - 2N_I^w \tag{60}$$

The fatigue strength exponents of plain plate, as-welded and post-treated weldments can be assumed to be nearly equal:

$$b_p \simeq b_w \simeq b_t \tag{61}$$

7.2 Fatigure Life Recovery Resulting from Post-Weld Treatments

The best possible weldment performance will occur when the recovered life (RL) becomes equal to the maximum recoverable life (MRL). For this condition:

$$\frac{K_f^t}{K_f^p} \leq \frac{\sigma_f'^t - \sigma_o^t}{\sigma_f'^p - \sigma_o^p} \tag{62}$$

Now $$\sigma_o^p = K_f^p S_o \quad \text{and} \tag{63}$$

$$\sigma_0^t = K_f^t S_0 + \sigma_r \tag{64}$$

where: S_0 = Remote mean stress and

σ_r = weld toe residual stress.

Therefore, Eqs. 62-64 result in

$$\frac{K_f^w}{K_f^p} \leq \frac{\sigma_f'^w - \sigma_r}{\sigma_f'^p} \tag{65}$$

Equation 65 shows the quantitative relation between the three controllable factors for completely regaining the recoverable fatigue life and implies that complete recovery does not depend on stress range (ΔS) nor stress ratio (R), but strongly depends on the factors; geometry (K_f), residual stress (σ_r) and material property (σ_f'). Therefore, complete recovery can be accomplished by manipulating these controllable factors through post-weld treatments.

The predicted conditions for complete recovery by post-weld treatments utilizing the empirical relationships of Appendix C are given in Table 20 for three kinds of steels: Mild Steel (MS), High Strength Low Alloy Steel (HS) and Quenched and Tempered Steel (QT). Dressing treatments generally produced large increases in hardness in the remelted zones. The $\sigma_f'^t$ predicted from hardness measurements made after dressing did not show any relationship to the prior material properties. Thus, the $\sigma_f'^t$ of the remelted zones used for the mild and quenched and tempered steels were measured values; see Table 17 and 20. The actual percentages of recovery resulting from the post-weld treatment investigated are given in Table 21.

It appears that shot-peening is a particularly effective post-weld treatment. For quenched and tempered steel, for example, the $K_{f,max}$ value of shot-peened weldments can be up to 3.6 for complete recovery. In the current

study, the shot-peened A514/E110 weldments for which the $K_{f,max}$ value was 3.3 (which satisfied the complete recovery conditions of 3.6) generally gave longer lives than plain plate at long lives. Most shot-peened A36/E60S specimens gave complete recovery even at high stress levels (40 Ksi) and short lives, even though the complete recovery conditions for mild steels were not quite satisfied (K_f = 2.6 maximum predicted in Table 20, K_f = 2.8 actual).

Laser and TIG dressing appear to also be effective post-weld treatments because th conditions for complete recovery are easily achieved by these methods for a wide range of steel strengths: see Table 20. The lower strength steel weldments require a smaller reduction of K_f by dressing process to accomplish complete recovery (K_f = 2.8). As shown in Table 21, the laser-dressed A514/E110 and TIG-dressed A36/E60S specimens gave complete recovery of their lost fatigue life at low stress levels. Unfortunately, the laser-dressed A36/E60S specimens could not recover their lost life completely simply because the resultant toe geometry of most dressed weldments had a substantial undercut and was not smooth.

At short lives for which N_p is dominant, most post-weld treatments did not give complete recovery, though TIG-dressed and shot-peened A36/E60S specimen gave a high percentage of recovery. Therefore, most post-weld treatments have the greatest potential of improving fatigue life at low stress levels. The advantage of increase in N_p at high stress levels due to the reduction of geometry factor, M_k, for dressed weldments should not be underrated. Consequently, though some difficulty was experienced in laser-dressing mild steel weldments, laser dressing treatment is a promising process for further development.

The maximum recoverable life concept may be applied to any kind of weldment of notched member and provides a bench mark for complete fatigue life recovery.

VIII. CONCLUSIONS

1) Shot-peening was found to be the most effective method of improving weld fatigue life for the post-treatments investigated. However, the improvements resulting from shot-peening may be temporary because the induced compressive residual stresses may be eliminated by heat or relaxed by high plastic cyclic strains. Shot-peening was more beneficial for the high strength materials due to the higher compressive residual stresses possible and at long lives due to the minimal mean stress relaxation.

2) Weld toe dressing was as effective as shot-peening if it produced a flawless weld toe geometry. Dressing was more beneficial for lower strength materials due to lower tensile residual stresses and at short lives due to larger increase in N_p (lower stress intensity factor). The changes in geometry and material properties resulting from dressing treatments are permanent. From this viewpoint, laser-dressing is one of the most promising methods for future study.

3) It appears that the I-P model as modified herein can predict the weld fatigue life for any kind of post-treated weldment as well as that of the plain plate.

4) According to the maximum recoverable life concept, the fatigue life lost due to welding can in most cases be recovered if a suitable post-weld treatment is undertaken.

TABLES

TABLE 1

Chemical Compositions of Base Metal
and Welding Electrode

	Base Metal		Welding Electrode	
	A36*	E-60S-3* (Linde 82)	A514** (U.S.S. T-1)	E110* Murex Hy Loy 110)
Element	5/8-in. Plate	1/16-in. Bare Wire	1/2-in. Plate	1/16-in. Bare Wire
C	0.23	0.09	0.16	0.08
Mn	1.17	1.00	0.82	1.70
P	0.1	0.017	0.012	0.005
S	0.24	0.024	0.019	0.009
Si	0.02	0.50	0.23	0.46
Cu	< 0.10	---	0.27	---
Ni	< 0.10	---	0.76	2.40
Cr	< 0.08	---	0.54	0.05
Mo	< 0.10	---	0.47	0.50
V	---	---	0.06	0.02
B	---	---	0.004	---
Al	---	---	---	0.003
Ti	---	---	---	0.025

* Compositions supplied by manufacturer.

** Ladle composition.

TABLE 2

Mechanical Properties of Base, Weld, and Heat-Affected Materials for ASTM A514F/E110 Welds (71)

Material	A514-BM	A514-HAZ	E110-WM
Hardness, DPH/BHN	320/303	496/461	382/362
Modulus of Elasticity, E, x 10^3 ksi (MPa)	30.3 (210)	30.3 (210)	30.3 (210)
0.2% Offset Yield Strength, ksi (MPa)	129 (890)	171 (1180)	121 (835)
Ultimate Tensile Strength, Su, ksi (MPa)	136 (938)	204 (1408)	150 (1035)
Percent Reduction in Area, %RA	63.0	52.7	57.6
True Fracture Strength, σ_f, ksi (MPa)*	216 (1490) 184 (1269)	326 (2250) 288 (1986)	320 (2208) 277 (1910)
True Fracture Ductility, ε_f	0.994	0.750	0.857
Strain Hardening Exponent, n	0.060	0.092	0.092
Strength Coefficient, K, ksi (MPa)	127 (1187)	306 (2110)	266 (1560)

* The first value is the load just before it is suddenly decreased prior to fracture divided by the final area of the fracture specimen. The second value is corrected for triaxial stress due to necking as proposed by Bridgman (72,73).

TABLE 3

Cyclic and Fatigue Properties of Base, Weld, and Heat-Affected Materials for ASTM A514F/E110 WELDS (71)

Material	A514-BM	A514-HAZ	E110-WM
Cyclic Yield Strength, 0.2% Offset, ksi (MPa)	87.6 (604)	136 (938)	94.2 (650)
Cyclic Strain Hardening Exponent, n'	0.091	0.103	0.177
Cyclic Strength Coefficient, K', ksi (MPa)	158 (1090)	256 (1765)	293 (2021)
Fatigue Strength Coefficient, σ_f', ksi (MPa)	189 (1305)	290 (2000)	274 (1890)
Fatigue Ductility Coefficient, ε_f'	0.975	0.783	0.848
Fatigue Strength Exponent, b	-0.079	-0.087	-0.115
Fatigue Ductility Exponent, c	-0.699	-0.713	-0.734
Transition Fatigue Life, $2N_{tr}$, Reversals	3,461	1,138	1,536

TABLE 4

Mechanical Properties of Base, Cross-Rolled, Weld, and Heat-Affected Materials for ASTM A36/E60S-3 Butt Welds (71,81)

Material	A36-BM	A36-HAZ	E60S-3-WM	Cross-Rolled*
Hardness, DPH/BHN	175/166	245/233	245/233	221/210
Modulus of Elasticity, E, x 10^3 ksi (MPa)	30.2 (208)	30.4 (210)	27.4 (189)	30.2 (208)
0.2% Offset Yield Strength, ksi (MPa)	40.2 (277)	82.0 (565)	84.1 (580)	104.8 (723)
Ultimate Tensile Strength, Su, ksi (MPa)	78.0 (538)	106 (731)	103 (710)	109 (752)
Percent Reduction in Area, %RA	62	49	44.6	33.0
True Fracture Strength, σ_f, ksi (MPa)**	162 (1117) 141 (972)	164 (1131) 146 (1007)	143 (987) 129 (889)	143 (985)
True Fracture Ductility, ε_f	0.96	0.78	0.590	0.40
Strain Hardening Exponent, n	0.182	0.113	0.098	0.0534
Strength Coefficient, K, ksi (MPa)	103 (710)	160 (1103)	143 (987)	150 (1034)

* A36 plates of 5/8" thickness were cross-rolled in 60% reduction and strain aged for 1 hour at 100°C. These test pieces were cut from the plate which Higashida used (71).

** The first value is the load just before it is suddenly decreased prior to fracture divided by the final area of the fracture specimen. The second value is corrected for triaxial stress due to necking as proposed by Bridgman (72,73).

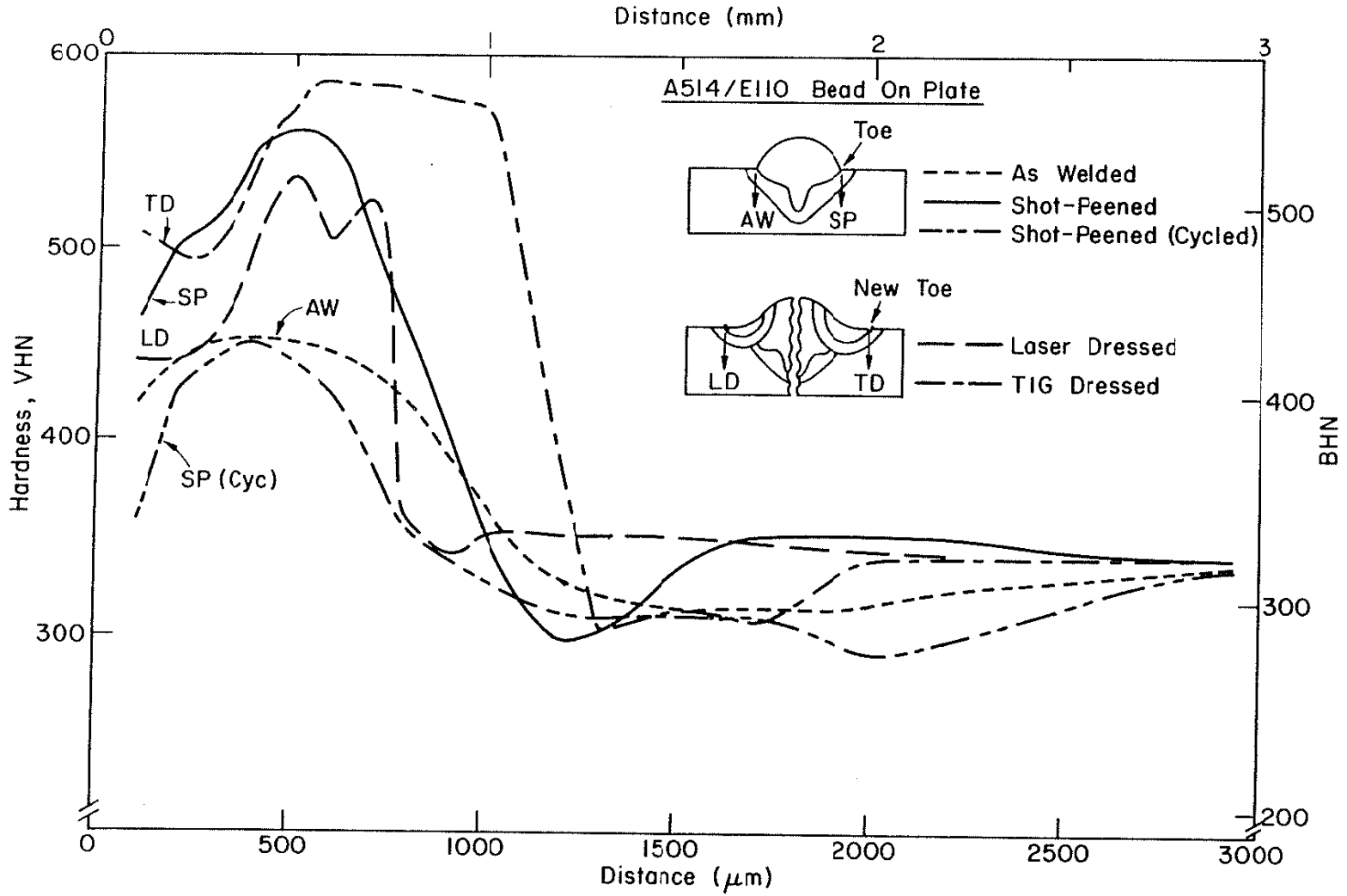

Fig. 15 Microhardress Traverse Inward from the Toe for As-Welded, Shot-Peened before and after Cycling and from New Toe for TIG-Dressed and Laser-Dressed A514/E110.

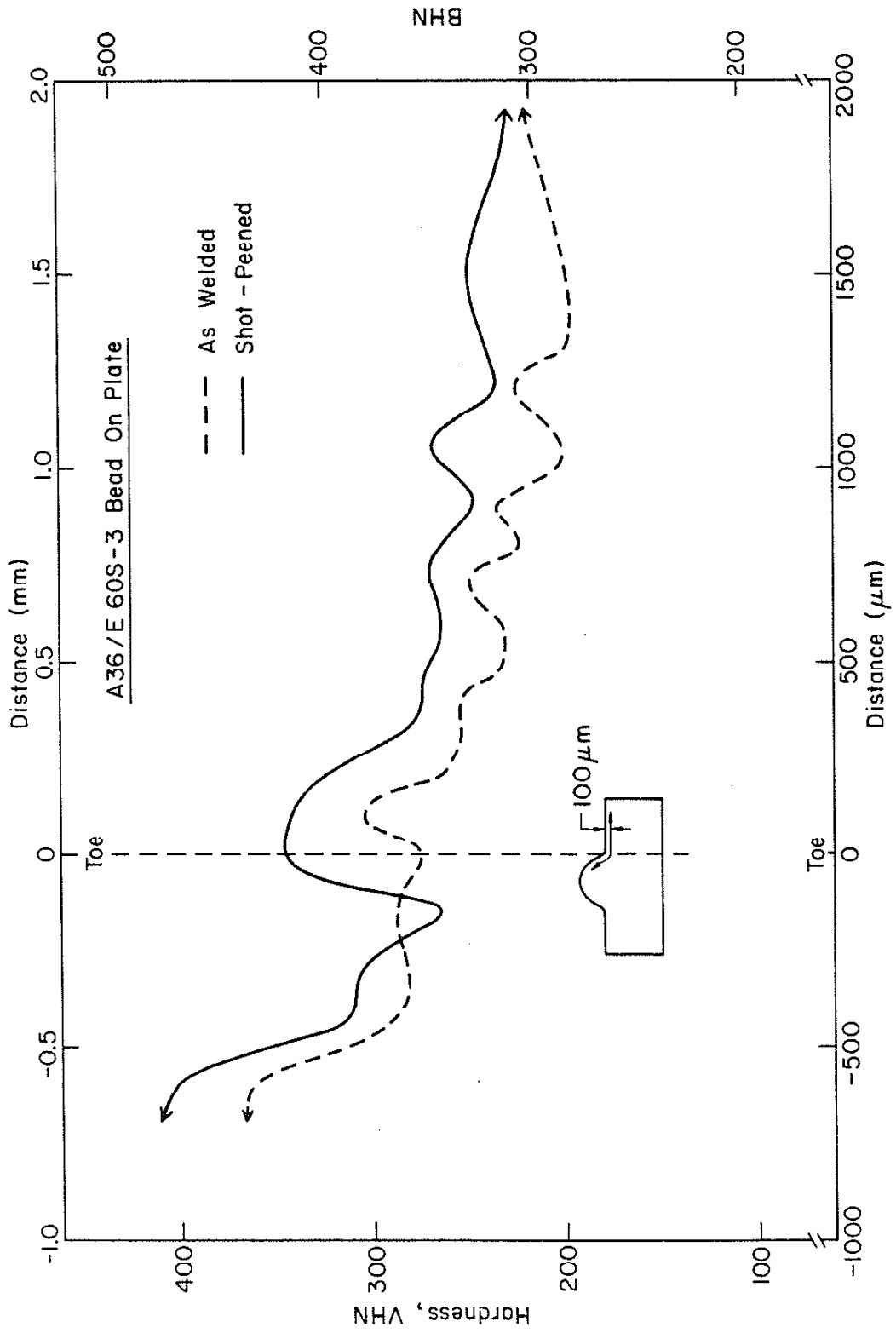

Fig. 16 Microhardness Traverse at 100μ below the Surface for As-Welded and Shot-Peened A36/E60S (Positive Direction into BM).

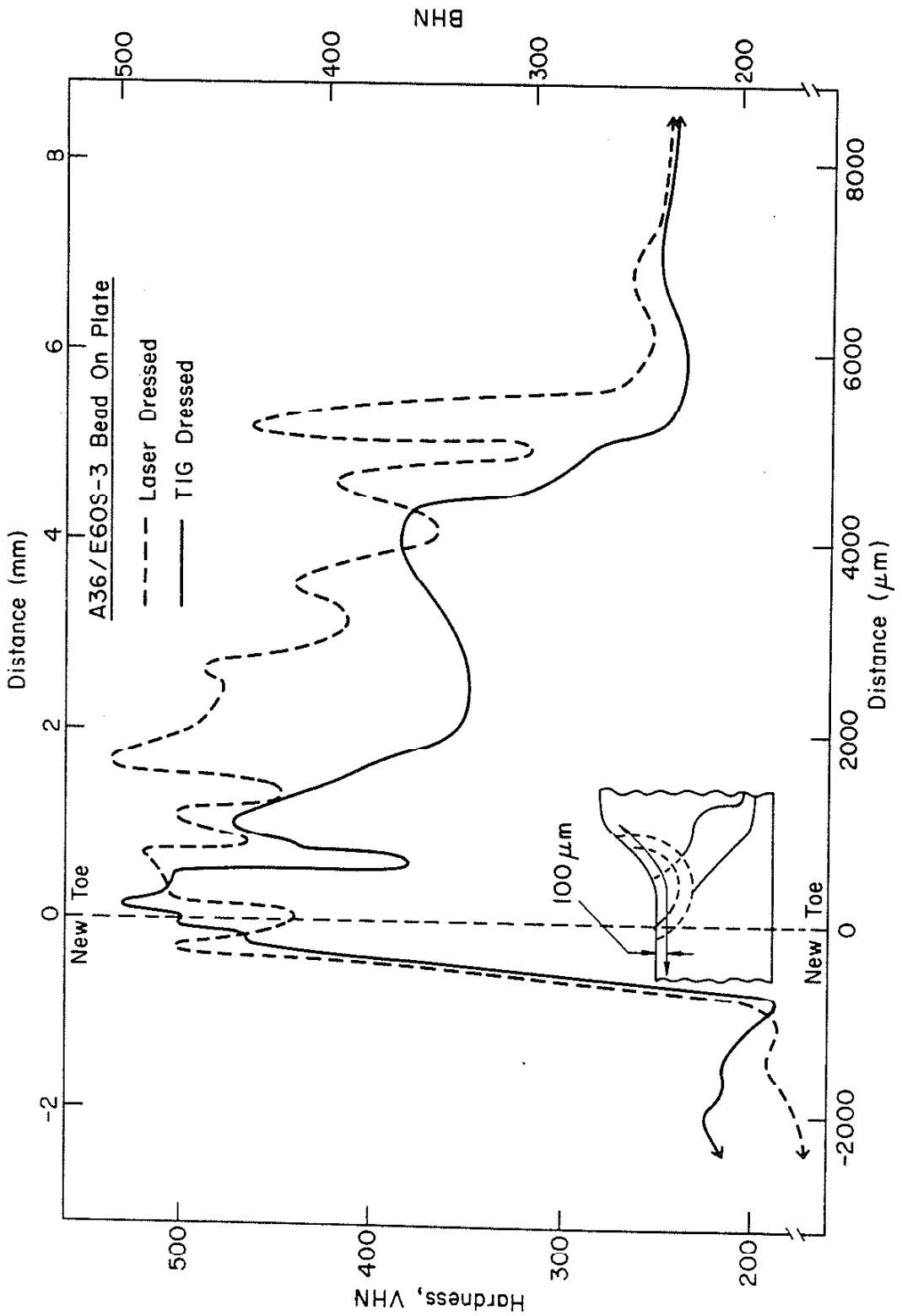

Fig. 17 Microhardness Traverse at 100μ below the Surface for TIG-Dressed and Laser-Dressed A36/E60S (Positive Direction into WM).

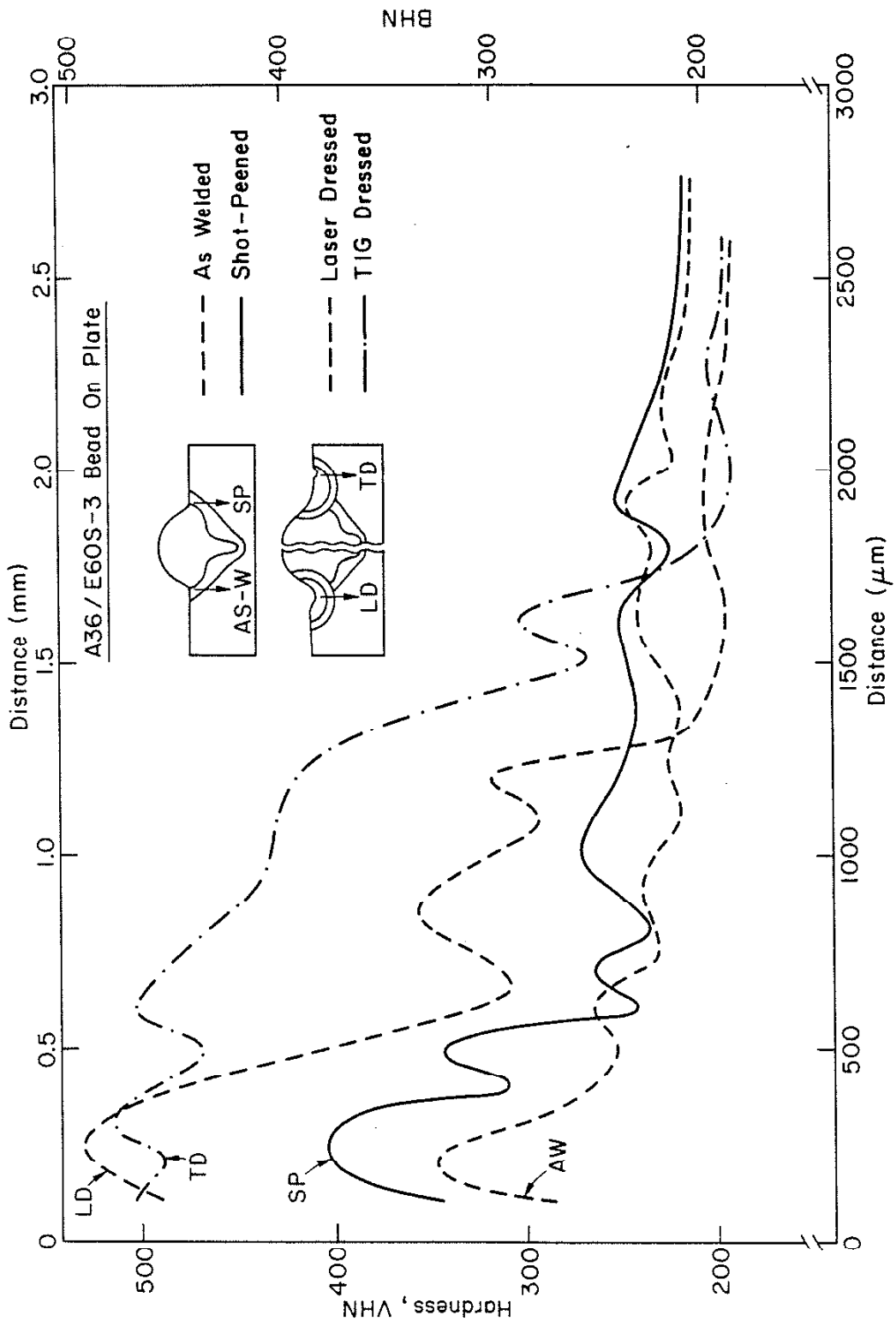

Fig. 18 Microhardness Traverse Inward from the Toe for As-Welded and Shot-Peened, from New Toe for TIG-Dressed and from Undercut on Dressed Bead for Laser-Dressed A36/E60S.

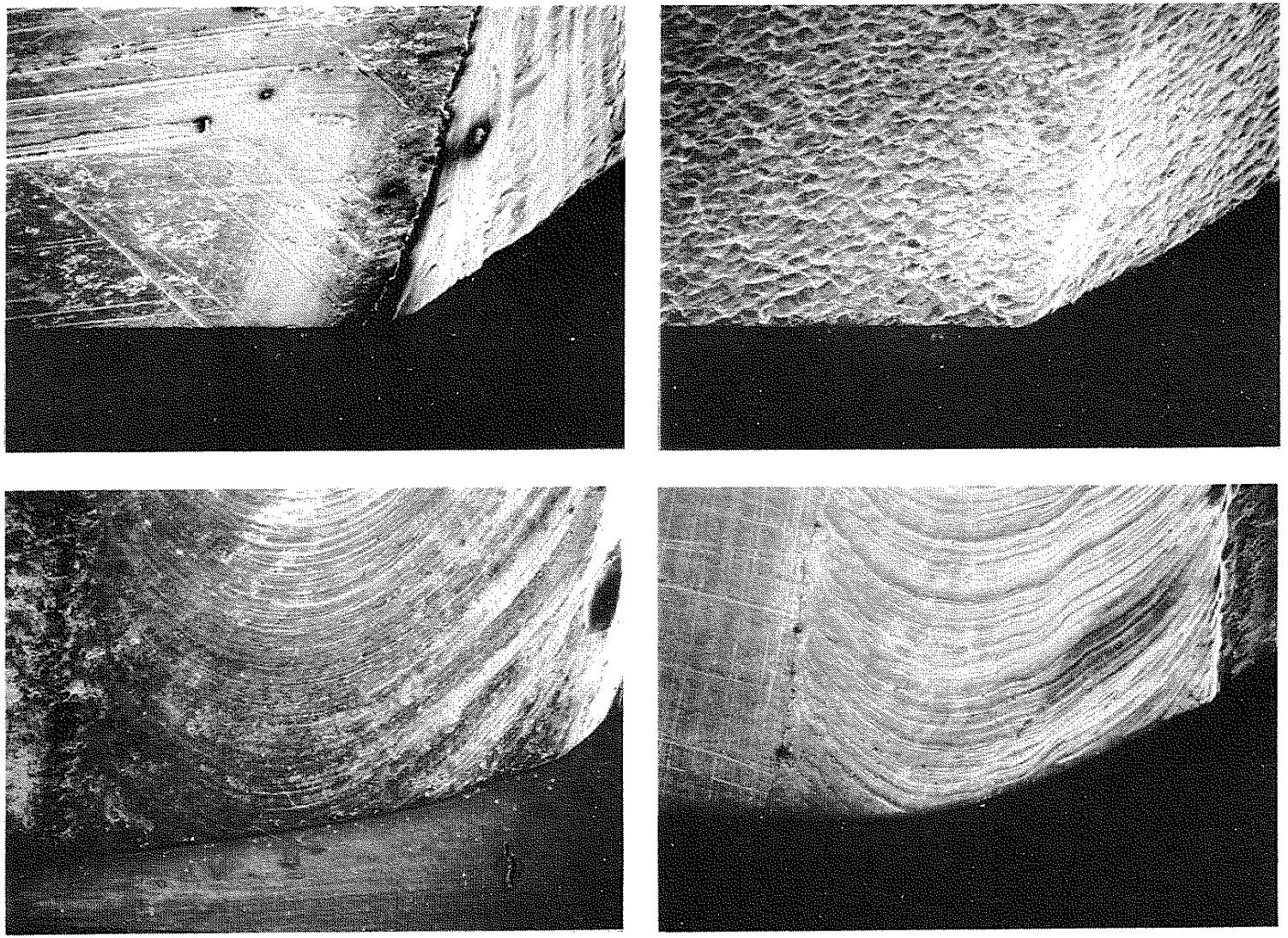

Fig. 19 SEM Photographs (15x) of Various Toe Configurations of A514/E110 Specimens: (a) As-Welded (Toe); (b) Shot-Peened (Toe); (c) TIG-Dressed (New Toe with Severe Undercut); (d) Laser-Dressed (New Toe with Nearly No Perceptible Undercut). All Four Treatments Would Give $K_{f,max}$ Conditions.

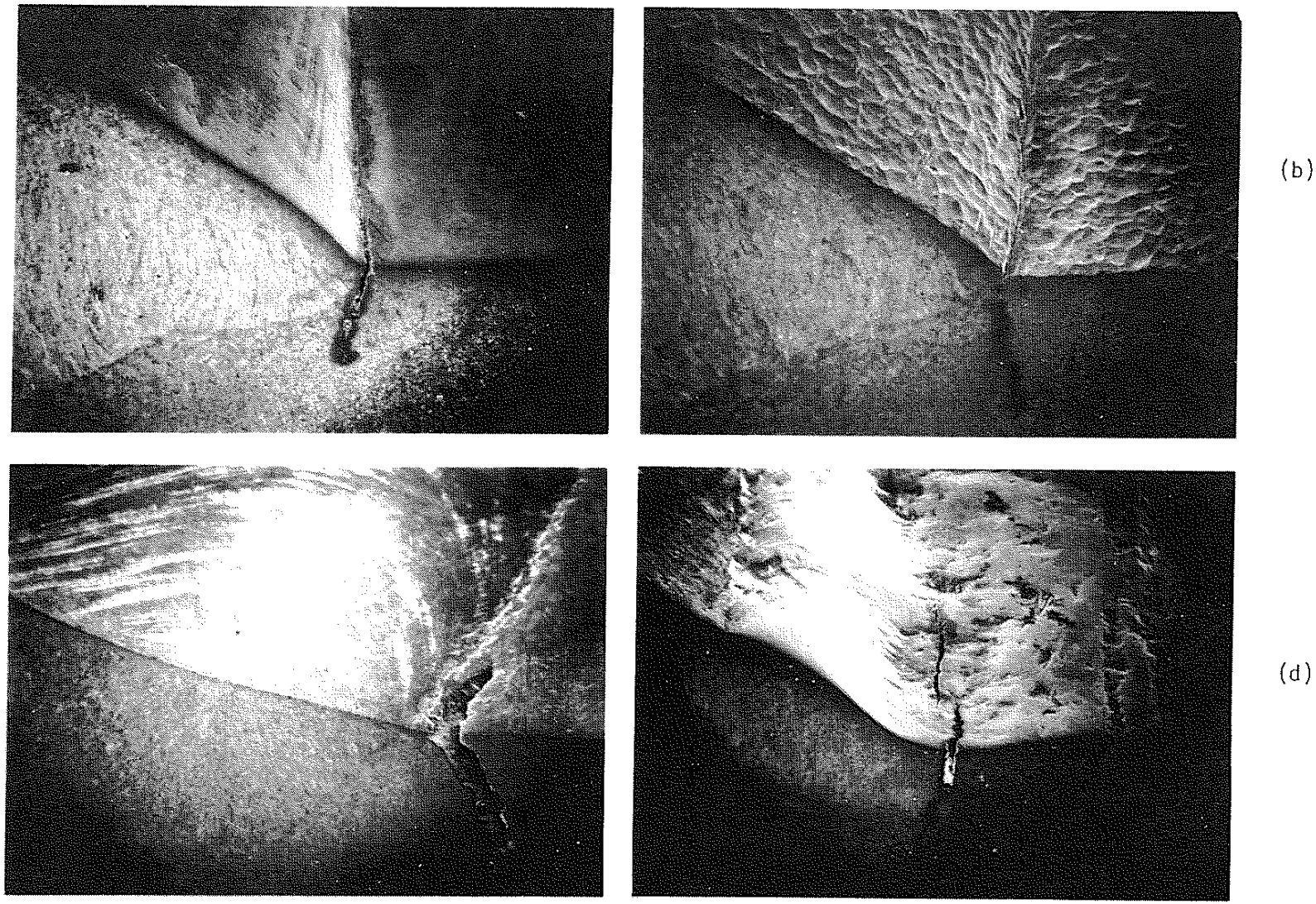

Fig. 20 SEM Photographs (15x) of Toe Configurations of A36/E60S Specimens with Developed Fatigue Cracks; (a) As-Welded: Crack at Toe; (b) Shot-Peened: Crack at Toe; (c) TIG-Dressed: Crack at New Toe with Undercut; (d) Laser-Dressed: Crack at Dressed Bead with Severe Undercut.

(a)

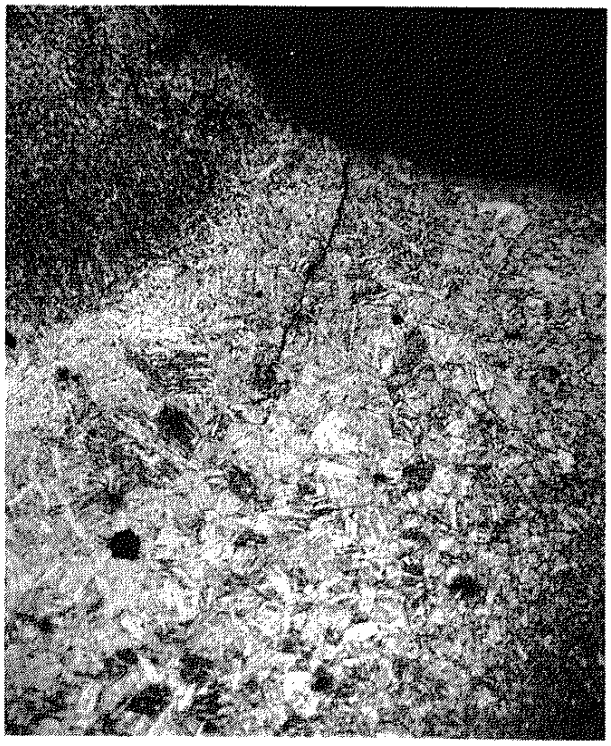

(b)

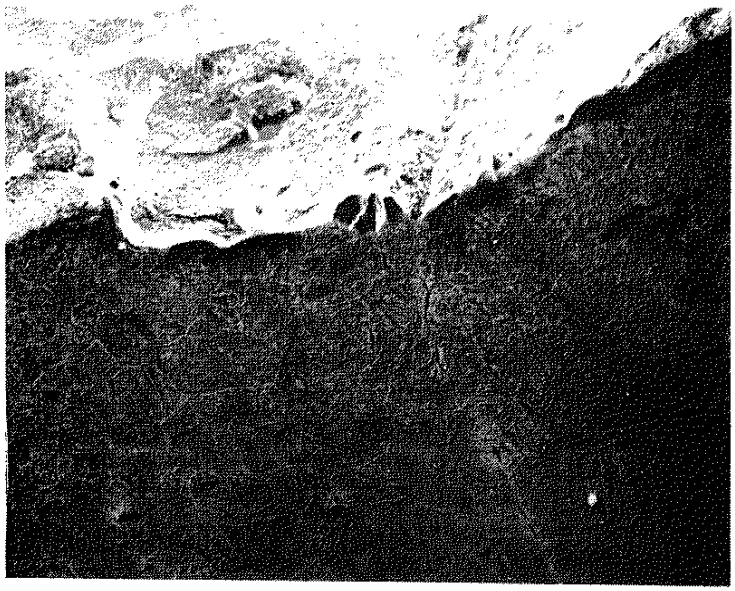

Fig. 21 (a) Micrograph (130x) of Fatigue Crack Starting at Toe and Propagating through Grain-Coarsened HAZ (Both As-Welded and Shot-Peened).
(b) SEM Photograph (200x) of Fatigue Crack Starting at Sharp Notch Root of Toe in Shot-Peened Specimen.

(a)

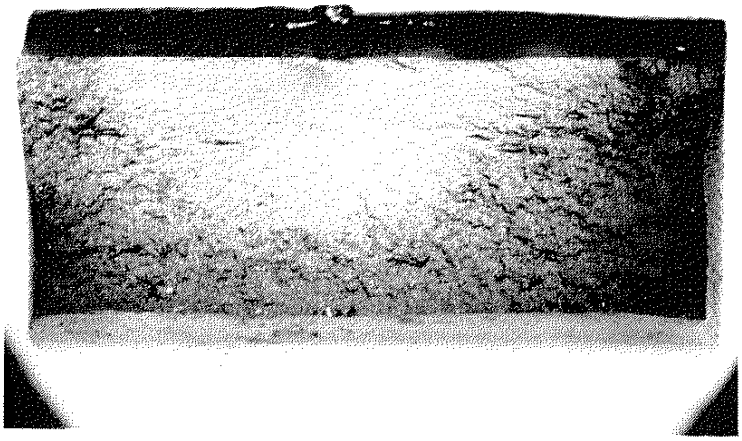

(b)

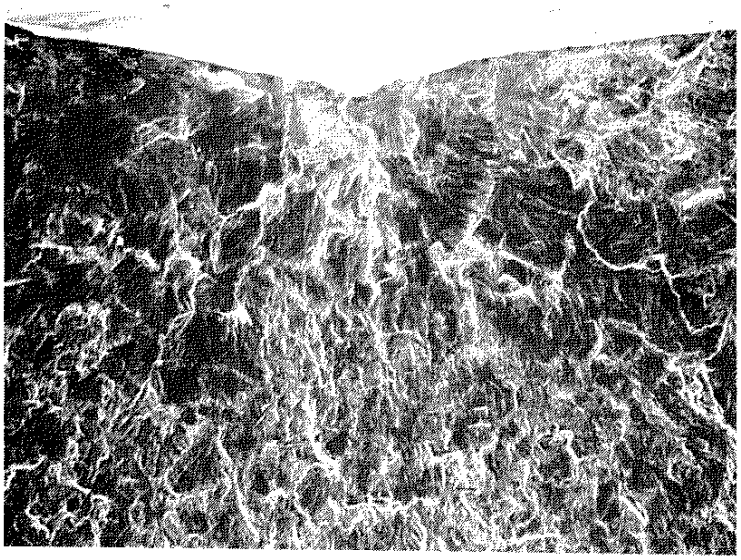

Fig. 22 TIG-Dressed A36/E60S Bead on Plate.
(a) Fracture Surface (2.3x) Showing Fatigue Crack Initiated at Middle of Surface and Semi-Circular Crack Front at High Stress Level (40 KSI).
(b) SEM Photograph (100x) for the Region of Crack Initiation Site of (a) Showing Crack Start at Undercut and Propagate Radially.

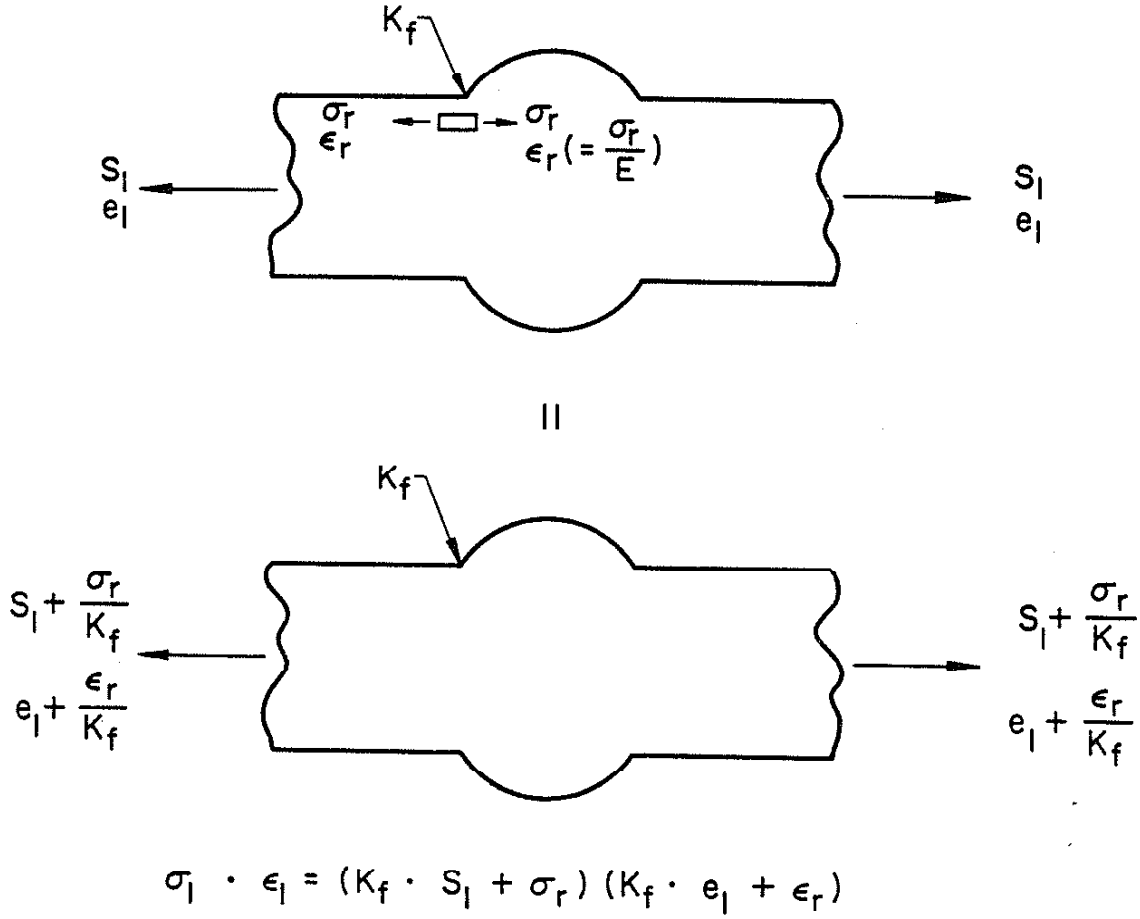

Fig. 23 Mechanical Simulation of Residual Stress (σ_r) at the Weld Toe Using Neuber's Rule with Elastic Superposition of Both Stress and Strain for the First Reversal.

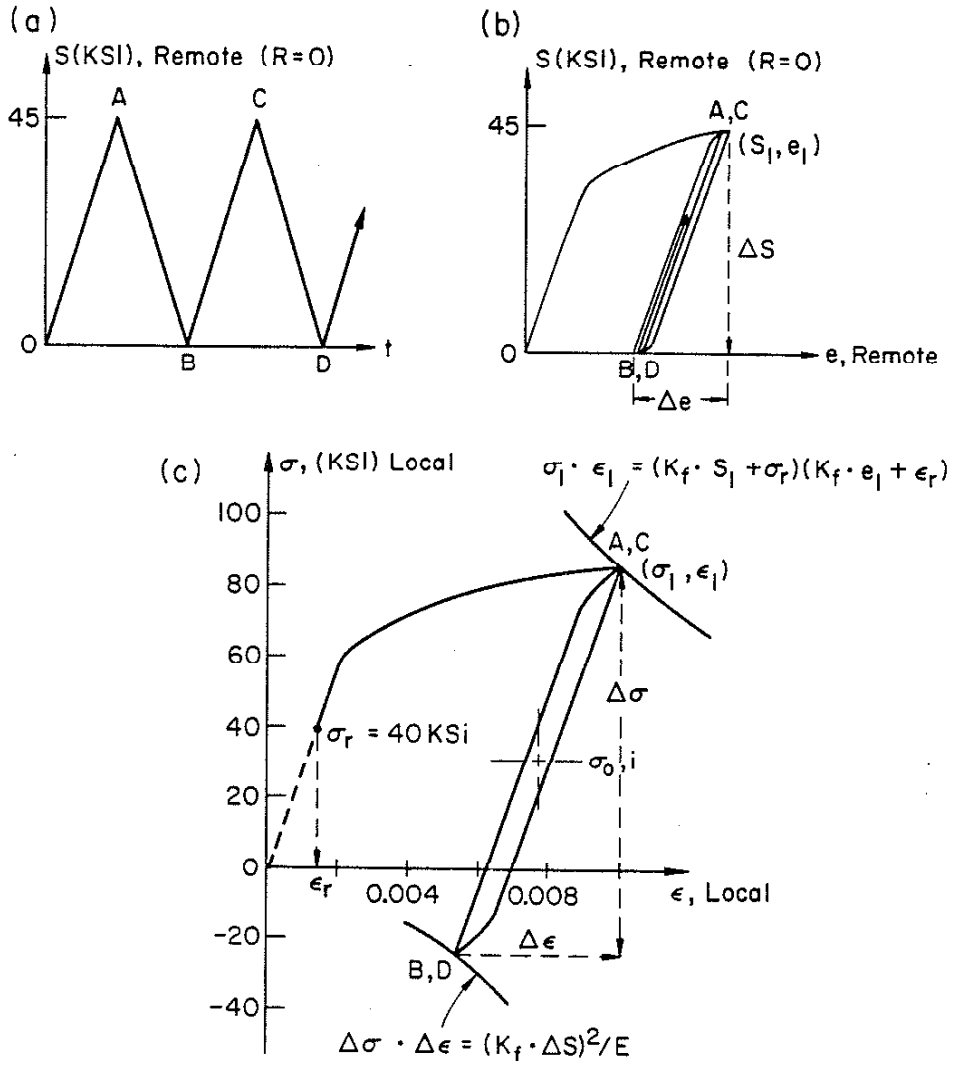

Fig. 24 Determination of Initial Mean Stress ($\sigma_{0,i}$) Using Set-Up Cycle Analysis for a Notch Root with Tensile Residual Stress (σ_r) for BM Plastic Case (a) Remote Stress vs. Time (b) Remote Stress-Strain Behavior (c) Local Stress-Strain Response Using Neuber's Rule.

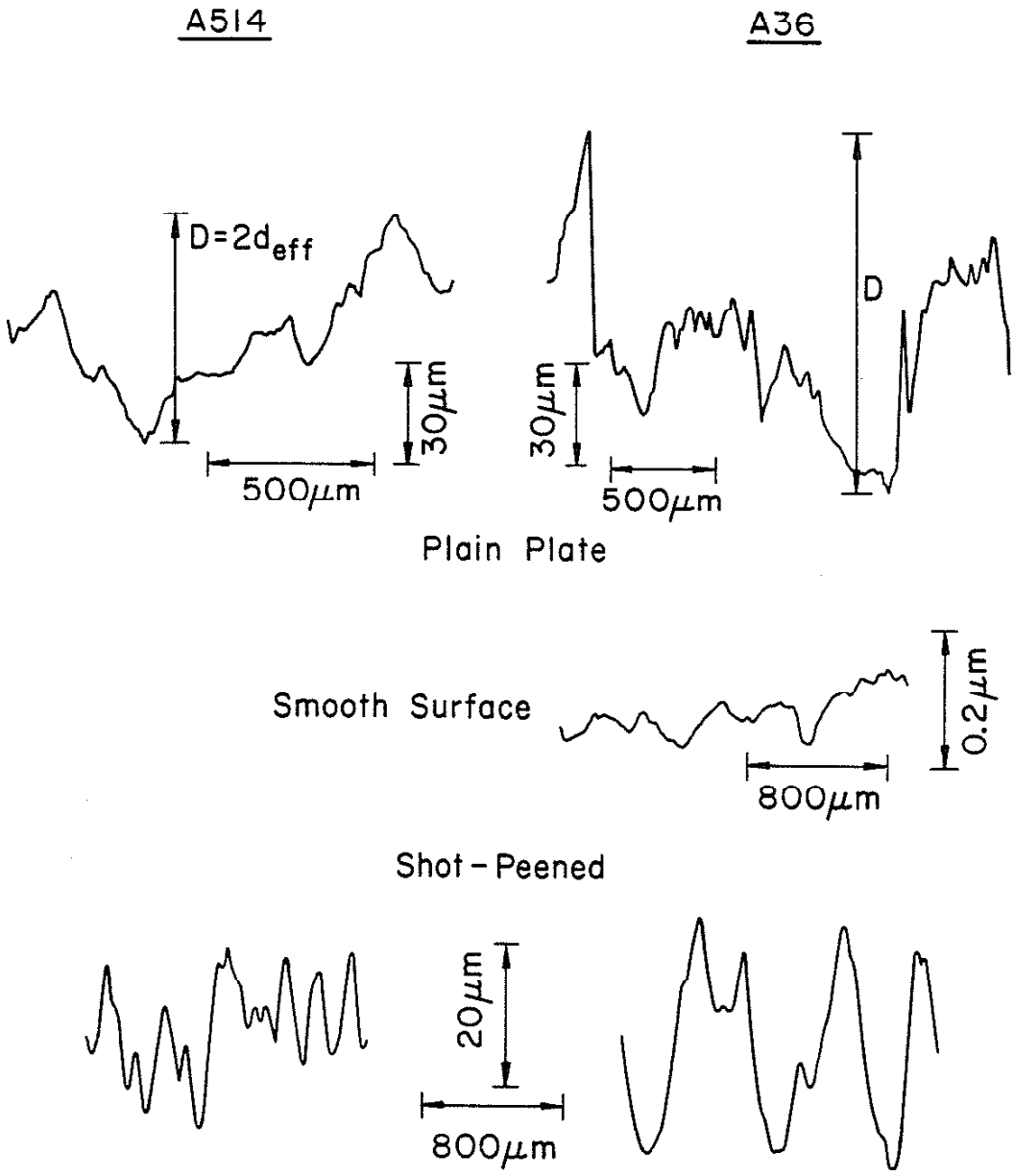

Fig. 25 Surface Roughness Profile: Plain Plate and Shot-Peened Specimens for A514 and Plain Plate, Smooth, and Shot-Peened Specimens for A36.

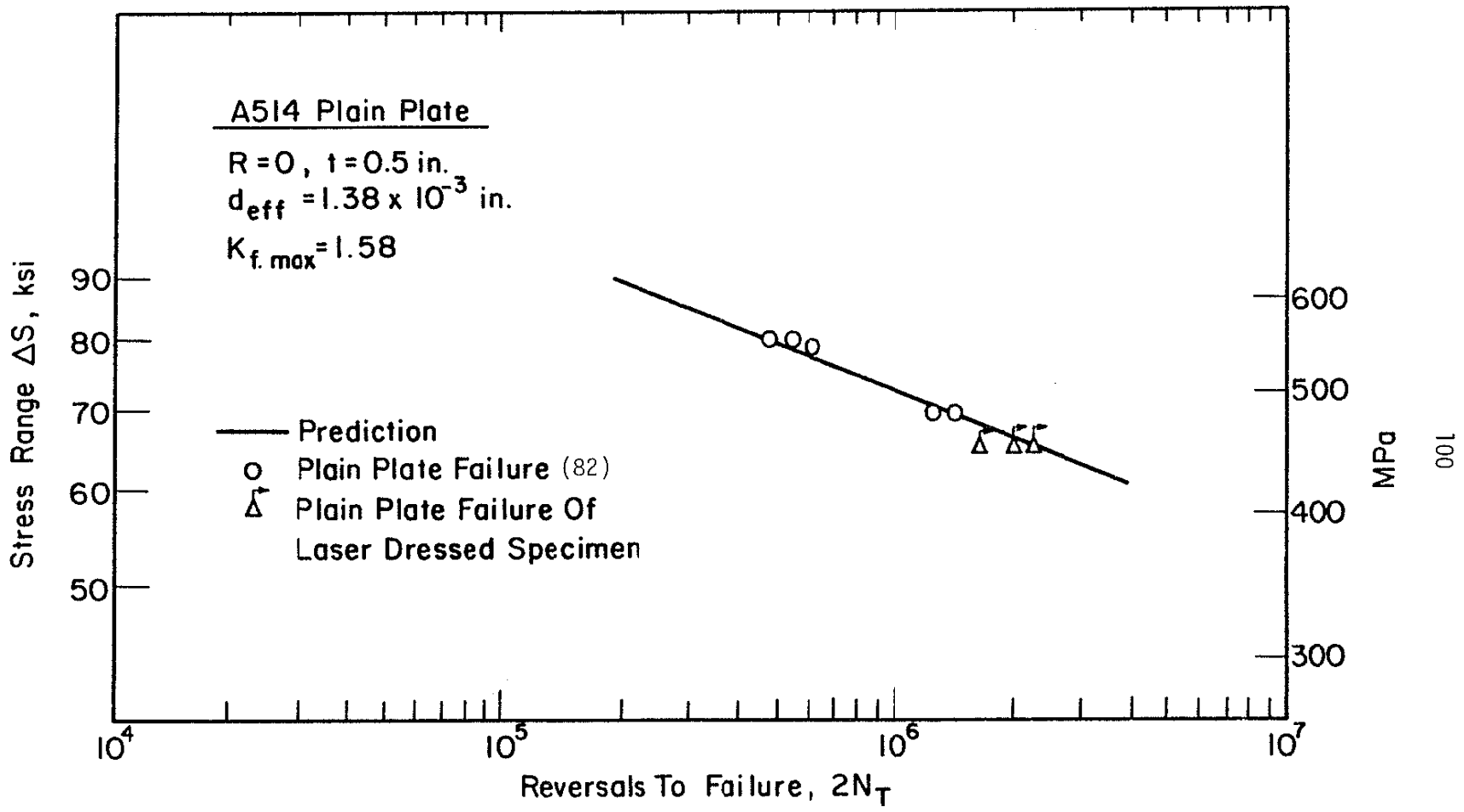

Fig. 26 Total Fatigue Life Prediction (Line) and Test Data for A514 Plain Plate (As-Received) Using K_f, max Concept Calculated from Surface Roughness Measured with Profilometer.

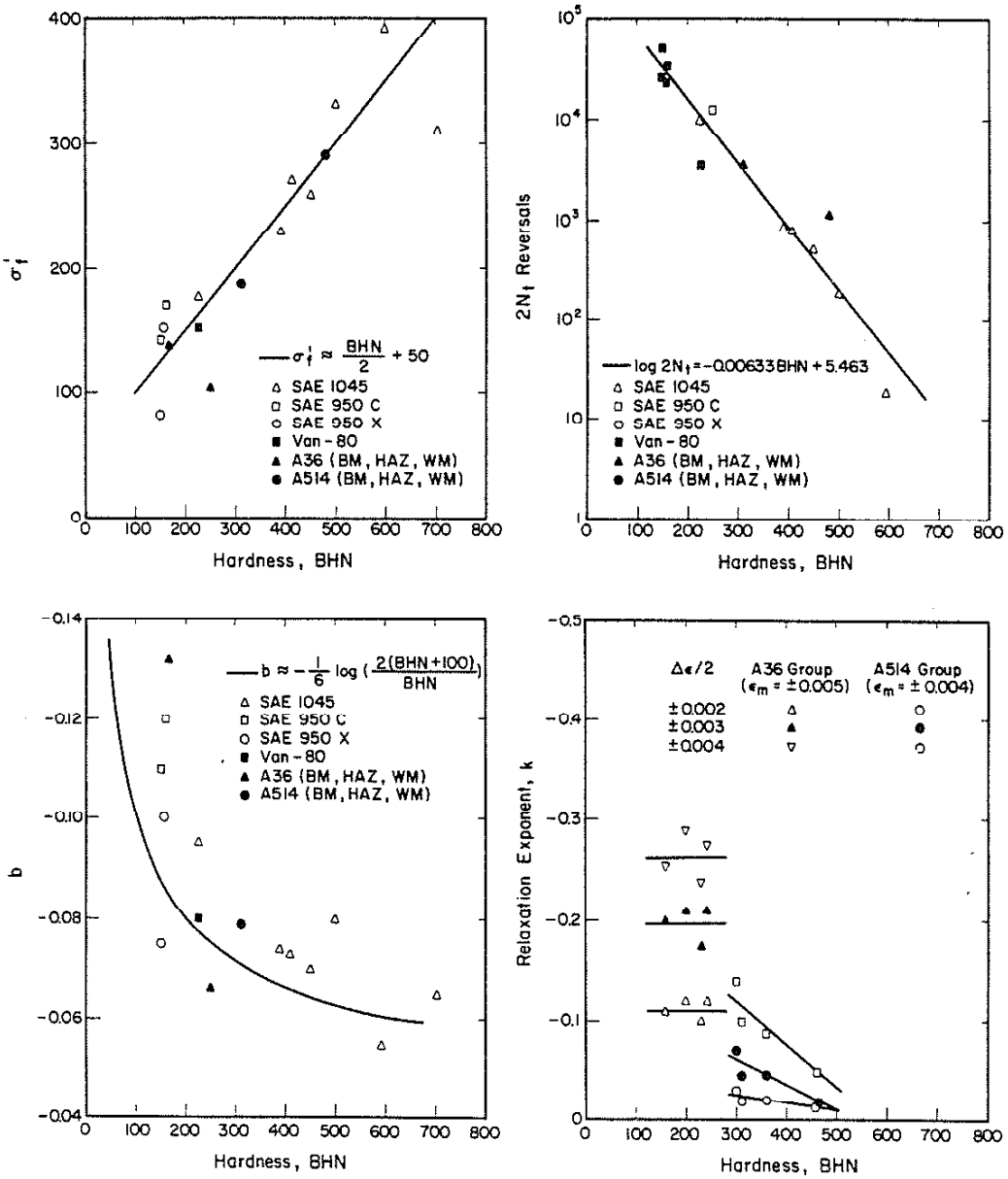

Fig. 27 Variation of σ'_f, b, $2N_{tr}$, and k with Brinell Hardness (1,71).

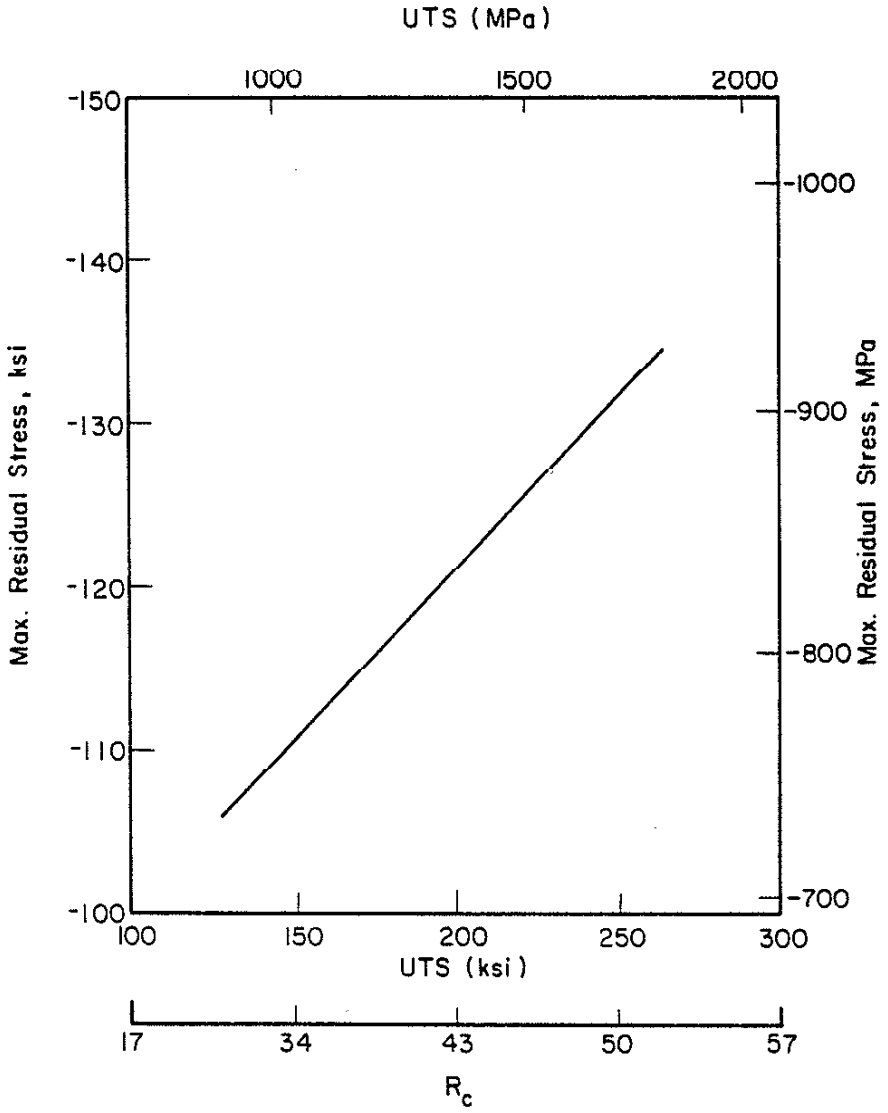

Fig. 28 Residual Stress Produced by Shot-Peening versus Tensile Strength of Steel before Peening (78).

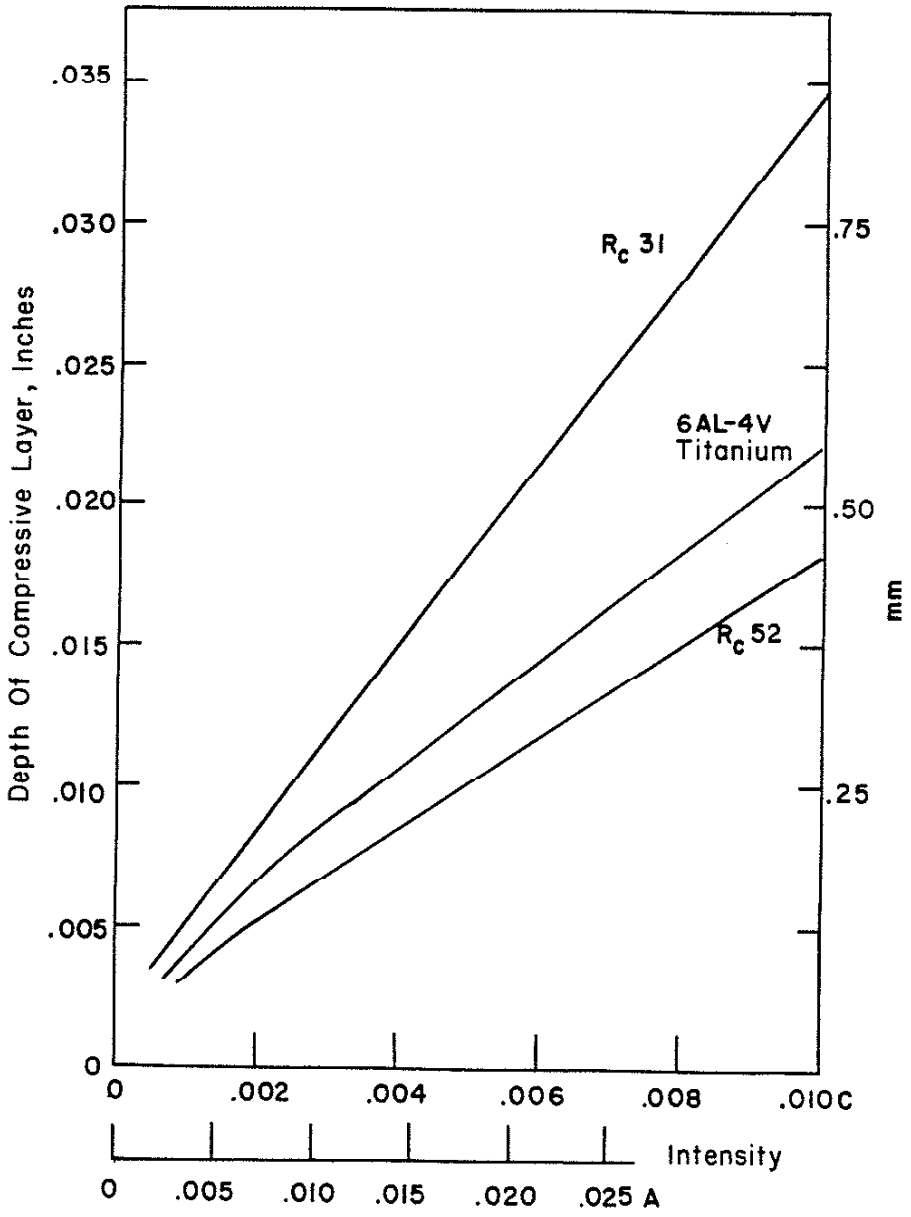

Fig. 29 Depth of Compressive Residual Stress versus Almen Intensity for Steel and Titanium (78).

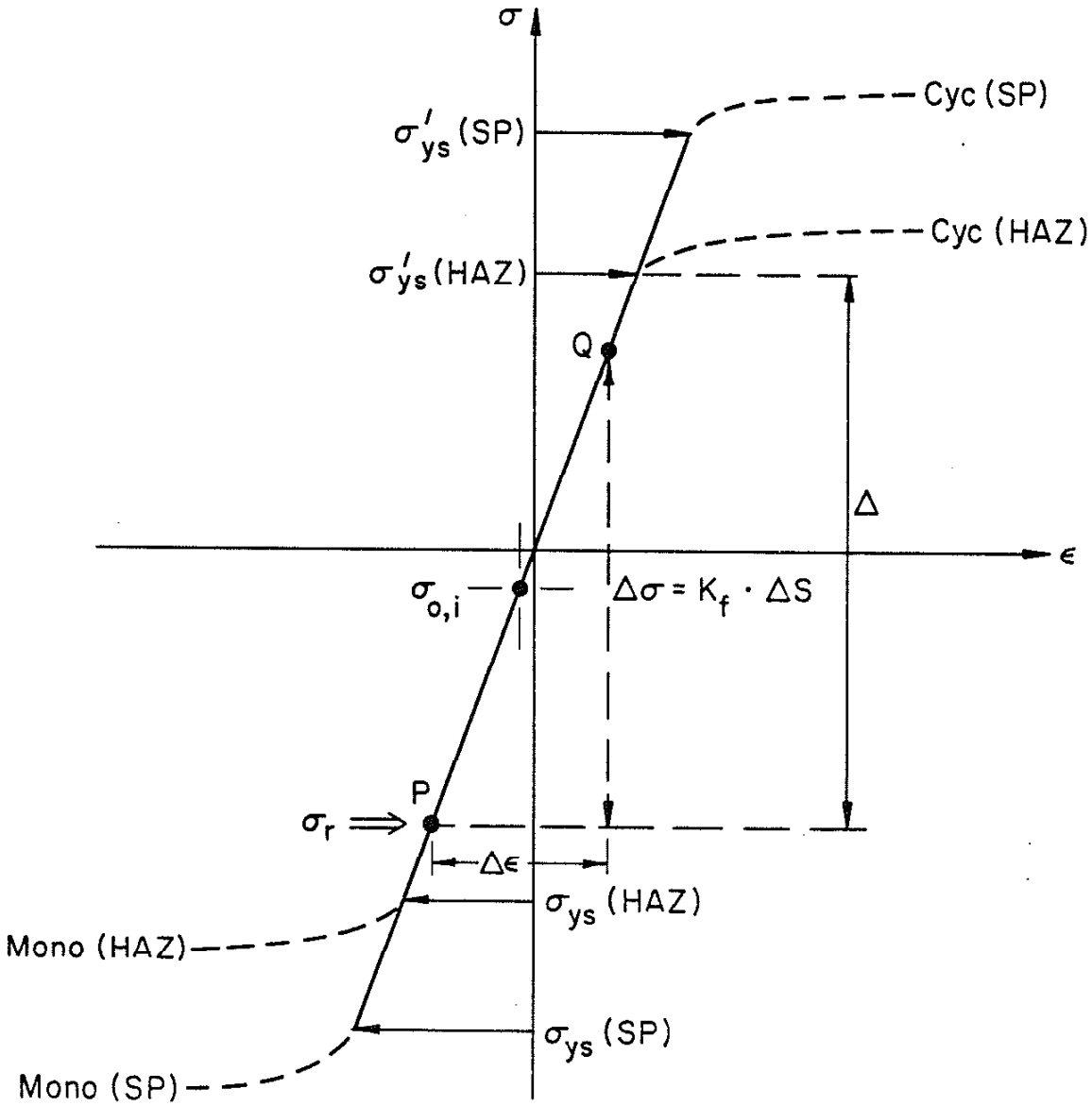

Fig. 30 Stress-Strain Response (Set-up Cycles) of Material at Shot-Peened (SP) Weld Toe Root with Residual Stress (σ_r) Showing the Determination of $\sigma_{o,i}$.

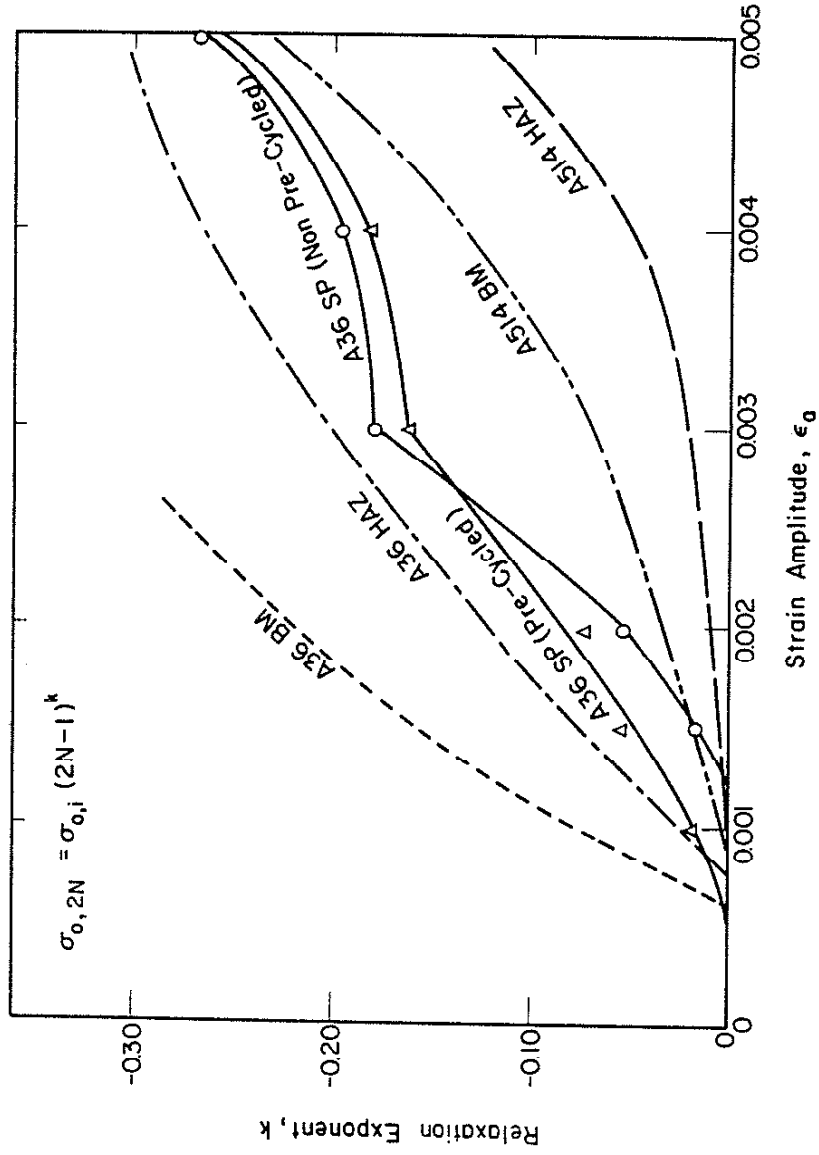

Fig. 31 Mean Stress Relaxation Exponent (k) as a Function of Strain Amplitude for the Materials Investigated. All are Pre-cycled Test Data (71) Except A36 SP (Pre-Cycled) and A36 SP (Non Pre-Cycled).

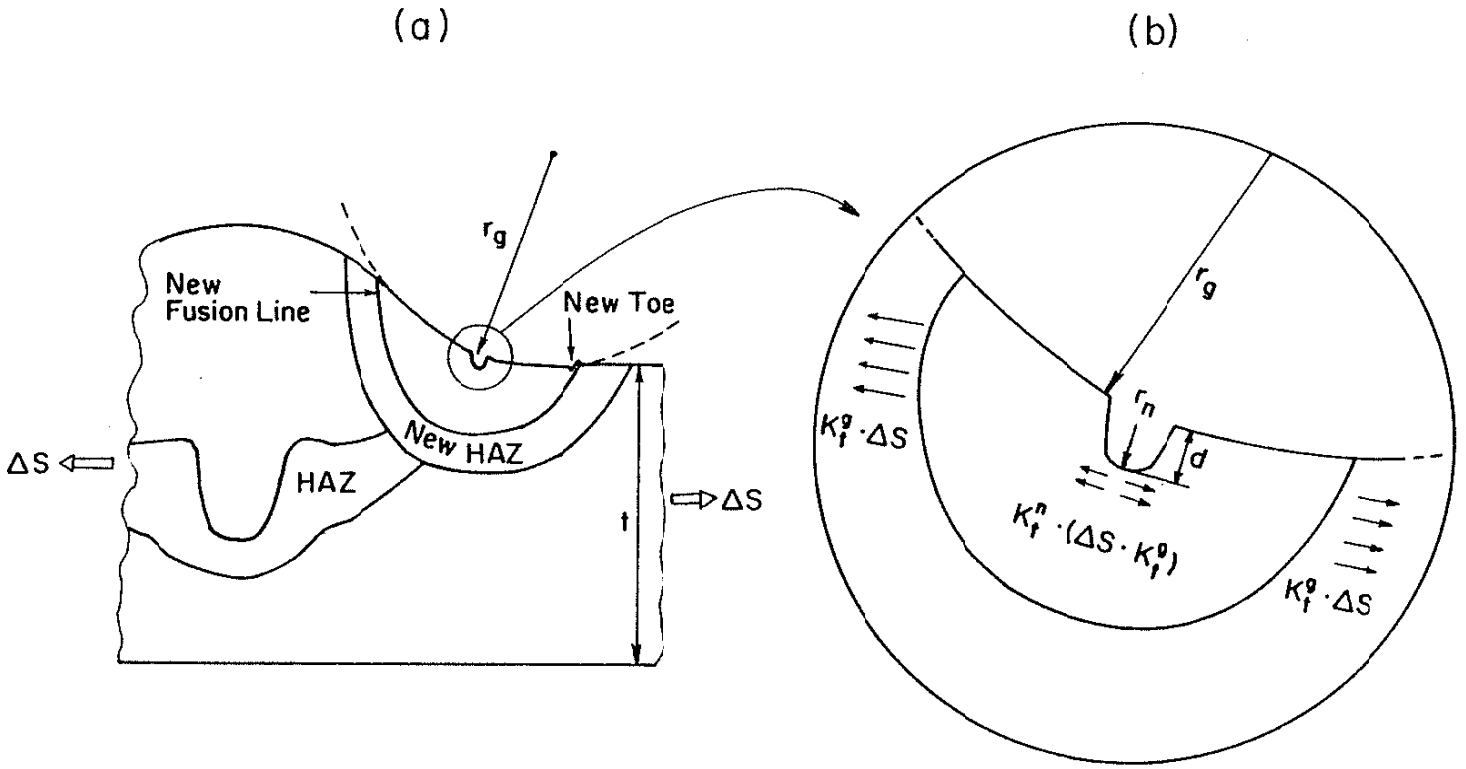

$$K_t^g = 1 + \alpha \sqrt{t/r_g}$$

$$K_t^n = 1 + 2 \sqrt{d/r_n}$$

$$K_t^s = K_t^g \times K_t^n$$

Fig. 32 Schematic diagram of Dressed Weldment: (a) Overall View of Dressed Bead (with Surface Undercut) Considered as a Geometrical Notch with Radius r_g. (b) Enlarged View of Undercut Considered as a Surface Notch Including Stress State at Notch Root with Depth (d) and Notch Root Radius (r_n).

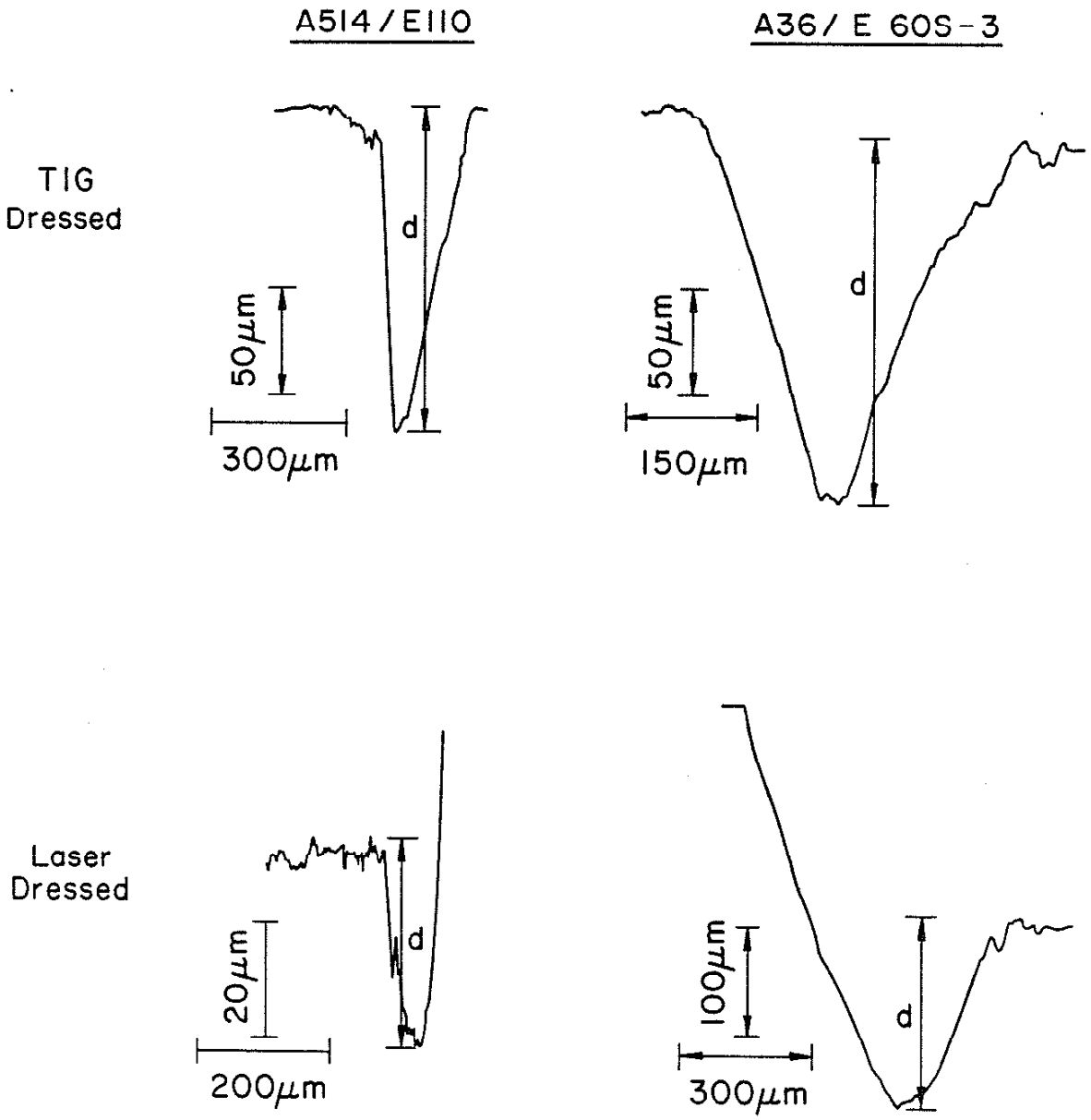

Fig. 33 Roughness Profile and Depth of Undercut at Fatigue Failure Sites: Dressed Bead for Laser-Dressed A36/E60S and New Toes for All Others.

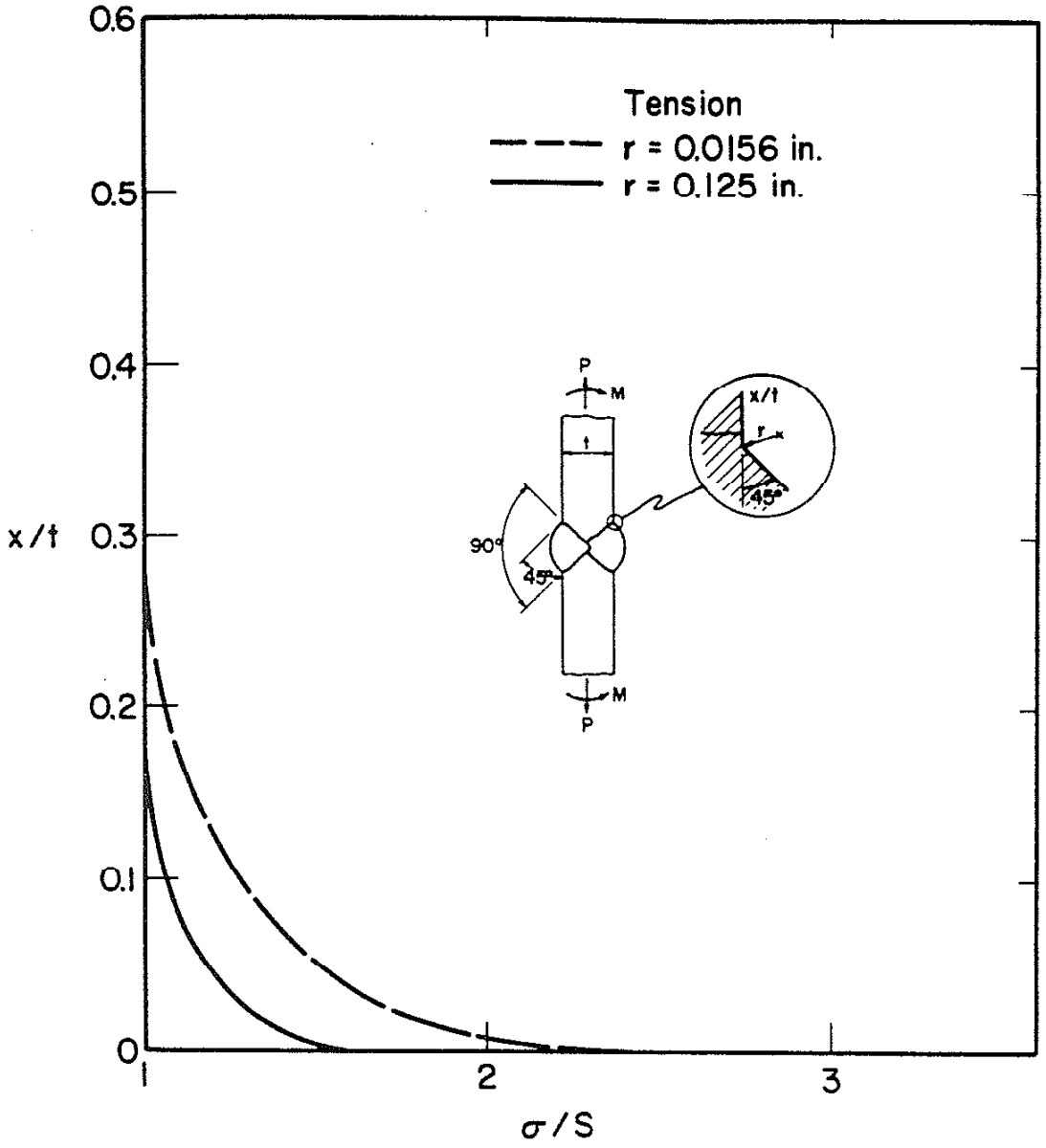

Fig. 34 Concentration of Stress at Plate Surface (σ/S) as a Function of Distance from the Weld Toe (x/t) for Double-V Butt Weld, Tension (80).

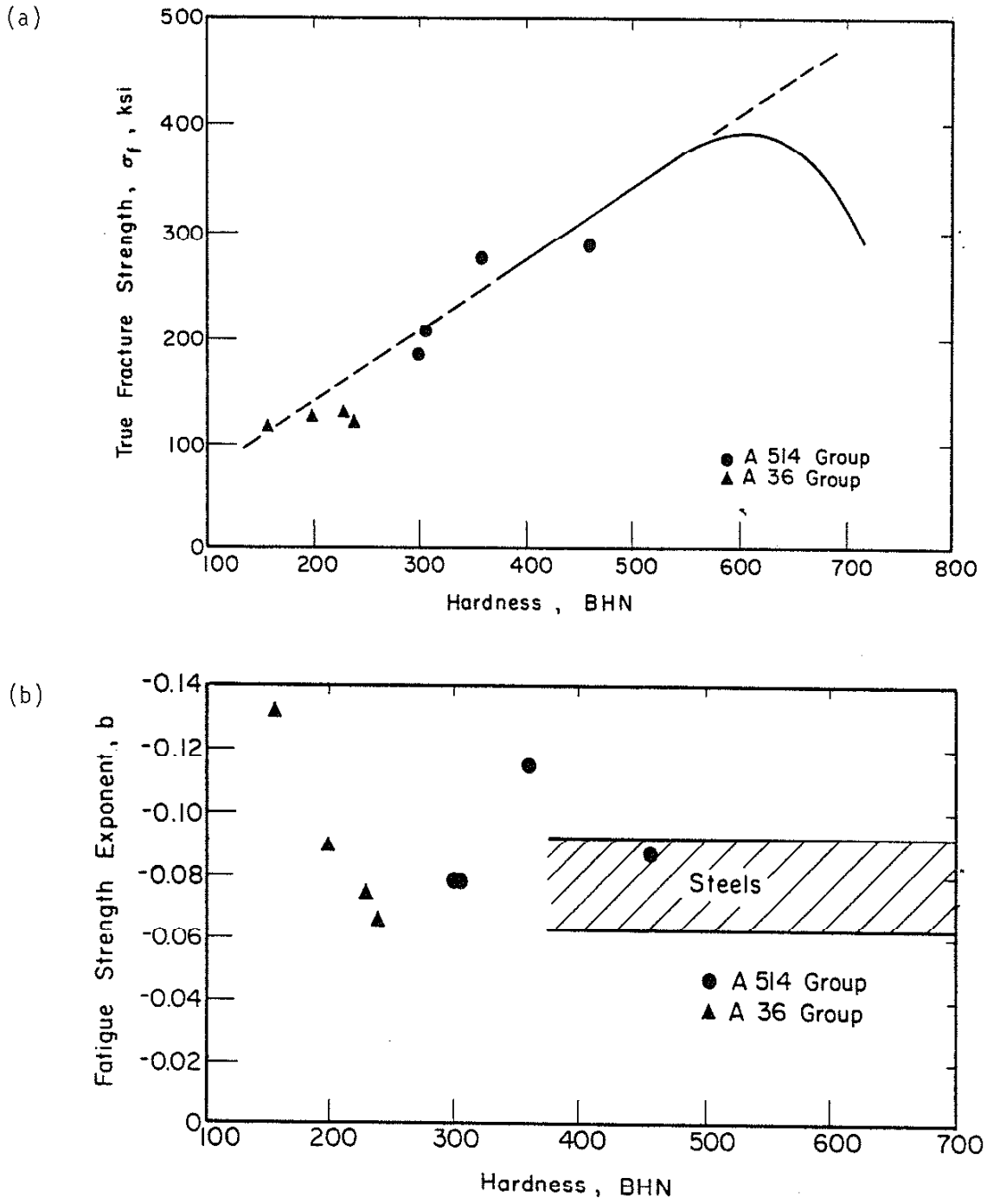

Fig. 35 Fatigue Properties as Functions of Hardness (71):
(a) True Fracture Strength as a Function of Hardness.
(b) Fatigue Strength Exponent as a Function of Hardness.
A36 Group Does Not Follow the General Trends in Both Fatigue Properties.

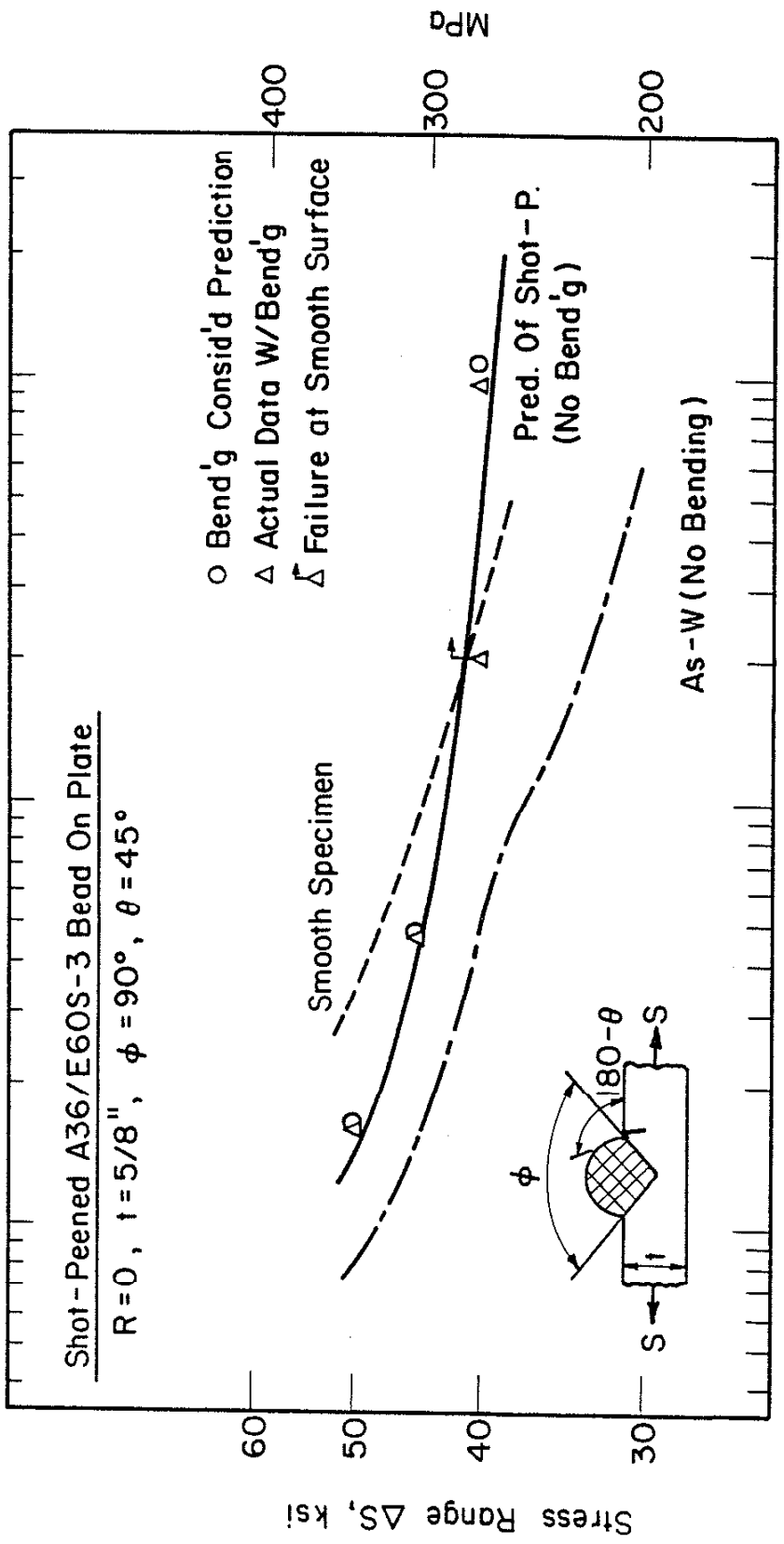

Fig. 36 Total Fatigue Life Predictions (Lines) with and without Bending Being Considered and Experimental Results of Stress Control (R = 0) Fatigue Test for Shot-Peened A36/E60S Bead on Plates.

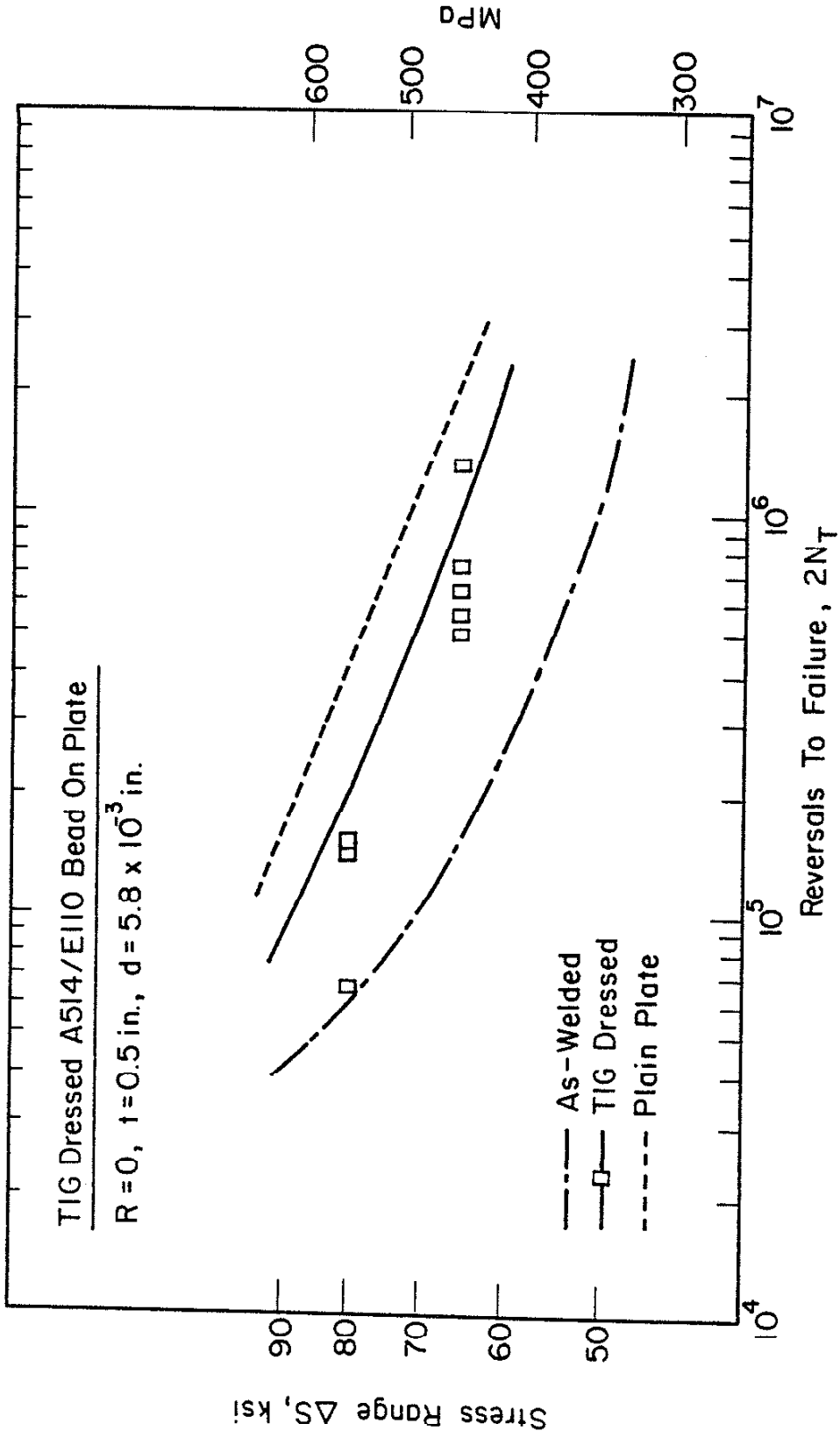

Fig. 37 Total Fatigue Life Predictions (Lines) and Experimental Results for Stress Controlled (R = 0) Fatigue Test of TIG Dressed A514/E110 Bead-on-Plate Specimens (Bending Stress Was Not Considered in the Prediction).

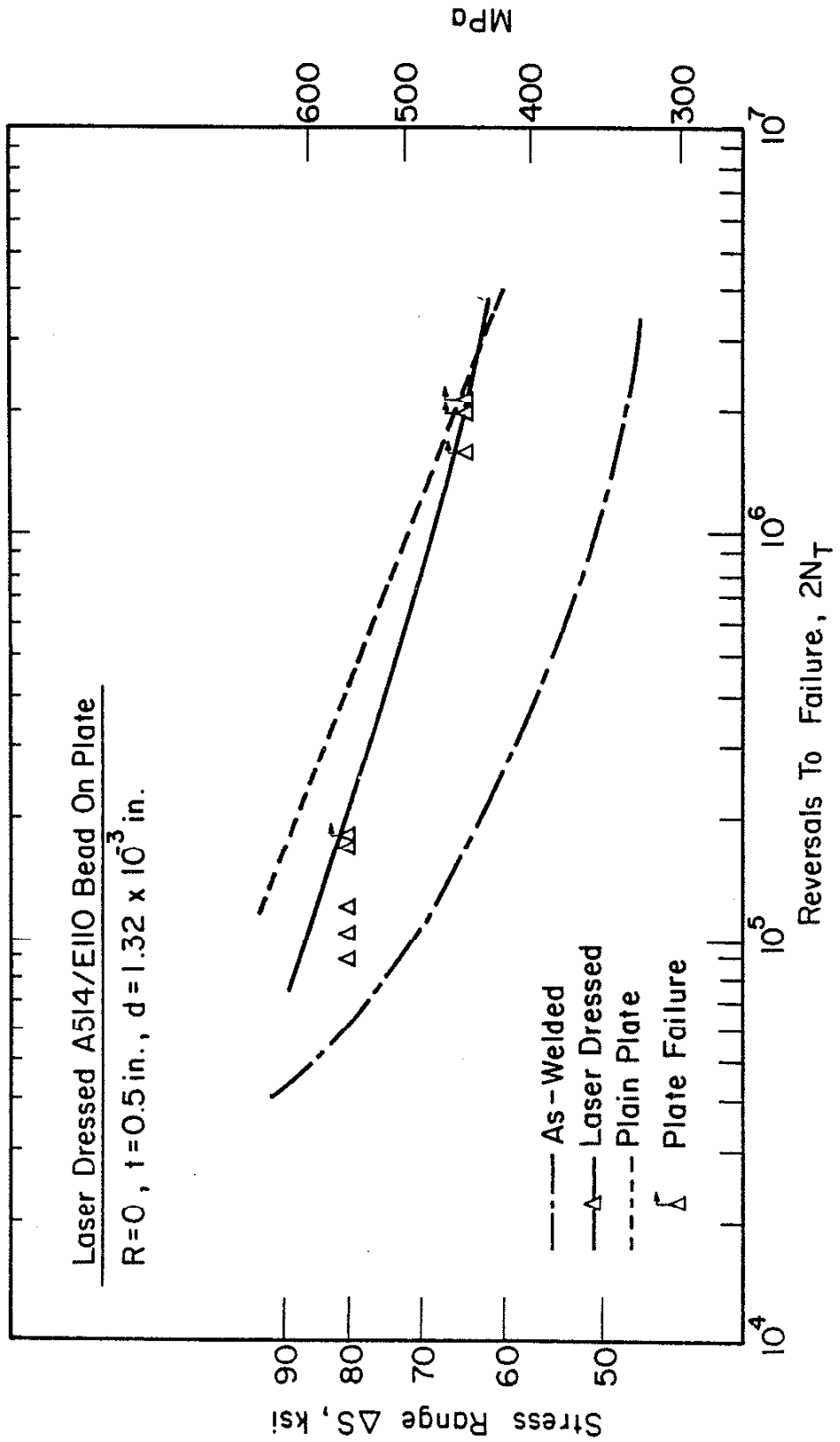

Fig. 38 Total Fatigue Life Predictions (Lines) and Experimental Results of Stress Controlled (R = 0) Fatigue Test for Laser-Dressed A514/E110 Bead on Plate (Bending Stress Was Not Considered in the Prediction).

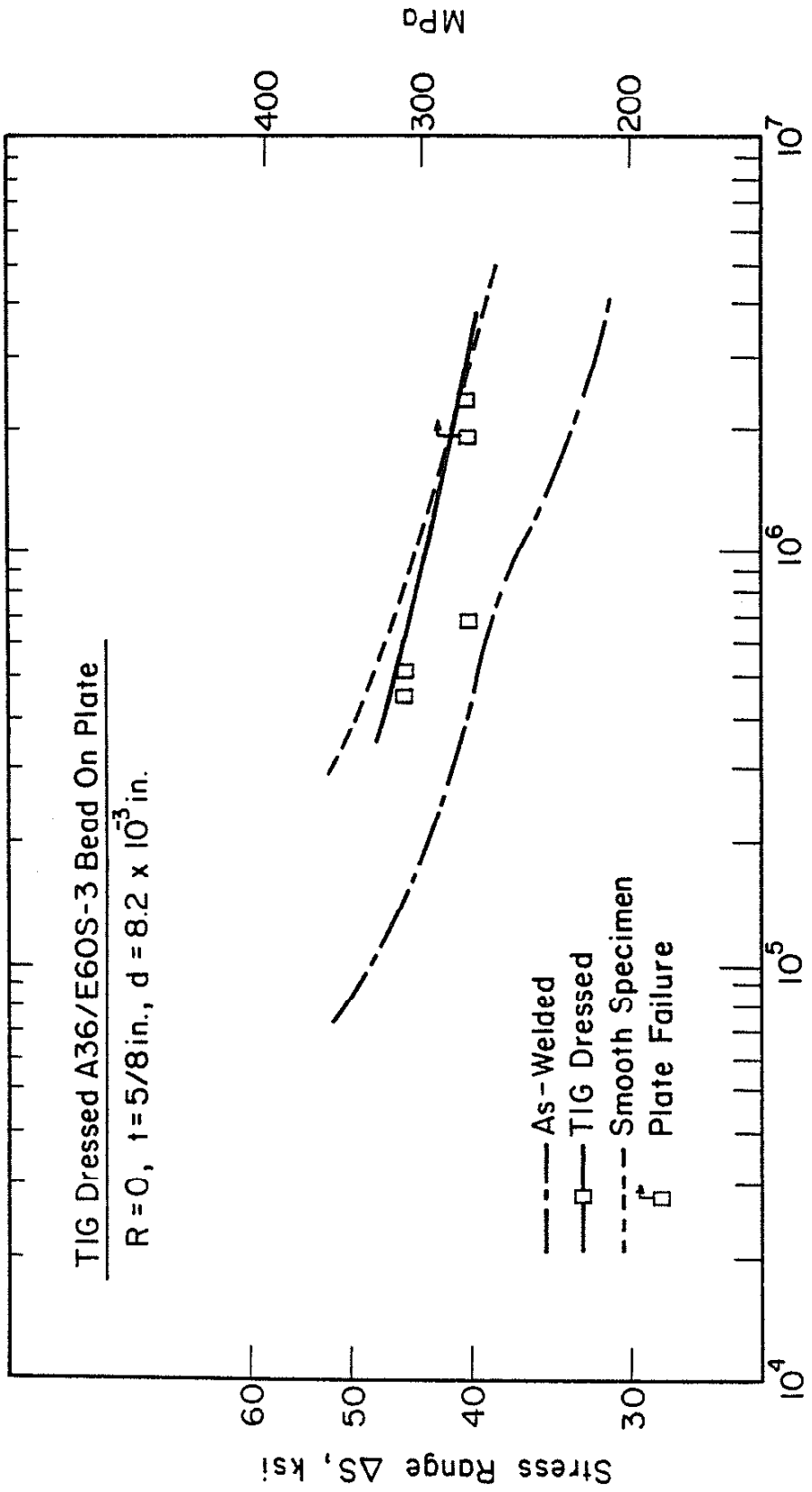

Fig. 39 Total Fatigue Life Predictions (Lines) and Experimental Results of Stress Controlled (R = 0) Fatigue Test for TIG-Dressed A36/E60S Bead on Plate (Bending Stress Was Not Considered in the Prediction).

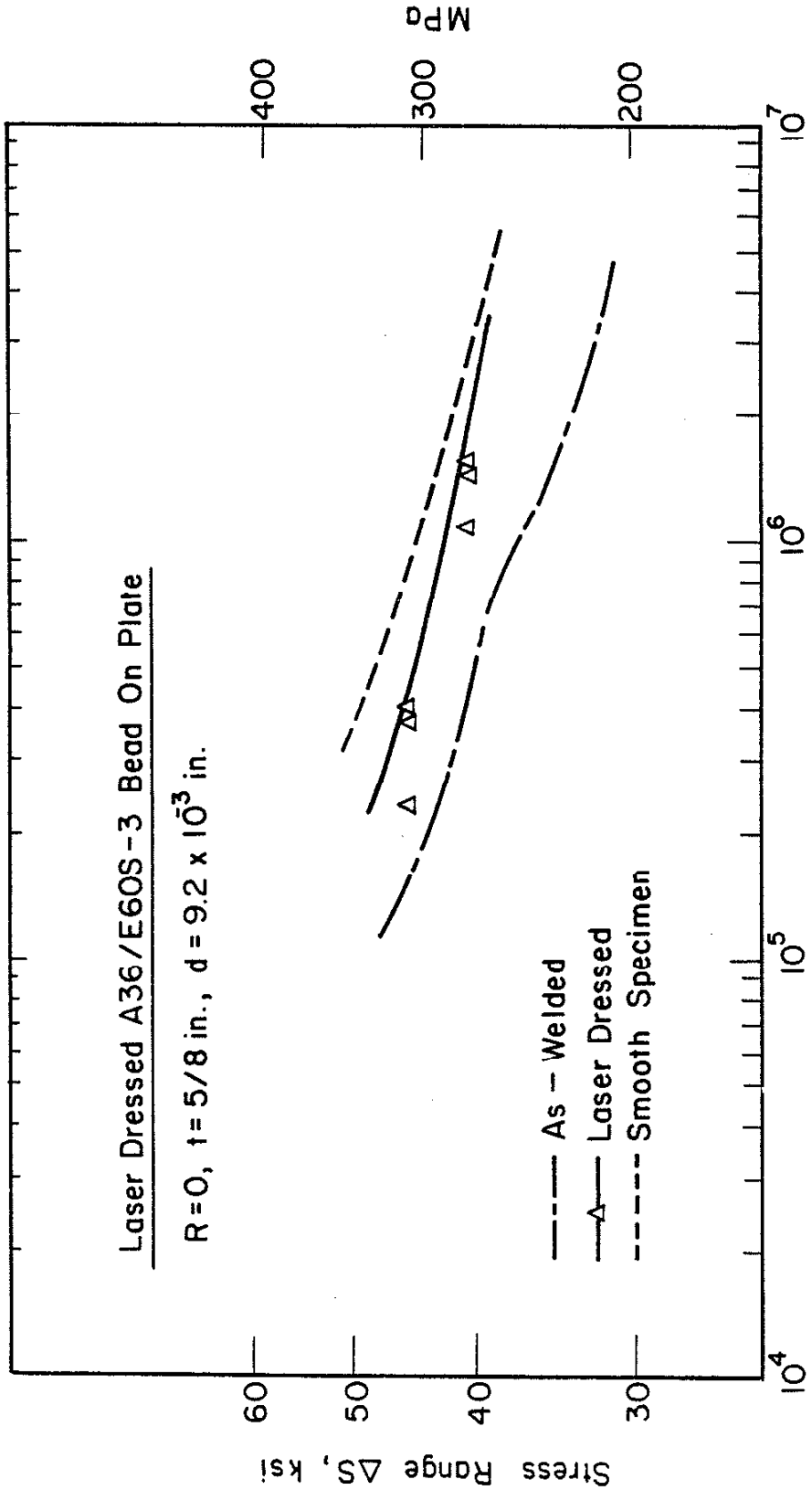

Fig. 40 Total Fatigue Life Predictions (Lines) and Experimental Results of Stress Controlled (R = 0) Fatigue Test for Laser-Dressed A36/E60S Bead on Plate. Bending Stress Was Not Considered in the Prediction. All Failures Occured Not at New Toe But at Laser-Dressed Beads.

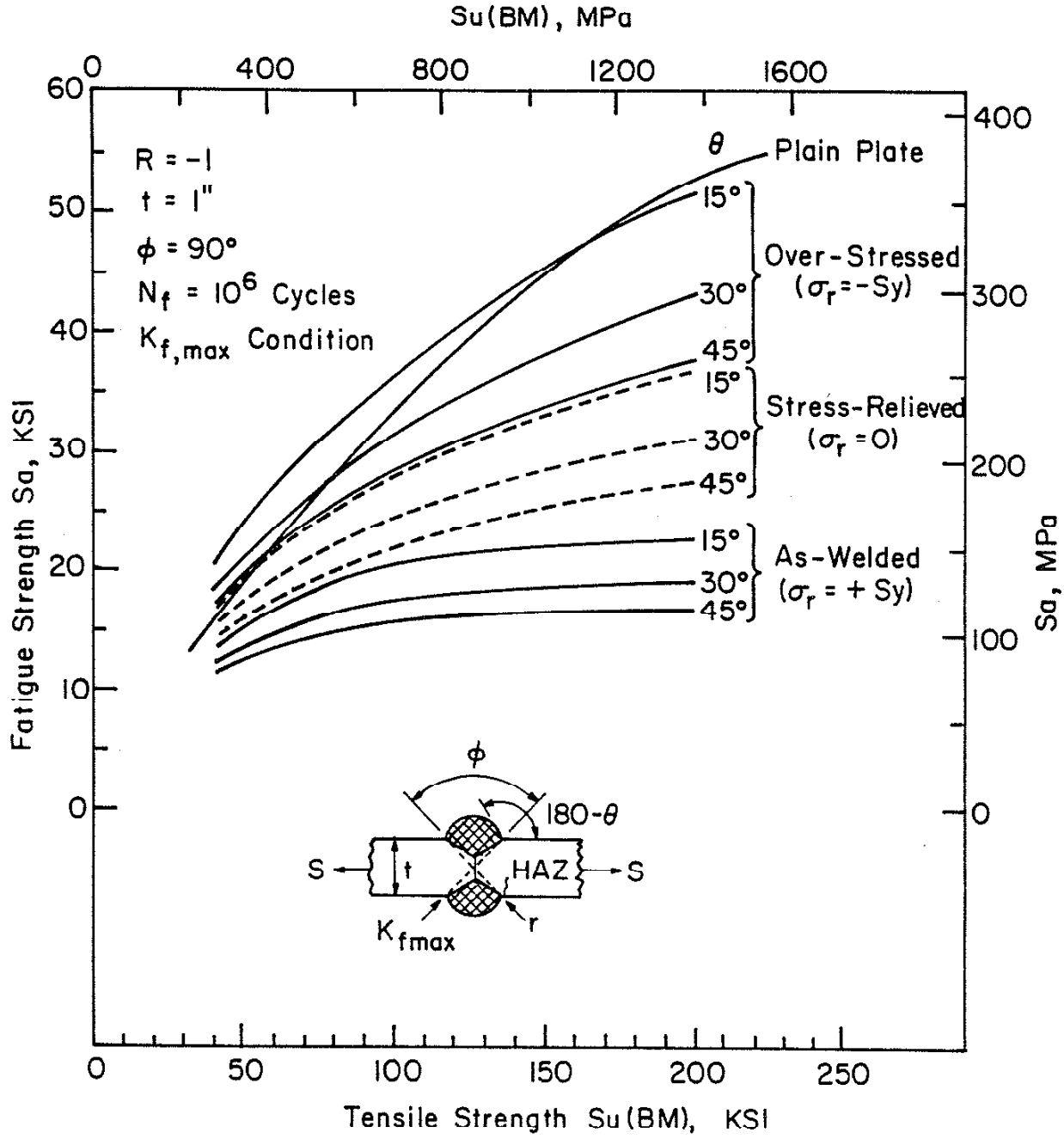

Fig. 41 Predicted Influence of BM Ultimate Tensile Strength and Flank Angle (θ) on the Fatigue Strength of Several Kinds of Post-Treated Butt Weldments (Hot-Rolled Steels) at 10^6 Cycles (ϕ = 90°, R = -1).

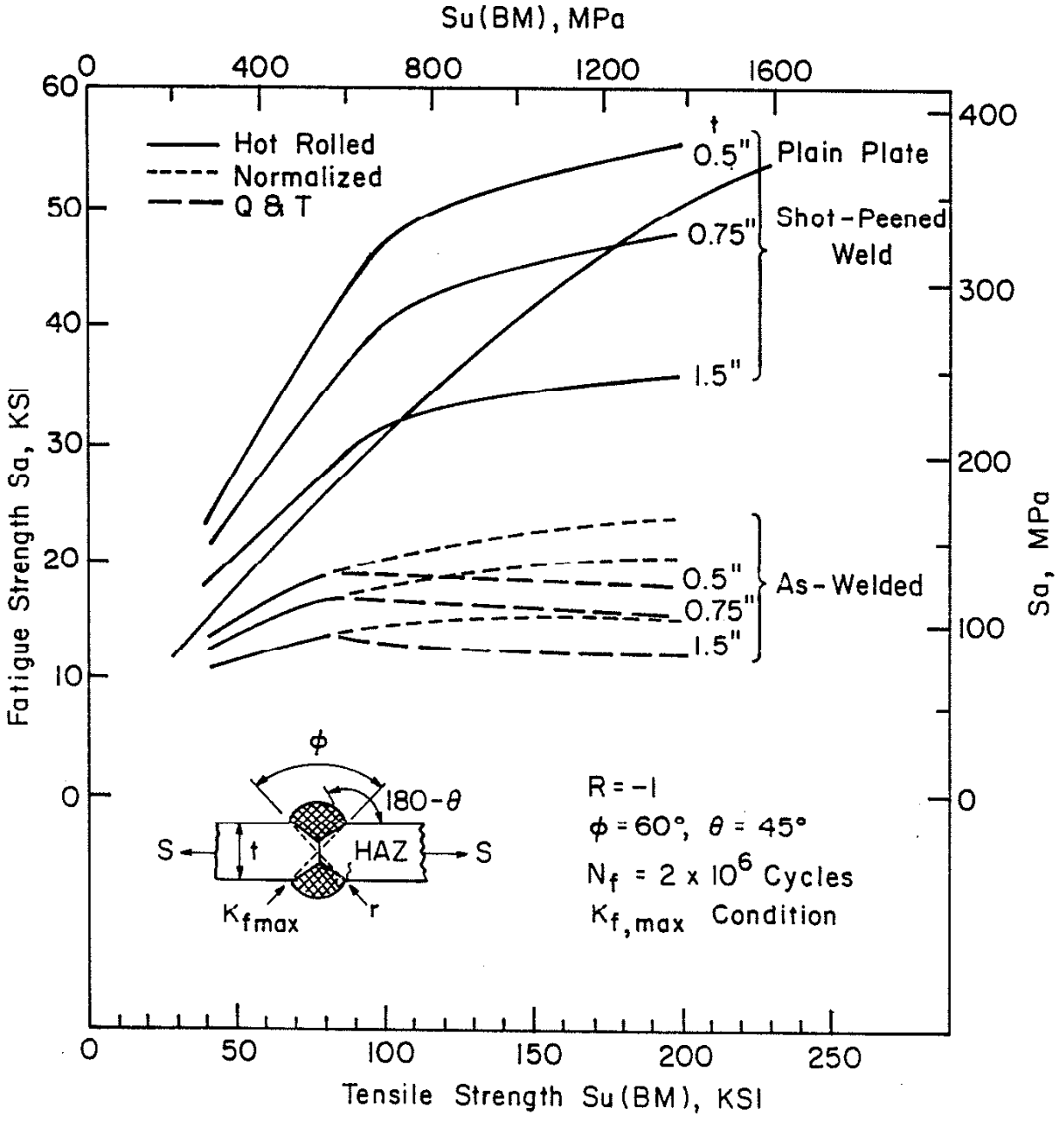

Fig. 42 Predicted Effect of Thickness (t) of Weldment on Fatigue Strength as Function of BM Tensile Strength for As-Welded and Shot-Peened Weldments (R = -1).

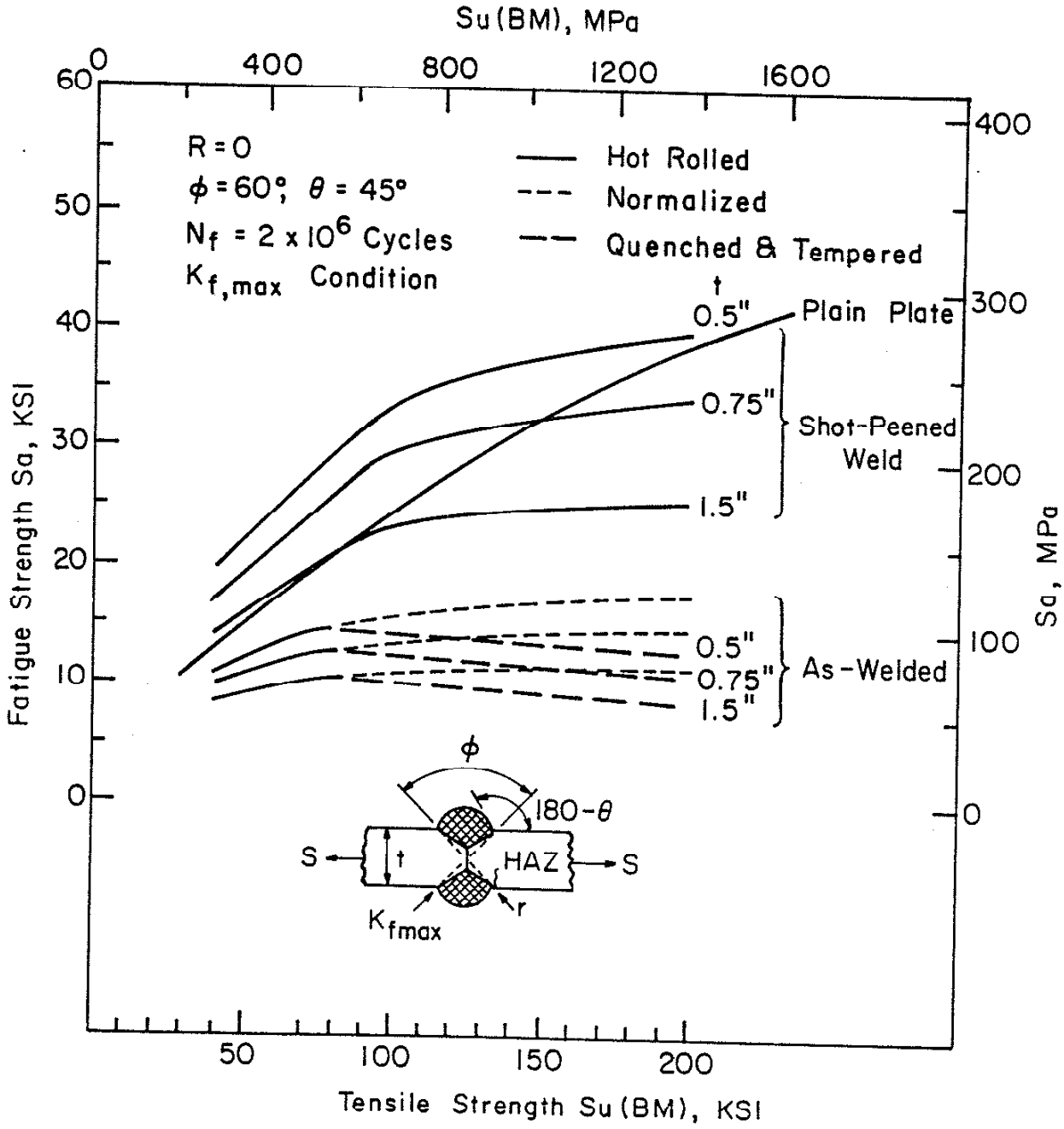

Fig. 43 Predicted Effect of Thickness (t) of Weldment on Fatigue Strength as Function of BM Tensile Strength for As-Welded and Shot-Peened Weldments (R = 0).

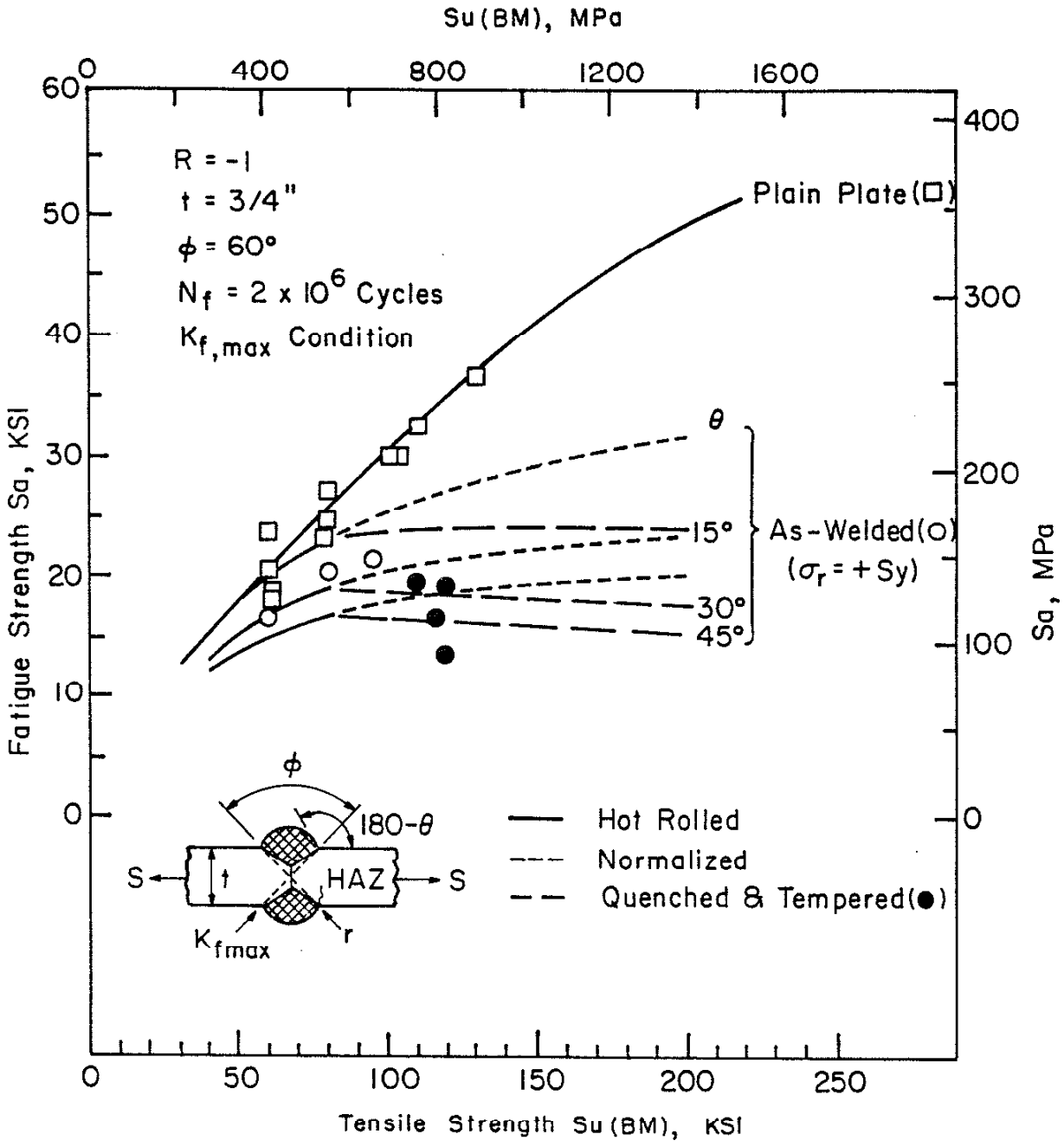

Fig. 44 Predictions and Actual Data for Fatigue Strength of Plain Plate and As-Weld as Function of BM Ultimate Tensile Strength for Steels (R = -1, t = 3/4").

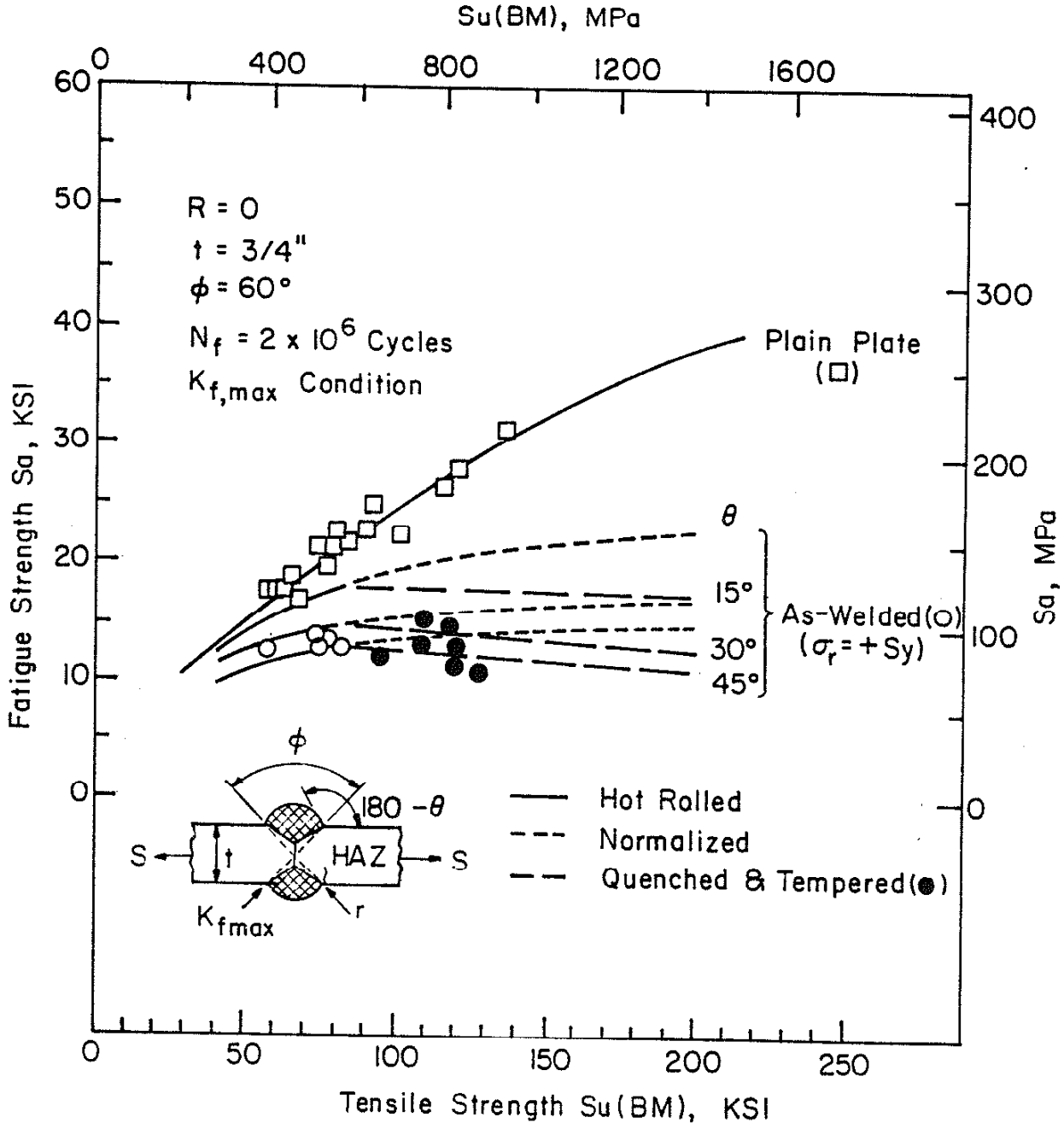

Fig. 45 Predictions and Actual Data for Fatigue Strength of Plain Plate and As-Weld as Function of BM Ultimate Tensile Strength for Steels (R = 0, t = 3/4").

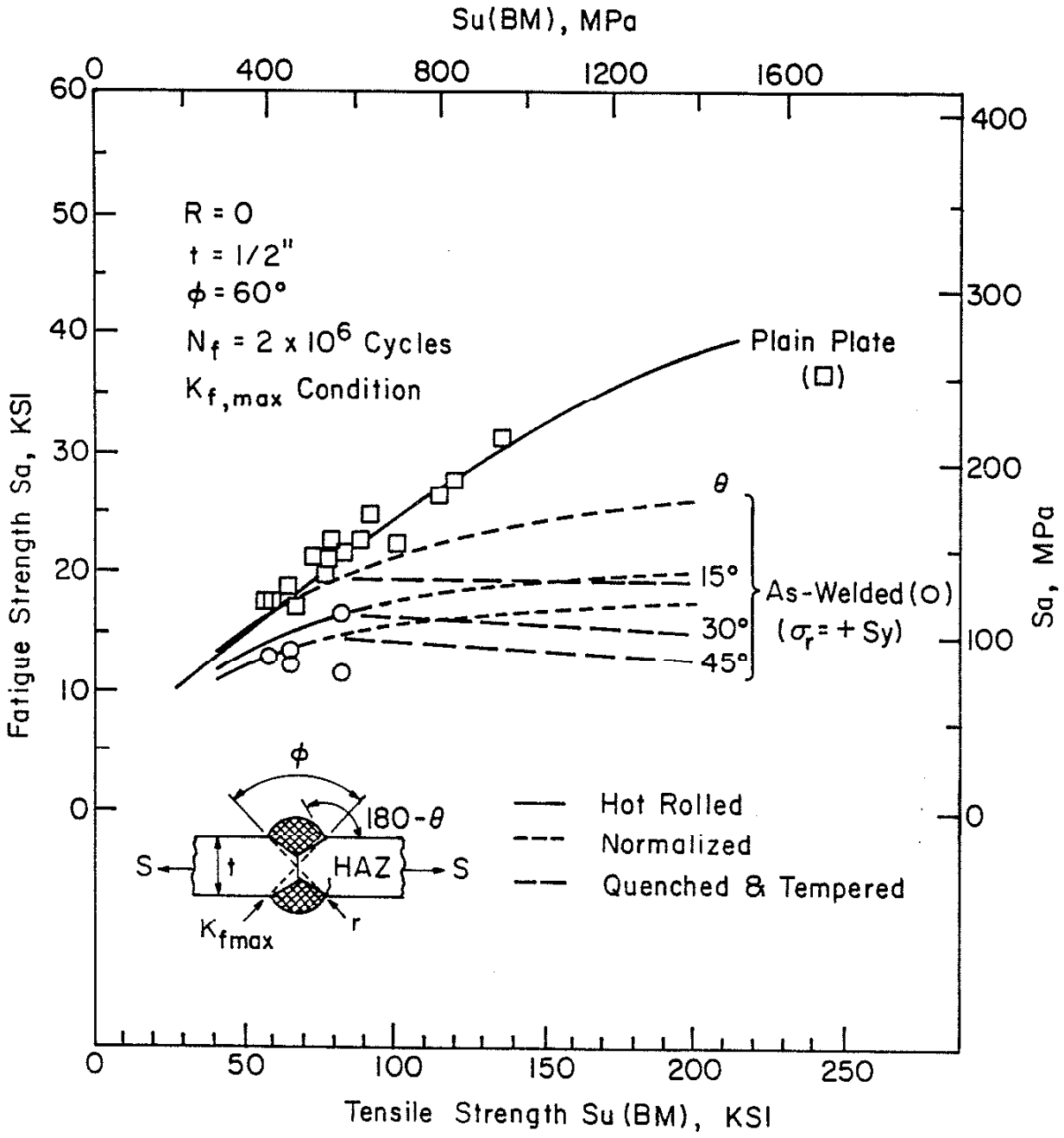

Fig. 46 Predictions and Actual Data for Fatigue Strength of Plain Plate and As-Weld as a Function of Su(BM) for Steels (t = 1/2", R = 0).

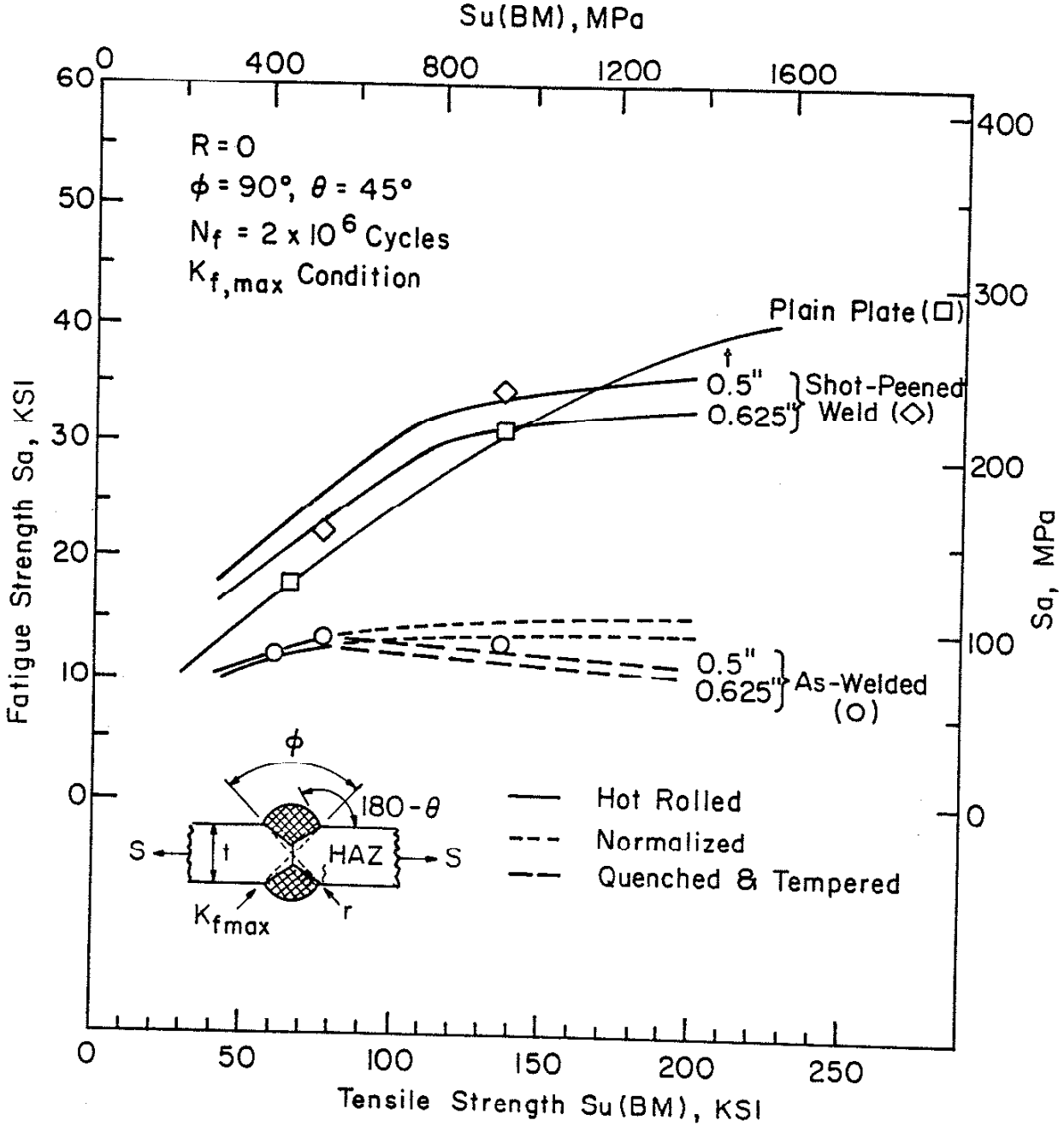

Fig. 47 Predictions and Test Data of Fatigue Strength for As-Weld and Shot-Peened Weldments.

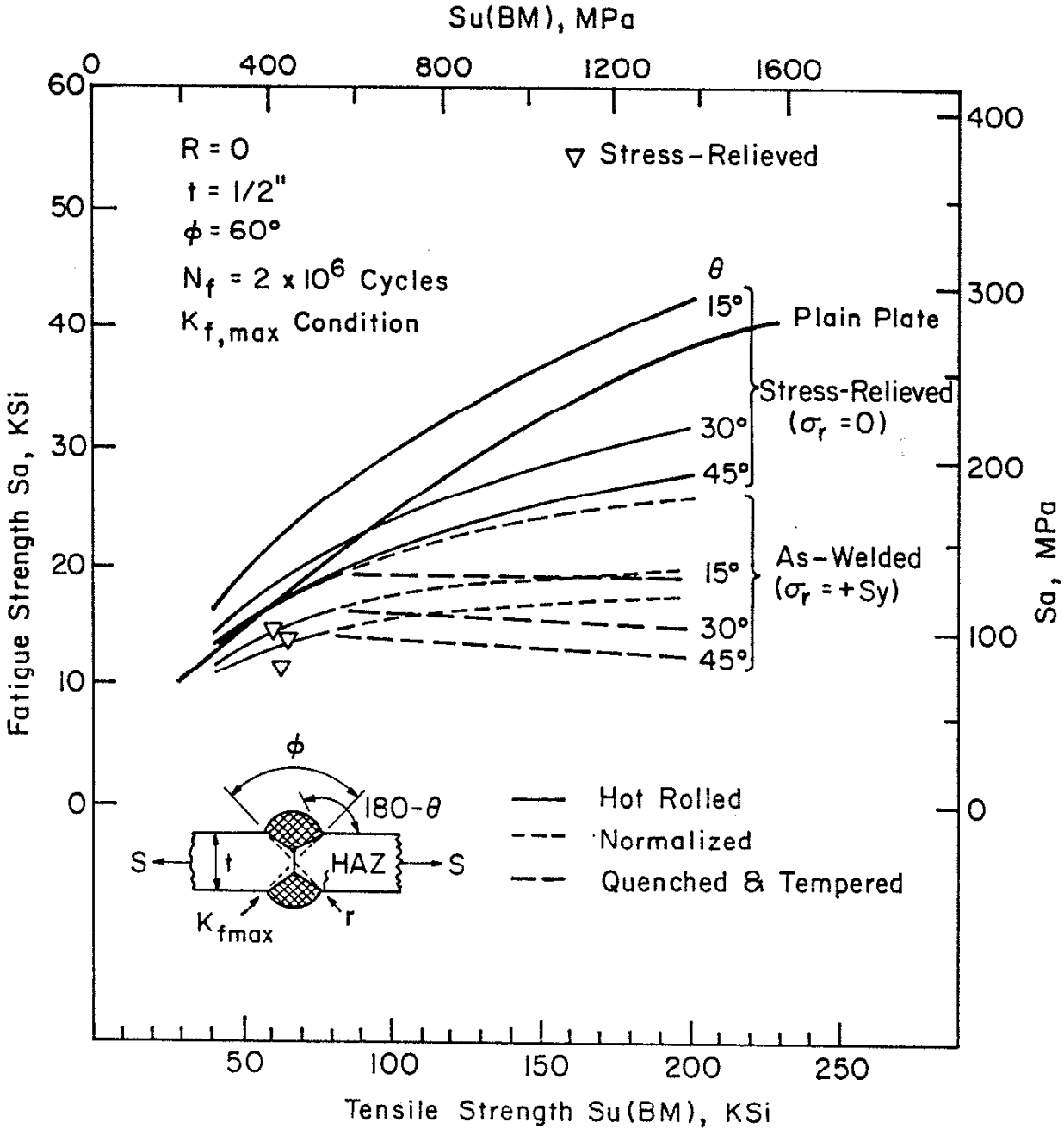

Fig. 48 Predictions and Actual Data for Fatigue Strength of Stress-Relieved Weldments for Steels (t = 1/2", R = 0).

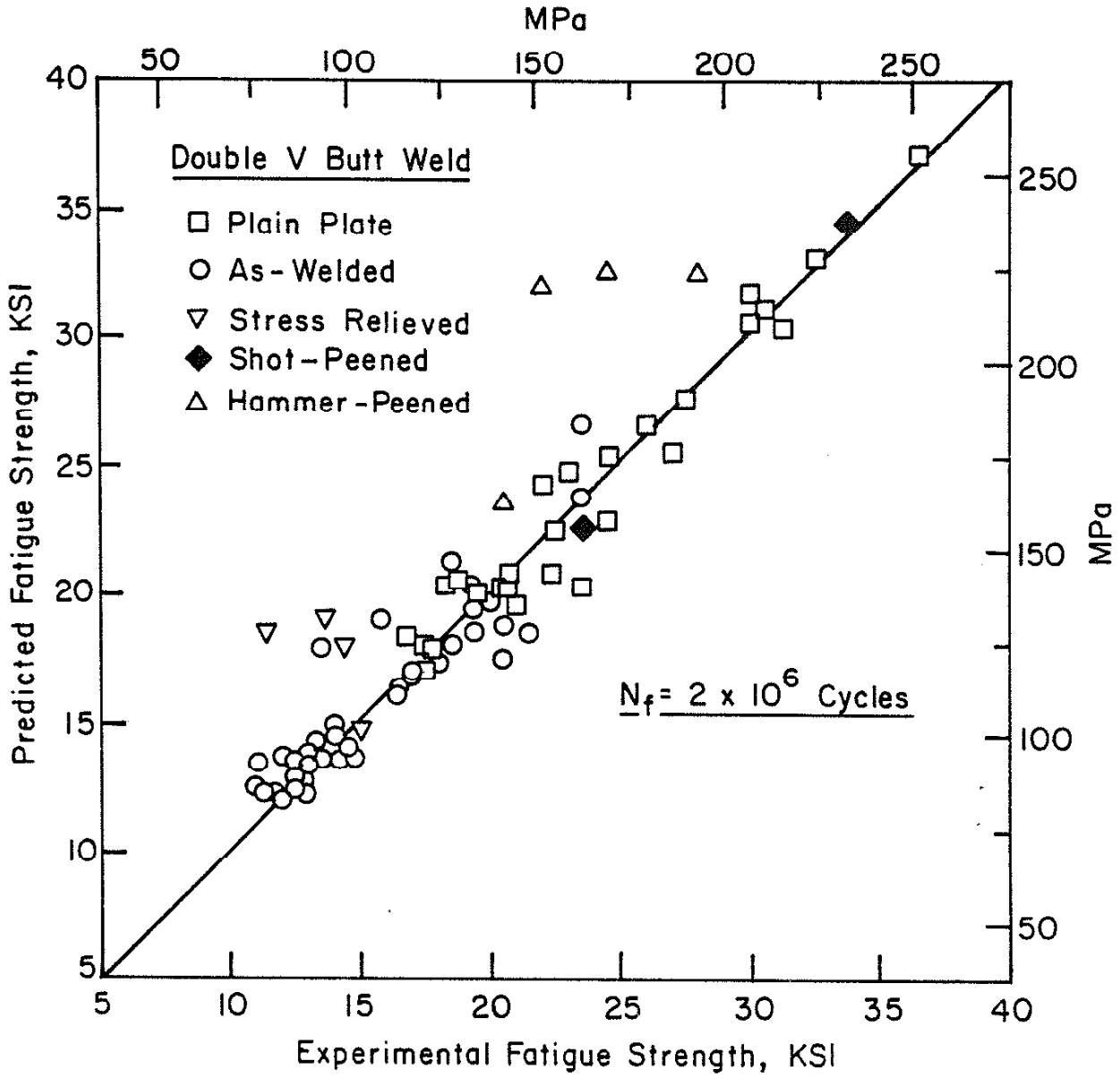

Fig. 49 Comparison of Predicted Fatigue Strength with Experimental Data.

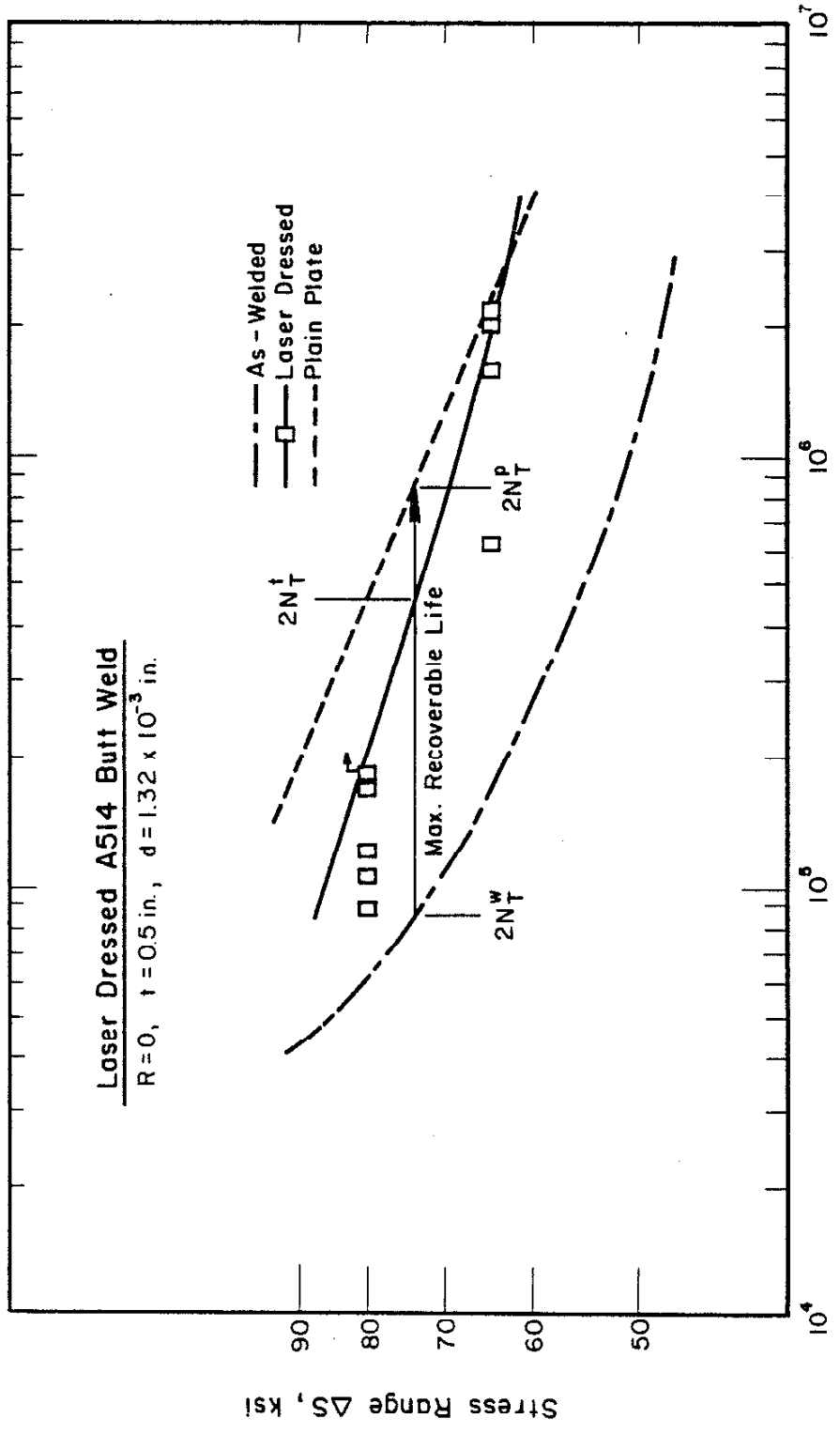

Fig. 50 The Maximum Recoverable Life (MRL) and Recovered Life (RL) for A514/E110 Butt Weldments. Laser-Dressed A514 Butt Weldments Show Complete Recovery at and below 65 ksi. $2N_T^W$: As-Weld, $2N_T^l$: Post-Treated Weld, $2N_T^p$: Plain Plate.

APPENDIX A

THE OBSERVATIONS IN DEVELOPING LASER-DRESSING PROCESS

The laser was utilized to remelt the weld toe in a controlled manner in order to improve the toe geometry, and thus to cause an increase in the weld fatigue life. Murzyn, a coworker in developing the laser dressing process, conducted a series of preliminary tests and discussed the process parameters which needed to be defined and optimized for laser-dressing process (86):

1. Beam Characteristics
    a. Power
    b. Spot size and shape (area of beam impingement upon surface)
    c. Angle of incidence
    d. Impingement location
2. Specimen Characteristics
    a. Surface condition and coating
    b. Surface inclination with respect to horizontal
    c. Traverse speed
3. Inert gas delivery system
    a. Gas type
    b. Direction and flow characteristics

At reasonable traverse speeds, the depth of remelted region was varied with the factors (beam power, traverse velocity, spot size) which determined the amount of heat input per unit volume and time, while the width was naturally determined by the spot size. Surface roughness, that is the magnitude and the spacing of surface ripples, decreased with higher traverse velocities due to fewer perturbations in the travel velocity and lesser

vibrations of the moving panel, but increased with lower beam energies due to an increase in the spattering of the molten metal. The laser dressing process (and the TIG dressing process, as well) produced some undercut at new toes. The most generous weld toe curvature without any noticeable undercutting resulted from directing the laser beam at the specimen with the proper angle.

The curvature of the remelted zone and tendency to undercut were extremely sensitive to the position of the beam on the surface of the work with respect to the old toe. As found by Kado et al. (28) for TIG-dressing, the least undercut and greatest curvature resulted when the beam center was approximately 0.04 inches away from the old toe: see Fig. 6. In general, it was important to keep the amount of remelted metal large enough to fill in the old toe but not so large as to overflow and create a new toe with considerable steepness and/or undercut.

The geometrical consistency along the length of the original toe was another important factor influencing the geometry of the new toe. The many irregularities along the old toe required a large spot size accompanied by a higher beam power to remelt sufficient metal to eliminate the effect of these irregularities on the new toe curvature. The A36/E60S weldments which exhibited a larger flank angle required a more dispersed beam of higher power (Table 7) to remelt sufficient metal. The presence of slag (from the welding process) caused spattering and irregularities in the remelted toe, which could be eliminated by wire-brushing the toe before dressing. A thin coat of ultra-flat black paint (or similar coating) prior to dressing reduced the reflection of the incident beam (87).

The complete shielding of the regions which were molten or still at a reasonably high temperature during the process was an extremely important factor in producing an oxide-free surface. A proper shielding produced glassy beads which resulted from the slag in weld metal and this residue could be easily removed.

APPENDIX B

CROSS-ROLLING FOR SIMULATION OF SHOT-PEENING AND ITS SMOOTH SPECIMEN TESTS

B.1 Specimen

A36 steel plates of 5/8 inches thickness were heavily cross-rolled to the thickness of 1/4 inches to simulate shot-peening. Smooth specimens of hour glass shape were cut and carefully machined from cross-rolled flat plates to the dimensions and geometry shown in Fig. 4a. Then, all the specimens were strain-aged in an oil bath at 100°C for one hour before testing.

B.2 Mechanical and Fatigue Tests

Monotonic tension tests were conducted under strain control up to necking, then stroke was controlled to final failure with the same testing equipment used in fatigue test described below.

Cyclic and fatigue tests were conducted on a ± 20 kips MTS close-loop, servo-controlled, axial, hydraulic test system at frequencies from 0.05 to 7 H_2 at room temperature. Wood's metal grips were used to ensure the axial alignment of specimen during testing. A MTS clip-on extensometer with a 0.05-in. gage length was used to measure strains. A sine wave function generator was used to control strain amplitude. During the fatigue tests at high frequency, cold water was allowed to pass through the Wood's metal grip to maintain the specimen at isothermal condition of room temperature. All amplified signals from the load cell and clip-on extensometer were recorded on X-Y strip charts. All cyclic tests started in compression. Test results are shown in Tables 4 and 5 and Figs. B1-B4. Cross-rolled A36 specimens showed significant increase in hardness and strength and decrease in ductility thus increase in long life and decrease in short life regimes as expected. Strain softening occurred during the cyclic tests.

B.3 Cyclic Mean Stress Relaxation

Cyclic mean stress relaxation tests with constant mean strain (3×10^{-3} ε) but variable strain amplitude for both precycled and non-precycled (virgin) specimens were conducted until final fractures observe the delayed relaxation effects. For precycled tests, a stabilization block was applied to each specimen before inducing a mean stress to exclude the effect of softening or hardening on relaxation behavior; and each initial mean stress was induced by giving a mean strain before cycling. The relaxation behavior for several strain amplitudes are shown in Fig. B5, and they show fairly good agreement with a power function relationship.

The delayed relaxation effect was significant at the strain amplitudes of 3×10^{-3} and bigger, but was negligible at smaller strain amplitudes where fatigue crack initiation life (N_I) dominates. It was found that the difference in relaxation exponent (k) between precycled and non-precycled conditions at lower strain amplitudes became significant. This observation indicates that information from non-precycled specimens is more appropriate for predicting the mean stress relaxation behavior.

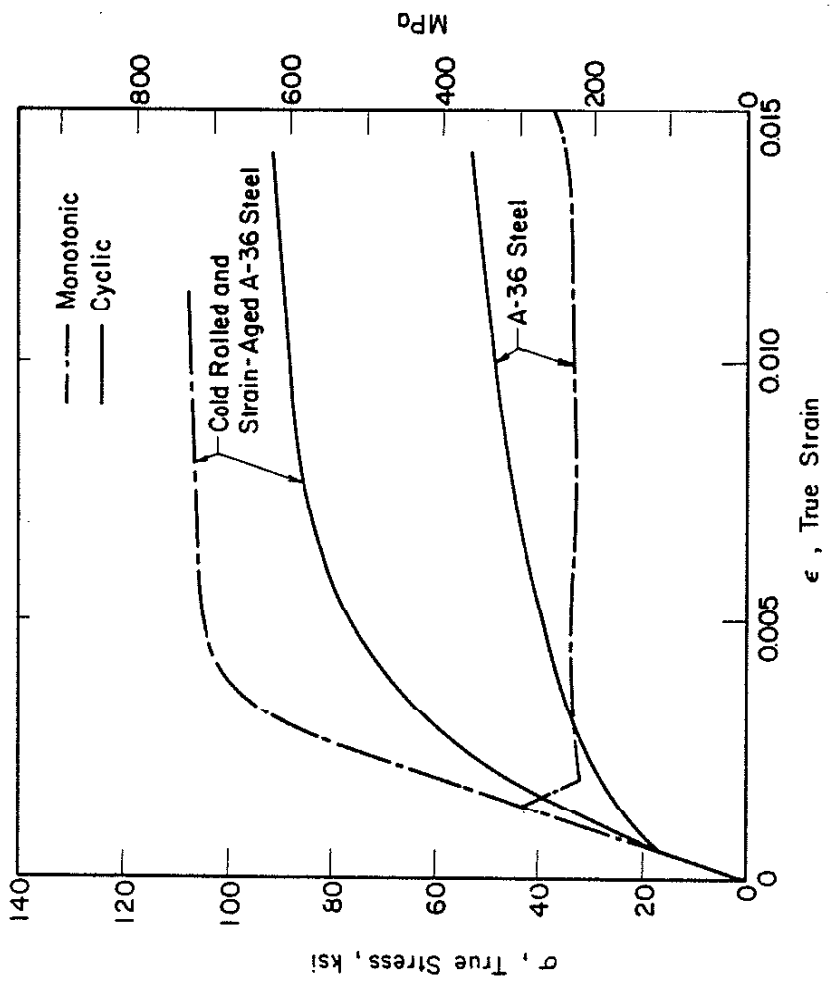

Fig. B-1 Monotonic and Cyclic True Stress-Strain Curves for A36 BM and Cross-Rolled and Strain Aged A36 Steel.

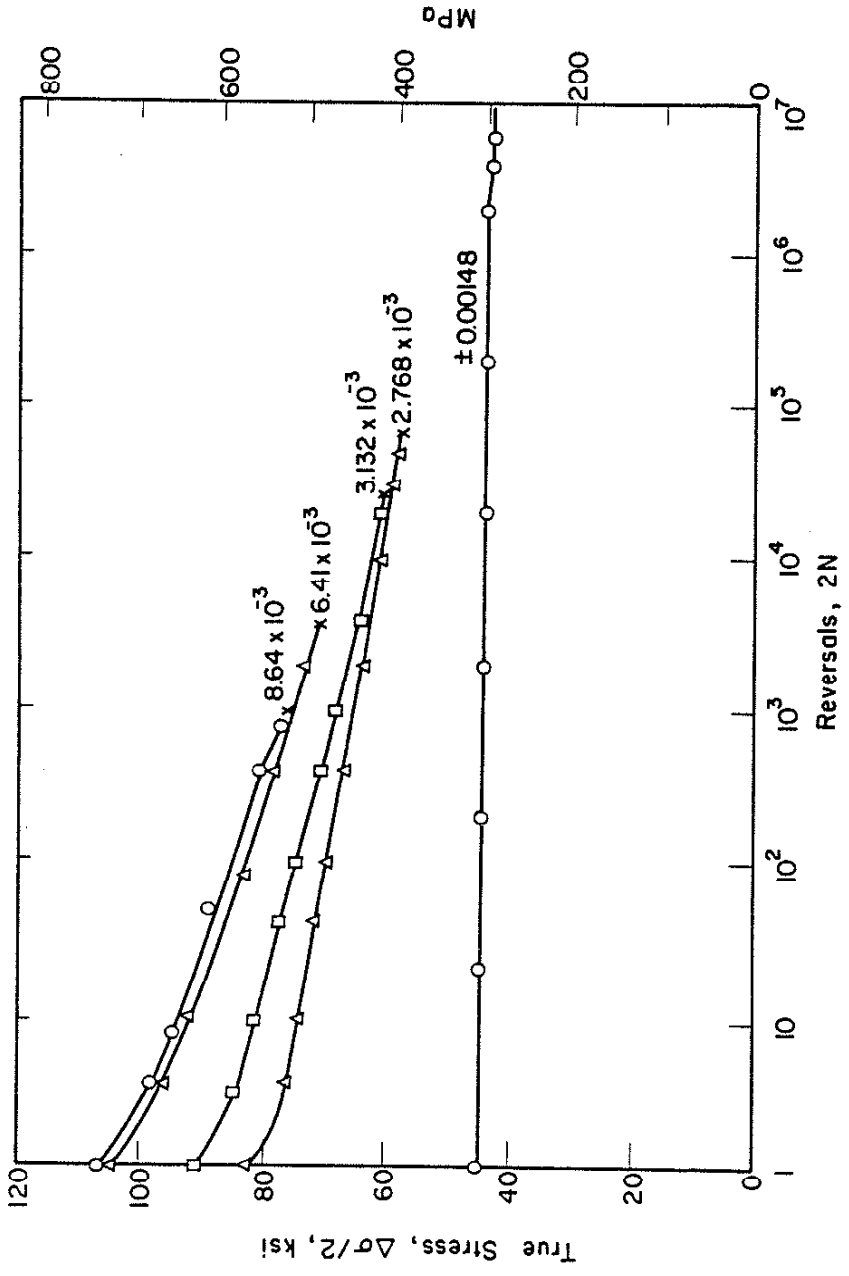

Fig. B-2 Cyclic Softening Behavior for Constant Amplitude Strain-Control Test on Cross-Rolled A36 Steel.

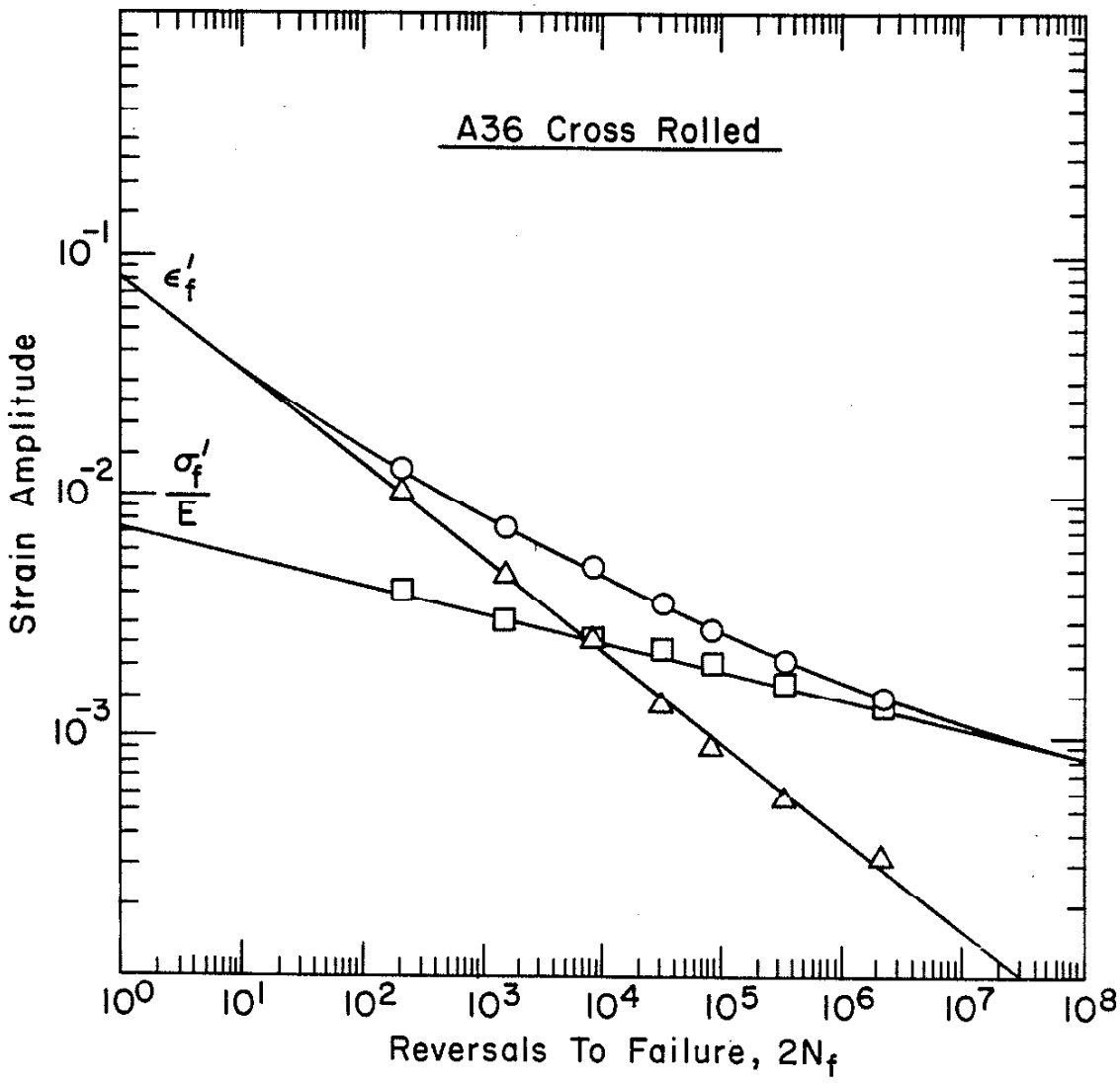

Fig. B-3 Strain Amplitude-Reseverals to Failure Data for Cross-Rolled and Strain-Aged A36 Steel.

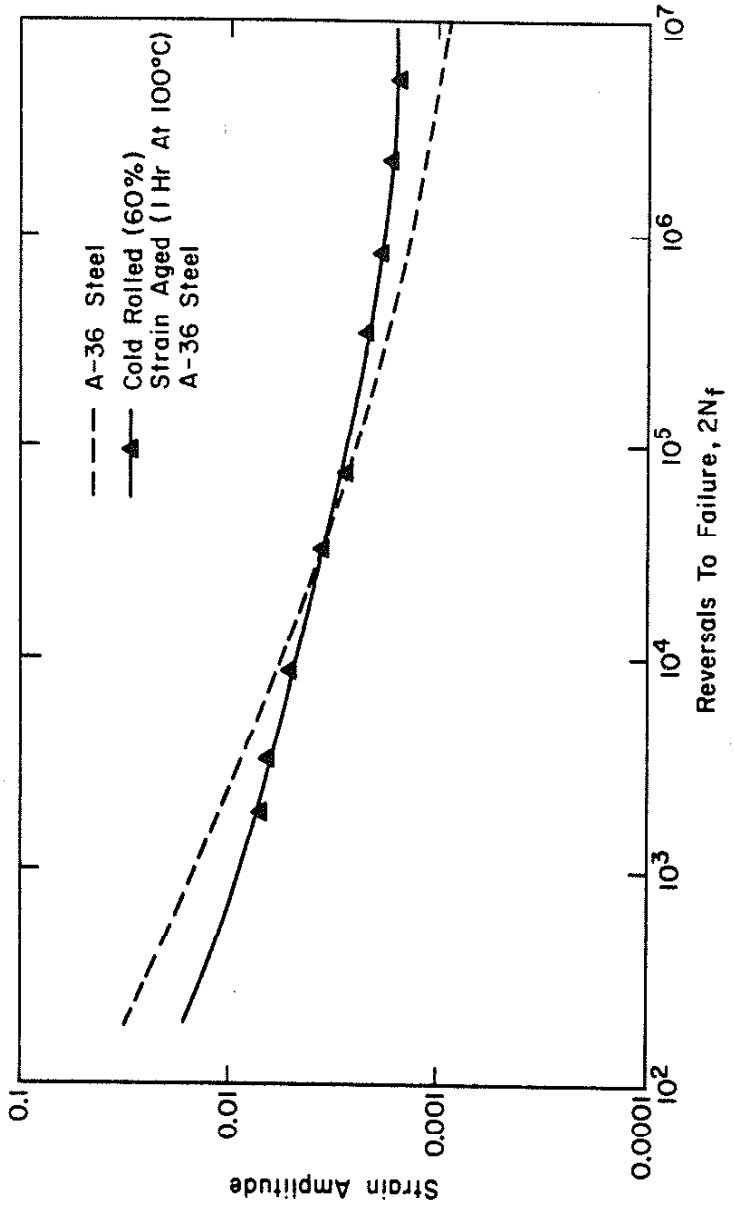

Fig. B-4 Summary Plots of Total Strain Amplitude-Reversals to Failure Data for A36 BM and Cross-Rolled and Strain-Aged A36 Steel.

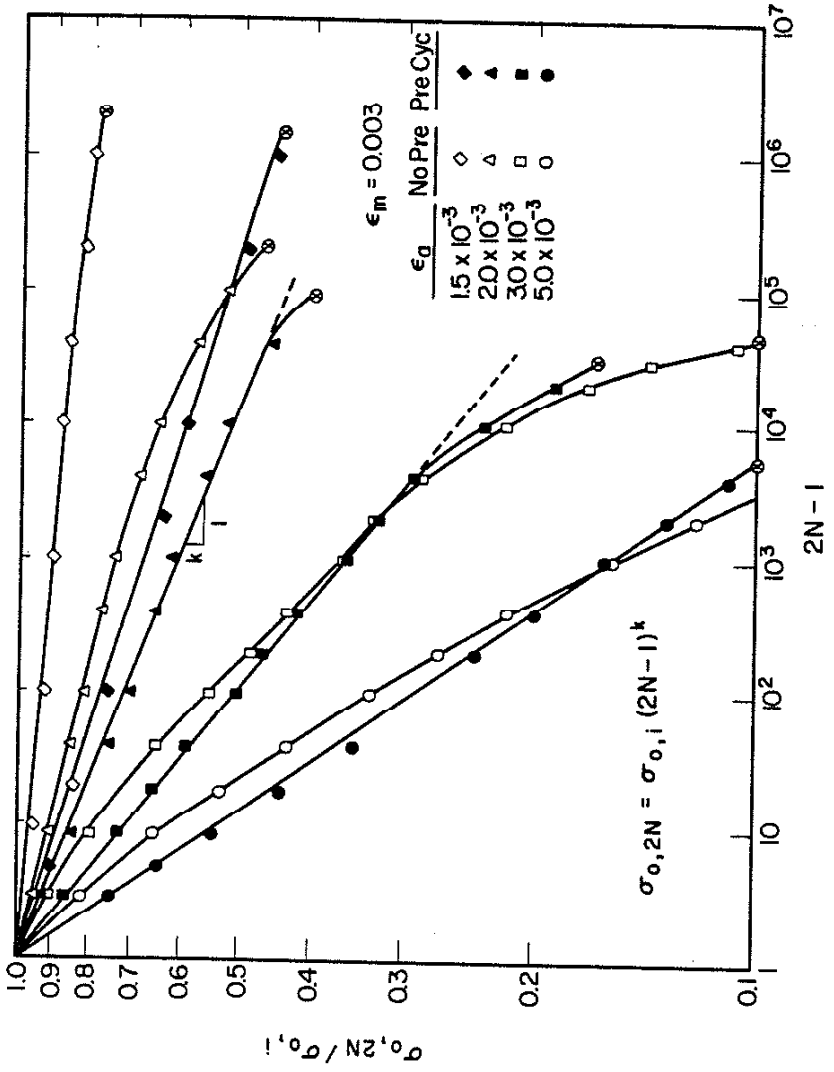

Fig. B-5 Normalized Mean Stress Relaxation Behavior of Cross-Rolled and Strain-Aged A36 Steel at Constant Mean Strain of 0.003.

APPENDIX C

MODEL TO PREDICT WELD FATIGUE STRENGTH FROM BASE METAL TENSILE STRENGTH

C.1 Estimation of HAZ Properties From Tensile Strength of Base Metal (S_u(BM))

To investigate the relationship between tensile strength (or hardness) of the HAZ (S_u(HAZ)), and the tensile strength (or hardness) of the base metal (S_u(BM)), the available data for the above properties (88-91) were plotted. Figure C1 shows a reasonably good linear relationship is apparent:

$$S_u(HAZ) \cong 1.5\ S_u(BM) \qquad C1$$

From Eqs. 44, 45, and C1,

$$\sigma_f'(HAZ) = 1.5\ S_u(BM) + 50 \qquad (ksi) \qquad C2$$

$$b = -\frac{1}{6} \log 2 \left(1 + \frac{100}{3S_u(BM)}\right) \qquad C3$$

From Eqs. 12 and C1.

$$K_{f,max} = 1 + 0.1343\ \alpha_A\ t^{0.5}\ \{S_u(BM)\}^{0.9} \qquad C4$$

C.2 Fatigue Strength (S_a) of Weldments

From the definition:

Stress ratio $R = \frac{S_{min}}{S_{max}}$, nominal stress range $\Delta S = S_{max} - S_{min}$, the nominal mean stress $S_o = 1/2(S_{max} + S_{min})$, and nominal stress amplitude (fatigue strength) $S_a = \Delta S/2$. As a result, the nominal mean stress can be expressed:

$$S_o = S_a \left(\frac{1+R}{1-R}\right) \qquad C5$$

For long life fatigue ($N_I > 1 \times 10^6$ cycles), the local stress-strain response to the corresponding nominal mean stress (S_o) and stress range (ΔS) may be assumed to be elastic. Therefore, the mean stress and stress range of local notch root can be expressed as:

$$\sigma_o = \sigma_r + K_{f,m} \cdot S_o \qquad C6$$

and

$$\sigma_a = K_{f,m} \cdot S_a \qquad C7$$

Substituting Eq. C5 into Eq. C6,

$$\sigma_o = \sigma_r + K_{f,m} \cdot S_a \left(\frac{1+R}{1-R}\right) \qquad C8$$

From Basquin's relationship (Eq. 2) and Eqs. C7 and C8:

$$\sigma_a = K_{f,m} \; S_a = \{\sigma_f' - \sigma_r - K_{f,m} \; S_a\left(\frac{1+R}{1-R}\right)\} \; (2N_I)^b \qquad C9$$

Rearranging Eq. C9 and substituting Eqs. C2-C4, the fatigue strength in long life range ($N_I > 1 \times 10^6$ cycles) is:

$$S_a = \frac{(1.5\, S_u\,(BM) + 50 - \sigma_r)(2N_I)^{-\frac{1}{6}} \; \log 2\left(1 + \frac{100}{3}\,\frac{1}{S_u(BM)}\right)}{\left(1 + 0.1343\alpha_A t^{0.5} S_{u(BM)}^{0.9}\right)\left\{1 + \frac{1+R}{1-R}(2N_I)^{-\frac{1}{6}} \; \log 2\left(1 + \frac{100}{3}\,\frac{1}{S_u(BM)}\right)\right\}} \qquad C10$$

Eq. C10 implies fatigue strength can be estimated for a given life ($N_T = 10^6$ cycles) if the geometrical information (α_A and t), the stress ratio (R), the base metal strength ($S_u(BM)$) and the residual stress (σ_r) can be estimated.

C.3 Determination of Yield Strength (S_y) as Function of BM Tensile Strength (S_u) for Three Most Common Classes of Heat-Treated Steels

Residual stresses of as-welded, stress-relieved, and over-stressed weldments are assumed to be equal to the yield strength of base metal in tension ($\sigma_r = +S_y$), zero ($\sigma_r = 0$)), and yield strength of base metal in compression as maximum ($\sigma_r = -Sy$), respectively.

Therefore, a relationship between S_u(BM) and S_y(BM) is necessary. A sufficient number of steels of each category were selected from recent data (92) for a reasonable range of strength on the basis of weldability without any special complicated pre or post heat-treatment (Table C-1); and then the relationships between S_y vs. S_u were plotted in Fig. C2. Each category shows its own simple linear relation between S_u and S_y, i.e.:
For hot rolled steels (S_u < 90 ksi.),

$$S_y \cong \frac{5}{9} S_u \qquad C11$$

for normalized (at 1600°F) steels (90 ksi < S_u 180 ksi),

$$S_y \cong \frac{7}{9} S_u - 20 \qquad C12$$

and for quenched and tempered (at 800°F) steels (S_u > 90 ksi),

$$S_y \cong 1.2\ S_u - 50 \qquad C13$$

Therefore, residual stress (σ_r) in Eq. C10 can be substituted by the corresponding equation of its category for individual case of base metal according to the post-weld treatment it received. Then, Eq. C10 implies that estimation of fatigue strength (S_a) is possible when only the base metal

tensile strength (S_u) is specified.

C.4 Fatigue Strength (S_a) of Shot-Peened Weldment and Plain Plate

The same development is used in estimating the material properties of shot-peened heat affected zone as of the as-welded heat affected zone.

Available data (93-97) are plotted in Fig. C3 to investigate the relationship between tensile strength (S_u^p) after peening and tensile strength (S_u^b) before peening. The tensile strength values (S_u^p) were obtained from the hardness data which are the only available information, since no other acceptable method has been developed to determine directly the material properties of such thin, shot-affected layers. Even the small amount of data available shows a good simple linear relationship between S_u^p and S_u^b (see Fig C3):

$$S_u^p = 1.2\ S_u^b \qquad \text{C14}$$

From Eq. C1 and C14,

$$S_u^p(\text{HAZ}) = 1.8\ S_u(\text{BM}) \qquad \text{C15}$$

From Eqs. 12, 44, 45, and C15,

$$\sigma_f'^p(\text{HAZ})\ 1.8\ S_u(\text{BM}) + 50 \qquad \text{(ksi)} \qquad \text{C16}$$

$$b^p = -\frac{1}{6} \log 2 \left(1 + \frac{50}{1.8} \frac{1}{S_u(\text{BM})} \right) \qquad \text{C17}$$

$$K^p_{f,\max} = 1 + 0.1582\ \alpha_A\ t^{0.5} S_u^{0.9}(\text{BM}) \qquad \text{C18}$$

Therefore, the fatigue strength of shot-peened weldments is:

$$S_a = \frac{(1.8S_u(BM) + 50-\sigma_r)\ (2N_I)^{\frac{1}{6}} \log 2(1 + \frac{50}{1.8}\frac{1}{S_u(BM)})}{\{1+0.1582\alpha_A\ t^{0.5}\ S_u^{0.9}(BM)\}\ \{1+\frac{1+R}{1-R}(2N_I)^{\frac{1}{6}} \log 2(1+\frac{50}{1.8S_u(BM)})\}} \quad C19$$

Residual stress (σ_r) of shot-peened steels in Eq. C19 can be predicted by Eqs. 46 and 47 for two different base metal strength ranges (see Sec. 4.5.2).

Plain Plate

From Eqs. 10 and 42

$$K_{f,max} = 1 + 0.1865\ \ d^{0.5}\ \ S_u^{0.9} \quad C20$$

As a result, the fatigue strength of plain plate is:

$$S_a = \frac{(S_u+50)(2N_I)^{\frac{1}{6}} \log 2(1 + \frac{50}{S_u})}{\{1+0.1865\ d^{0.5}S_u^{0.9}\}\{1+\frac{1+R}{1-R}(2N_I)^{\frac{1}{6}} \log 2(1+\frac{50}{S_u})\}} \quad C21$$

C.5 Fatigue Strength (S_a) for Combined Axial and Bending Stresses

If L_1 and L_2 are the ratios of the static bending (S_1^B) and cyclic bending (ΔS_2^B) stresses to the axial stress (ΔS), respectively, i.e.,

$$\frac{S_1^B}{S_1^A} = L_1 \text{ and } \frac{\Delta S_2^B}{\Delta S_A} = L_2 \quad C22$$

where S_1^B and ΔS_2^B can be calculated by bending strain measurements: see Sec. 3.4. Then, Eq. C6 becomes:

$$\sigma_o = \sigma_r + S_o^A \{K_{f,m}^A (L_1 + L_2)\} \left(\frac{1+R}{1-R}\right) \quad \text{C23}$$

Thus, Eq. C8 becomes:

$$\sigma_o = \sigma_r + S_a^A \{K_{f,m}^A + K_{f,m}^B (L_1 + L_2) \left(\frac{1+R}{1-R}\right)\} \quad \text{C24}$$

Since only cyclic bending stress (ΔS_2^B) can affect the stress amplitude, Eq. C7 becomes:

$$\sigma_a = S_a^A (K_{f,m}^A + L_2 K_{f,m}^B) \quad \text{C25}$$

Then Eq. C10 becomes:

$$S_a = \frac{(\sigma_f' - \sigma_r)(2N_I)^b}{(K_{f,m}^A + L_2 K_{f,m}^B) + \{K_{f,m}^A + K_{f,m}^B (L_1 + L_2)\} \left(\frac{1+R}{1-R}\right)(2N_I)^b} \quad \text{C26}$$

where:

$$K_{f,m}^A + L_2 K_{f,m}^B = 1 + L_2 + 1/2(\alpha_A + L_2 \alpha_B)(t/a)^{1/2} \quad \text{C27}$$

and

$$K_{f,m}^A + K_{f,m}^B (L_1 + L_2) = 1 + L_1 + L_2 + 1/2\{\alpha_A + (L_1 + L_2)\alpha_B\}(t/a)^{1/2} \quad \text{C28}$$

If the initial static bending stress (S_1^B) equal to zero, then Eq. C26 becomes:

$$S_a = \frac{(\sigma_f' - \sigma_r)(2N_I)^b}{(K^A_{f,m} + L_2 K^B_{f,m})\{1 + \frac{1+R}{1-R}(2N_I)^b\}} \qquad C29$$

Equation C29 can be reexpressed in the form of Eq. 55 by substituting b, σ_r, and the term $(K^A_{f,m} + L_2 K^B_{f,m})$ with the same kinds of expressions used to obtain Eq. 55.

TABLE C-1

Selected Weldable Alloy Steels (92)

Treatment	AISI-SAE No	Tensile Strength ksi (MPa)	Yield Strength ksi (MPa)	Hardness BHN
Hot-Rolled	1006	43 (296)	24 (165)	86
	1015	50 (345)	27.5 (190)	101
	1021	61 (421)	33 (228)	116
	1030	68 (469)	37.5 (259)	137
	1044	80 (552)	44 (303)	163
Normalized at 1600° F (871° C)	8620	91.75 (633)	51.75 (357)	183
	1141	102.5 (707)	58.75 (405)	201
	4320	115 (793)	67.25 (464)	235
	9310	131.5 (907)	82.75 (571)	269
	4140	148 (1020)	95 (655)	302
	4340	185 (1276)	125 (862)	363
Quenched and Tempered at 800° F (427° C)	1040	110 (758)	80 (552)	241
	1137	127 (876)	106 (731)	262
	1141	169 (1165)	150 (1034)	331
	4140	181 (1248)	165 (1138)	370
	8630	185 (1276)	170 (1172)	375
	5140	190 (1310)	170 (1172)	365
	4340	213 (1469)	198 (1365)	430
	8640	200 (1379)	188 (1296)	400

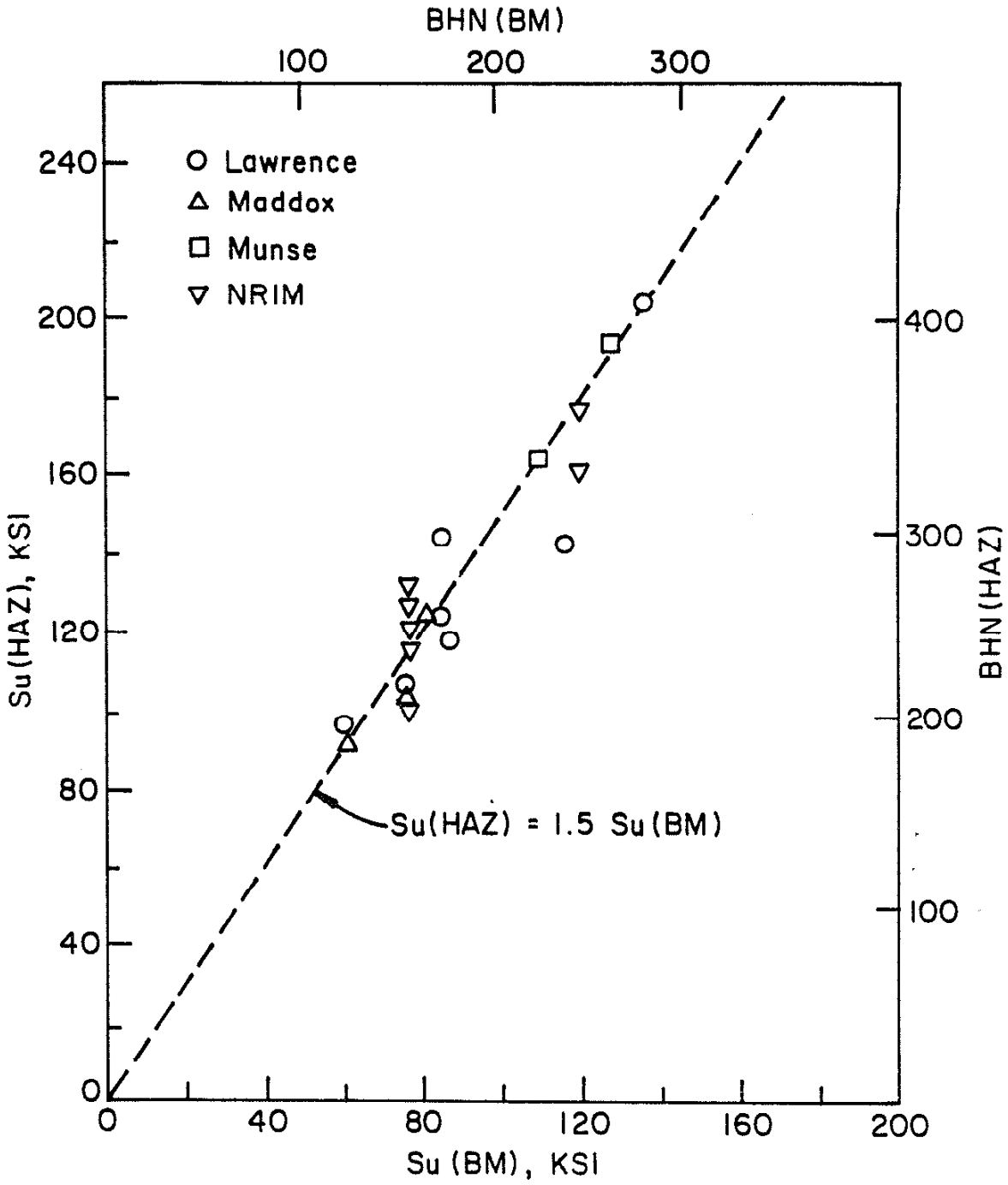

Fig. C-1 Empirical Relationship between Tensile Strength of HAZ and Tensile Strength of BM for Steels (Some of the Values for Su(HAZ) Were Calculated from Hardness Measurements).

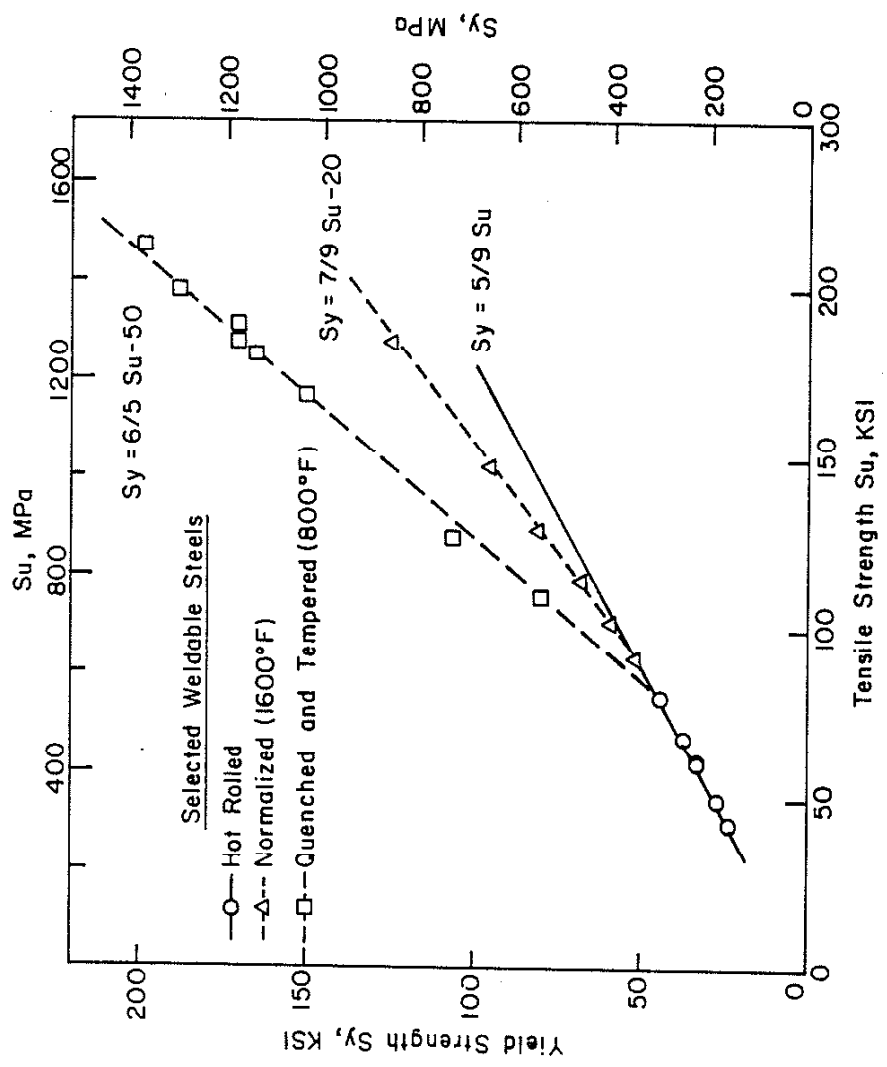

Fig. C-2 Relationship between Yield Strength and Tensile Strength of Selected Weldable Steels (92).

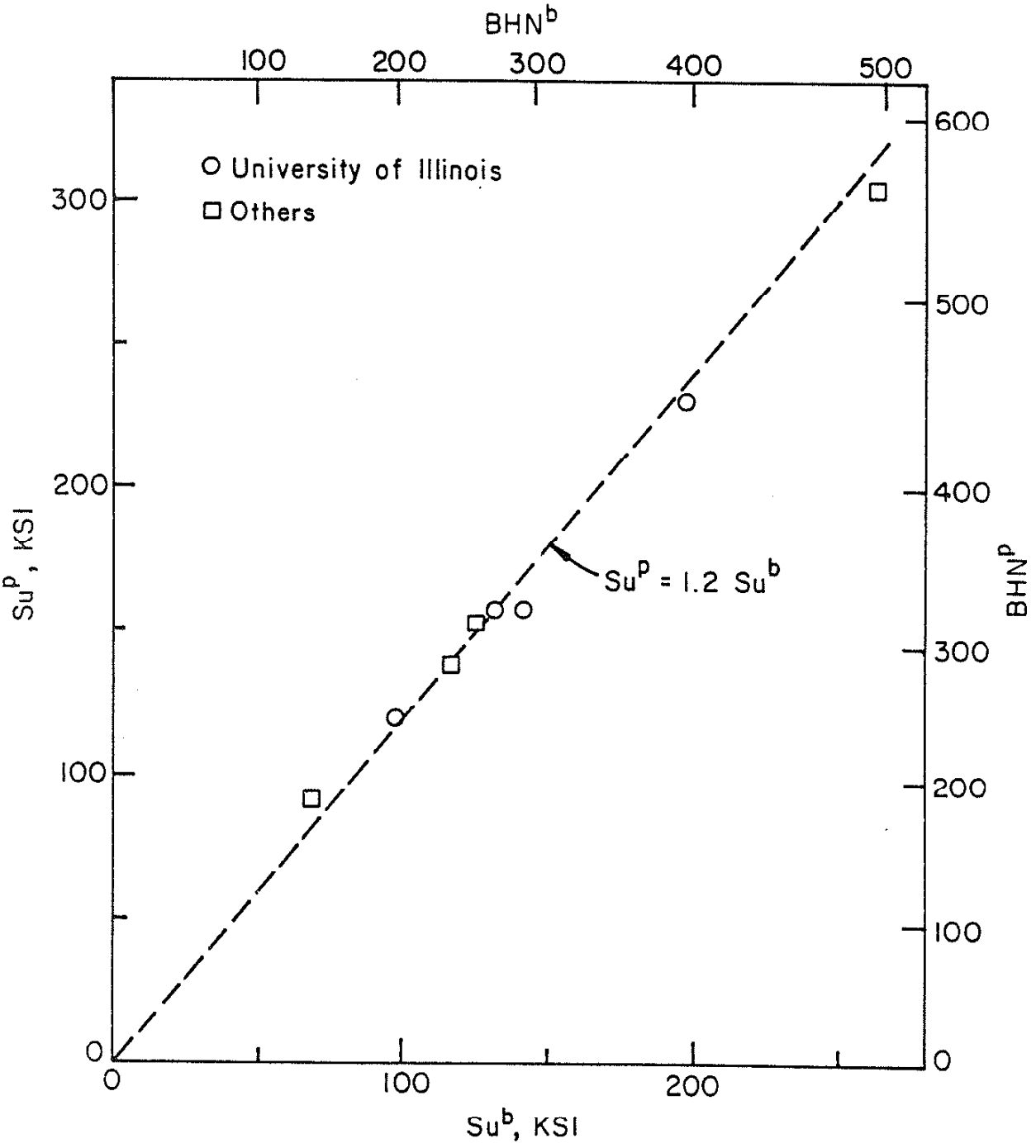

Fig. C-3 Relationship between the Tensile Strength of Steels before Shot-Peening (Su^b) and after Shot-Peening (Su^p).

REFERENCES

1. Landgraf, R. W., "Cyclic Deformation and Fatigue Behavior of Hardened Steels," Ph.D. Thesis, University of Illinois, Urbana, 1969.

2. Burk, J. D. and Lawrence, F. V., "Influence of Bending Stresses on the Fatigue Crack Propagation Life in Butt Welds," Welding Journal Research Supplement, Vol. 56, No. 2, February, 1977, pp. 615-665.

3. Friedman, E., "Thermomechanical Analysis of the Welding Process Using the Finite Element Method," J. Pressure Vessel Tech., 97, 3, p. 206, 1975.

4. Ros, M., "Experiments for the Determination of the Influence of Residual Stresses on the Fatigue Strength of Structures," Welding Research, BWRA, Vol. 4, No. 5, Oct., 1950, pp. 83r-93r.

5. Hebrant, F., Louis, H., Soete, W., and Vinckier, A., "The Relaxation of Residual Welding Stresses by Static and Fatigue Loading," Welding Research Abroad, Sept., 1957, pp. 58-63.

6. Dugdale, D. S., "Effect of Residual Stress on Fatigue Strength," Welding Journal, Vol. 38, No. 1, 1959, pp. 45s-48s.

7. Trufyakov, V. I., "Welded Joints and Residual Stresses," Welding Research Abroad, Vol. 5, No. 3, Mar., 1959, pp. 11-18.

8. Serensen, S. V., Trufiakov, V. I. and Babaer, A. V., "Influence of Welding Defects on a Fatigue Resistance of Joints Considering Residual Stressing," E. O. Paton Electric Welding Institute, Kiev, USSR National Welding Committee, Moscow 1969. Submitted as IIW Doc. Comn. XIII-552-69.

9. Gurney, T. R., "Influence of Residual Stresses on Fatigue Strength of Plates with Fillet Welded Attachments," British Welding Journal, Vol. 7, No. 6, 1960, pp. 415-431.

10. Kudryavtsev, I. V., "The Influence of Internal Stresses on the Fatigue Endurance of Steel," International Conference on Fatigue, Inst. Mech. Engr., 1956.

11. Selby, K. A., Stallmeyer, J. E., and Munse, W. H., "Influence of Geometry and Residual Stress on the Fatigue of Welded Joints," Structural Research Series No. 297, University of Illinois, Urbana, June, 1965.

12. Gurney, T. R., "Fatigue of Welded Military Structures," British Welding Journal, Vol. 15, No. 6, 1968, pp. 276-282.

13. Reemsnyder, H. S., "Some Significant Parameters in the Fatigue Properties of Weld Joints," Welding Journal, Vol. 48, No. 5, May, 1969 pp. 213s-220s.

14. Braglia, B. L., "Fatigue Resistance of Fillet Welds," General Motors Institute Fifth Year Thesis, February, 1975.

15. Navrotskii, D. I. and Savel'ev, V. N., "The Effects of Residual Stresses on the Fatigue Strengths of Specimens with Transverse Welds," Welding Research Abroad, Vol. 7, No. 9, November, 1961, pp. 63-67.

16. Reemsnyder, H. S., "The Development and Application of Fatigue Data for Structural Steel Weldments," Presented at the ASTM Symposium on Fatigue Testing of Weldments, Toronto, Canada, May 2-3, 1977.

17. Pollard, B. and Cover, R. J., "Fatigue of Steel Weldments," Welding Research Supplement, Nov., 1972, pp. 544s-554s.

18. Dutschinskii, B. N. Paper of All. Union Research Inst. for Railway Const. and Design (TSNIIS), No. 8, 1952.

19. Harrison, J. D., "Further Techniques for Improving the Fatigue Strength of Welded Joints," British Welding Journal, Vol. 13, No. 11, 1966, pp. 642-647.

20. Gurney, T. R., "Effect of Peening and Grinding on the Fatigue Strength of Fillet Welded Joints," Welding Research Abroad, Vol. 15, No. 3, March, 1969, pp. 13-21.

21. Suhr, R. W., "Bending Fatigue of Fillet Welds in 25.4 mm (1 in.) Mild Steel Plate Under Narrow Band Random Loading and the Effect of Weld Variables," Proceedings of the Conference on Fatigue of Welded Structures, (July 6-9, 1970), Vol. 2, The Welding Institute, 1971.

22. Harrison, J. D., "Techniques for Improving the Fatigue Strength of Welded High Strength Steels," The Welding Institute Contract Report, C215/7/68, May, 1968.

23. Millington, D., "TIG Dressing to Improve Fatigue Properties in Welded High Strength Steels," Welding Research Abroad, Vol. 19, No. 8, October, 1973, pp. 40-45.

24. Haagensen, P. J., "Effect of TIG Dressing on Fatigue Performance and Hardness of Steel Weldments," Paper presented at the ASTM Symposium on Fatigue Testing of Weldments, Toronto, Canada, May 2-3, 1977.

25. Watkinson, F., Bdoger, P. H., and Harrison, J. D., "The Fatigue Strength of Welded Joints in High Strength Steels and Methods for Its Improvement," Proceedings of the Conference on the Fatigue of Welded Structures, (July 6-9, 1970), Vol. 1, The Welding Institute, 1971, pp. 97-113.

26. Kado, S., Ishiguro, T., Hanzawa, M., and Yokota, H., "Influence of the Conditions in TIG Dressing on Fatigue Strength in Welded High Tensile Strength Steel," IIW-Doc.-XIII- 771-75, Japan, 1975.

27. Minner, H. H. and Seeger, T., "Fatigue Strength of Welded and TIG-Dressed High Strength Steels," 3JWS-39, 3rd Int. Symp. J.W.S., Tokyo, 1978.

28. Kado, S., Ishiguro, T., and Ishii, N., "Fatigue Strength Improvement of Welded Joints by Plasma Arc Dressing," IIW/IIS-Doc.-XIII-774-75, Japan, 1975.

29. Baxter, C.F.G., and Booth, G. S., "Improved Fatigue Strength by Plasma Dressing," Weld. Inst. Res. Bull., Sept., 1979.

30. Testin, R. A., "Fatigue Strength of Fillet Welds," Unpublished Reports, Electro-Motive Division, General Motors Corportation, September, 1977, Feb., 1978, June, 1978.

31. Faulkner, M. G. and Bellow, D. G., "Improving the fatigue strength of butt welded steel joints by peening," Weld. Res. Int., Vol. 5, No. 3, 1975, pp. 63-72.

32. Gurney, T. R., Fatigue of Welded Structures, 2nd. ed., Cambridge University Press, London, England, and New York, N.Y., 1979.

33. Braithwaite, A.B.M., "Fatigue tests on Bailey bridge transoms," Br. Weld. J., Vol. 11, No. 12, 1964, pp. 641-4.

34. Gurney, T. R., "Exploratory fatigue tests on plastic coated specimens," Br. Weld. J., Vol. 10, No. 10, 1963, pp. 530-33.

35. Harrison, J. D., "Some cumulative damage fatigue tests on an Al.Zn.Mg alloy," Inst. Weld., Autumn Meeting, 1967.

36. Knight, J. W., "Improving the fatigue strength of fillet welded joints by grinding and peening," Weld. Inst. Rep. 8/1976/E.

37. Booth, G. S., "The effect of mean stress on the fatigue lives of ground or peened fillet welded steel joints," Weld. Inst. Rep. 34/1977/E.

38. Nacher, A., "Influence of local heating and of surface peening on fatigue behaviour of welded jionts and details," IIW Doc. XIII-255-1961. (Part reported in contribution to discussion by U. Guerrera., Symp. on fatigue of welded structures. Br. Weld. J., Vol. 7, No. 8, 1960, pp. 513-16.)

39. Doty, W. D., "Properties and characteristics of a quenched and tempered steel for pressure vessles," Weld. Res. Suppl., Vol. 20, No. 9, 1955, pp. 425-41.

40. Nacher, A., "Report of a promising proceeding for improving the fatigue strength of butt welded joints," IIW Doc. XIII-290-1962.

41. Baron, H. G. and Brine, F. E., "A note on the improvement in fatigue properties of butt welds produced by shot peening or pre-stretching," Commonwealth Welding Conf., London, 1965.

42. Robakowski, T., "Fatigue strength and mechanical properties of submerged peening on the fatigue strength of St35 steel butt joints," Przeglad Spaw. Vol. 24, No. 8, Aug. 1972, pp. 188-92.

43. Konish, K., Takagi, O. and Shimada, K., "On the fatigue strengths of welded joints of high tensile structural steel," Proc. 1st Jap. Congr. on testing materials JSTM 1958, pp. 10-14.

44. Nordmark, G. E., "Peening increases fatigue strength of welded aluminium," Metal Prog., Vol. 84, No. 5, 1963, pp. 101-3.

45. Hedström, A., "Cumulative damage in specimens of Al-Zn-Mg tested by a new method for reducing the scatter," Weld. Inst. Conf. on Fatigue of Welded Structures, Brighton, July 1970.

46. Gurney, T. R., "Exploratory Fatigue Tests on Fillet Welded Specimens Subjected to Prior Overloading," British Welding Journal, Vol. 10, No. 10, 1963, pp. 526-529.

47. Harrison, J. D., "Further Fatigue Tests on Fillet Welded Specimens Subjected to Prior Overloading," British Welding Journal, Vol. 12, No. 5, 1965, pp. 255-258.

48. Albrecht, M., ASCE, Abtahi, A., and Irwin, G. R., "Fatigue of Periodically Overloaded Stiffener Detail," Journ. Struct. Div., II, P. 2103-2119, Nov., 1976.

49. Burk, J. D., and Lawrence, F. V., "The Effect of Residual Stresses on Weld Fatigue Life," Fracture Control Report 29, University of Illinois 1-26, January 1978.

50. Maddox, S. J., "Assessing the Significance of Flaws in Welds Subject to Fatigue," Welding Journal, 1974, 53:401s - 409s.

51. El Haddad, M. H., Topper, T. H., Smith, I.F.C., "Fatigue Life Predictions of welded Components Based on Fracture Mechanics," Journal of Testing and Evaluation, JTEVA, Vol. 8, No. 6, November 1980, pp. 301-307.

52. Lawrence, F. V., Jr., Mattos, R. J., Higashida, Y., and Burk, J.D., "Estimating the Fatigue Crack Initiation Life of Welds," ASTM STP 648, 1978, pp. 134-158.

53. Lawrence, F. V., Ho, N. J., Mazumdar, P. K., "Predicting the Fatigue Resistance of Welds," Amm. Rev. Mater. Sci., 1981, 11:401-25, pp. 401-425.

54. Tobe, Y. and Lawrence, F. V. Jr., "The Effect of Inadequate Joint Penetration on the Fatigue Resistance of High-Strength Structural Steel Welds., Welding Journal, Vol. 56, No. 9, 259s - 266s.

55. Landgraf, R. W., and Morrow, JoDean, "Effect of Mean Stress on the Fatigue Behavior of a Hard Steel," Master's Thesis, Dept. of Theoretical and Applied Mechanics, U. of Ill., 1966.

56. Topper, T. H., Wetzel, R. M., and Morrow, JoDean, "Neuber's Rule Applied to Fatigue of Notched Specimens," J. Mat., 4, p. 200, 1969.

57. Neuber, H., "Theory of Stress Concentration for Shear Strained Prismatical Bodies with Arbitrary Non-Linear Stress-Strain Law," J. App Mech., P. 544, 1961.

58. Peterson, R. E., "Notch Sensitivity," Chap. 13, Metal Fatigue, Sines and Waisman (ed.), McGraw-Hill, New York, 1959.

59. Morrow, JoDean, (ed.) Graham, J. A., Sec. 3.2, SAE Fatigue Design Handbook, Society of Automotive Engineers, 1968.

60. Mattos, R. J., and Lawrence, F. V., Jr., "Estimation of the Fatigue Crack Initiation Life in Welds Using Low Cycle Fatigue Concepts," FCP Rep. No. 19, U. of I., 1975.

61. Palmgren, A., "Die Lebensdauer von Kvgellagern," Verein Deutscher Ingenieure Zeitschrift, Vol. 68, pp. 339, 1924.

62. Miner, M. A., "Cumulative Damage in Fatigue," Journal of Applied Mechanics, Vol. 12, pp. A159, 1945.

63. Paris, P.C., and Erdogan, F., "A Critical Analysis of Crack Propagation Law," J. Basic Engr., ASME Trans., Vol. 85, series D, No. 4, pp. 528, 1963.

64. Maddox, S. J., "An Analysis of Fatigue Cracks in Fillet Welded Joints," Weld. Inst. Members Rep. E49/72.

65. Emery, A. F., "Stress-Intensity Factors for Thermal Stresses in Thick Hollow Cylinders," J. Basic Eng. ASME Trans. Seris D, Vol. 85, p. 45, 1966.

66. Socie, D. F., "Estimating Fatigue Crack Initiation and Propagation Lives in Notched Plates under Variable Loading Histories," TAM Report No. 417, University of Illinois, Urbana-Champaign, 1977.

67. Barsom, J. M., "Fatigue-Crack Growth Under Variable Amplitude Loading in ASTM A514 Grade B Steel," ASTM STP 536, American Society for Testing and Materials, 1973.

68. Elber, W., "The Significance of Fatigue Crack Closure," ASTM STP 595, American Society for Testing and Materials, 1971.

69. Bell, P. D., and Wolfman, A., "Mathematical Modeling of Crack Growth Interaction Effects," ASTM STP 595, American Society for Testing and Materials, 1976.

70. Elber, W., "Equivalent Constant-Amplitude Concept for Crack Growth Under Spectrum Loading," Fatigue Crack Growth Under Spectrum Loads, ASTM STP 595.

71. Higashida, Y., "Strain Controlled Fatigue Behavior of Weld Metal and Heat-Affected Base Metal in A36 and A514 Steel Welds," Ph.D. Thesis, University of Illinois, Urbana-Champaign, 1976.

72. Bridgman, P. W., "The Stress Distribution at the Neck of a Tension Specimen," Transactions of American Society of Metals, Vol. 32, 1944, pp. 553-574.

73. Dieter, G. E., Jr., Mechanical Metallurgy, 2nd. Ed., McGraw-Hill Book Co., Inc. New York, 1976, pp. 344-345.

74. Burk, J.D., "Prediction of the Fatigue Crack Propagation Lives of Butt Weldments," Master's Thesis, Dept. of Metallurgy, Univ. of Ill., 1974.

75. Shot-Peening, 4th Ed., American Wheelabrator & Equipment Corp., Mishawaka, Indiana, 1951, p. 21.

76. Chen, W. C. and Lawrence, F. V., Jr., "A Model for Joining the Fatigue Crack Initiation and Propagation Analyses," Fracture Control Program, Report No. 32, University of Illinois, November 1979.

77. Peterson, R. E., Stress Concentration Factors, Wiley and Sons, Inc. New York. 1974.

78. Shot Peening Applications, 6th ed., Metal Improvement Company, Inc., 1980.

79. Cichlar, D., Private Communication, Chicago Div., Metal Improvement Company, Chicago, IL, 1980.

80. Ho, N-J., "The Fatigue of Weldments Subjected to Complex Loadings," Ph.D. Thesis, Univ. of Il., Urbana, IL, 1982.

81. Yung, J-Y., et al., "Mechanical Testing of Welds," Research Report to GARD, Inc., Niles, Ill., 1982.

82. Radziminski, J. B., Srinivansan, R., Moore, D., Thrasher, C. and Munse, W. H. (1973), Structural Research Series No. 405, University of Illinois at U-C., Urbana, IL.

83. Monograph on Fatigue Strength of Welds, Royal Swedish Academy of Engineering Sciences, Stokholm, Sweden, 1969.

84. NRIM Fatigue Data Sheets, National Research Institute for Metals, Tokyo, Japan, 1978.

85. Munse, W. H. and Grover, L., Fatigue of Welded Steel Structures, Welding Research Council, New York, N.Y., 1968.

86. Murzyn, P. J., "An Experimental Study of the Means for Improving Weldment Fatigue Resistance," M.S. Thesis, Univ. of Ill., Urbana, 1981.

87. Koktuniak. F., "Laser Surface Heat Treating an Evaluation of Several Variables," GM Tech. Center 48090, Michigan, 1977.

88. Maddox, S. J., "Fatigue Crack Propagation in Weld Metal and Heat Affected Zone Material," Weld. Inst., Members Rep. E/29/69.

89. Maddox, S. J., "Some Further Fatigue Crack Propagation Result Relevant to Welded Joints in Steel," Weld. Inst., Members Rep. E37/70.

90. Maddox, S. J., "The Influence of Fracture Mode on Fatigue Crack Propagation," Weld. Inst., Members Rep. E49/72.

91. Hartmann, A. J., Bruckner, W. H., Mooney, J., and Munse, W. H., "Effect of Weld Flaws on the Fatigue Bahavior of Butt-Welded Joints in HY-80 Steel," SRS No. 275, Civil Engr. studies, Univ. of Ill., Urbana, 1963.

92. Metal Progess Materials and Processing Databook, ASM, Vol. 120, No. 1, June, 1981.

93. Chang, S.-T. and Lawrence, F.V., Jr., "Predicting the Effect of Shot Peening on Weld Fatigue Life," Shot-peening, Pergamon Press, pp. 461-476, First International Conference on Shot Peening, Paris, Sept., 1981.

94. Sato, S., Inoue, K., and Ohno, A., "The Effect of Shot-peening to Decarburized Spring Steel Plate," Shot Peening, Perg. Press, pp. 303-312, 1st Int. Conf. on Shot Peening, Paris, Sept., 1981.

95. Koibuchi, K., Hayama, T., and Kawai, S., "Residual Stress and Fatigue Strength of Surface Hardened Components," Shot Peening, Perg. Press, pp. 413-419, 1st Int. Conf. on Shot Peening, Paris, Sept., 1981.

96. Muller, M. P., Verpoort, C., and Gessinger, G. H., "The Influence of Shot Peening on the Fatigue and Corrosion Fatigue Behavior of an Austenitic Ferritic Stainless Steel," Shot Peening, Perg. Press, pp. 479-484, 1st Int. Conf. on Shot peening, Paris, Sept., 1981.

97. Cheng, M.-X., and Ao, B.-Q., "The Effect of Shot Peening on Contact Fatigue Life of Carburized Steel," Shot Peening, Perg. Press, pp. 333-339, 1st Int. Conf. on Shot Peening, Paris, Sept., 1981.